HIGH ENERGY SCATTERING IN QUANTUM CHROMODYNAMICS

THE UNIVERSITY
of MANCHESTER

A thesis submitted to the University of Manchester
for the degree of Doctor of Philosophy
in the Faculty of Science

By
Agustín Sabio Vera
Department of Physics and Astronomy
September 2000

Contents

List of Figures 6

Abstract 10

Declaration 12

Copyright and Ownership of Intellectual Property Rights 13

Dedication 14

Acknowledgements 15

The Author 18

1 Introduction 19

1.1 QCD 20

1.1.1 Asymptotic freedom 21

1.1.2 Factorization 25

1.1.3 Renormalization scale invariance 26

1.2 Deep inelastic scattering 28

1.2.1 The Altarelli-Parisi evolution equations 30

1.2.2 Solution to the DGLAP equations 36

1.2.3 Solution to the DGLAP equations at small x 40

1.2.4 BFKL formalism in deep inelastic scattering 43

1.2.5 Parton saturation 46

1.3 Small x processes at HERA 47

1.4 Total cross-sections 51

1.5 Other tests for BFKL 56

2 The BFKL equation at leading order **61**

2.1 The reggeization of the gluon 62

2.1.1 Tree level 62

2.1.2 One-loop 64

2.1.3 Two-loops 67

2.1.4 All-loops 71

2.2 The BFKL equation 74

2.2.1 One-loop 74

2.2.2 Two-loops 75

2.2.3 All-loops 75

2.3 Solution to the BFKL equation at leading order for forward scattering . 76

3 Coherence in QCD **79**

3.1 Coherence in Quantum Electrodynamics 80

3.2 Coherence in Quantum Chromodynamics 81

3.3 Small x final states 84

3.3.1 Introducing a resolution scale 88

3.3.2 Coherence with a resolution scale 93

3.3.3 Equivalence between BFKL and CCFM jet rates 97

3.3.4 Jet rates to all orders and the CCFM-BFKL equivalent description of final states at leading order 98

4 The BFKL equation at next-to-leading order 102

4.1 Introduction 103

4.2 The impact factors 104

4.3 Leading order case 105

4.4 Next-to-leading order case 107

5 Improving the BFKL expansion 115

5.1 Structure of the next-to-leading order corrections 116

5.2 Collinear limit of the BFKL kernel 119

5.3 Estimating the higher order corrections 122

6 Rapidity veto effects 124

6.1 Eliminating unphysical logarithms 125

6.2 Limiting the gluon emission. 132

6.3 The Rapidity Veto to all orders. 137

7 Solving the BFKL equation with running coupling **144**

7.1 Formalism to solve the equation at leading order 146

7.1.1 The γ-contours 150

7.1.2 Qualitative analysis of the solution for N=0 151

7.2 Accounting for Higher Order Corrections 155

8 Conclusions and future work **157**

A Example of integration in two-dimensional gluon phase space **161**

List of Figures

1.1 Experimental tests of the QCD running coupling 24

1.2 Electron-proton deep inelastic scattering 28

1.3 Scaling of the F_2 structure function [14] 30

1.4 Gluon radiation in photon-quark interaction 31

1.5 Contributions to F_2 from vertex diagrams and external wave function renormalization 33

1.6 Quark-quark ladder diagrams 34

1.7 Struck quark coming from a gluon parent 35

1.8 QCD fits to muon-proton DIS F_2 [14] 38

1.9 Parton density distributions as functions of x for $Q^2 = 20$ GeV^2 [15] . . 39

1.10 The proton structure function F_2 as a function of Q^2 for fixed x 41

1.11 A global NLO DGLAP fit to the measurements of F_2 by the H1 and fixed target collaborations. 45

1.12 The (x, Q^2) kinematic plane of some of the fixed target and of the HERA collider DIS experiments 47

1.13 The proton structure function as a function of x for three Q^2 values . . 48

1.14 A NLO QCD fit to F_2 as function of x for fixed Q^2 values (in GeV^2) . . 49

1.15 $\lambda(Q^2)$ from fits of the form $F_2 \sim x^{-\lambda}$ at fixed Q^2 and x <0.1 [29] 50

1.16 The ρ ($\circ$), ω ($\square$), ϕ ($\triangle$) and π ($\bullet$) trajectories. The ρ trajectory has been continued as measured in $\pi^- p \to \eta n$ [34] 52

1.17 The total cross section data and parameterization of $\bar{p}p$, pp and $\pi^\pm p$ as function of $\sqrt{s}$ 53

1.18 The total photoproduction cross section data as function of W. The full line and the dotted line are the Donnachie-Landshoff parameterization predictions for $\alpha_{\mathcal{P}}$=1.08 and 1.1. ALLM is a different parameterization. 54

1.19 Diffractive deep inelastic scattering 55

1.20 The differential cross section as a function of x for forward π^0s for $2 < Q^2 < 70$ GeV^2, $x_{\pi^0} > 0.01$ and the angle between the proton and pion between 5 and 25 degrees. The dotted line is a prediction calculated with DGLAP. The solid line is a modified LO BFKL calculation. 58

1.21 $\gamma^*\gamma^*$ cross section for Q^2 values of 3.5, 14 and 14.5 GeV^2 [111] 59

2.1 Simplest diagram contributing to leading order octet exchange 63

2.2 First graph contributing to one-loop corrections 65

2.3 Second graph contributing to one-loop corrections 66

2.4 Contributions to Im$\mathcal{A}^{(2)}_{2\to 2}$ at leading order 68

2.5 Contributions to Im$\mathcal{A}^{(2)}_{2\to 2}$ at leading order 69

2.6 Effective vertex in the leading logarithm approximation 70

2.7 $q + q \to q + q + n$ gluons amplitude in the leading logarithm approximation at tree level 72

3.1 Kinematics of $\gamma^* \to e^+e^-\gamma_{\rm soft}$ 80

3.2 Kinematics of $\gamma^* \to q\bar{q}g_{\rm soft}$ 82

3.3 Colour coherence effect in a gluonic cascade 83

3.4 Notation for DIS momenta with soft gluon radiation 85

3.5 Contributions to the structure function to order $\bar{\alpha}_S^3$ 90

4.1 Elements for high energy factorization 103

4.2 Born level amplitude in high energy scattering 105

4.3 Amplitude for real gluon emission in the central region 106

4.4 Graphs for real gluon emission in the fragmentation region 108

4.5 Graphs contributing to the $gB \to ggB$ amplitude 109

4.6 Graphs contributing to the $gB \to q\bar{q}B$ amplitude 109

4.7 Non-contributing diagram at NLO for $gB \to q\bar{q}B$ 110

4.8 Amplitudes for three partons production with a pair produced in the forward-rapidity region 112

4.9 Amplitudes for four partons production with a pair produced in the central-rapidity region 112

5.1 Comparison between LO and NLO kernels at $\gamma = \frac{1}{2} + i\nu$ 118

6.1 Behaviour of the next-to-leading order kernel compared to the collinear improved ones 132

6.2 Dependence of the LO kernel plus veto upon ν for $\bar{\alpha}_s = 0.2$ 135

6.3 Dependence of the NLO kernel plus veto upon ν for $\bar{\alpha}_s = 0.2$ 135

6.4 Dependence of the LO kernel plus veto upon $\bar{\alpha}_s$ for $\nu = 0$ 136

6.5 Dependence of the NLO kernel plus veto upon $\bar{\alpha}_s$ for $\nu = 0$ 136

6.6 Dependence of the 'Scheme 3 plus veto' NLO kernel upon ν for $\bar{\alpha}_s = 0.2$ 138

6.7 Dependence of the 'Scheme 3 plus veto' NLO kernel upon $\bar{\alpha}_s$ for $\nu = 0$ 139

6.8 Dependence of the 'Scheme 4 plus veto' NLO kernel upon ν for $\bar{\alpha}_s = 0.2$ 139

6.9 Dependence of the 'Scheme 4 plus veto' NLO kernel upon $\bar{\alpha}_s$ for $\nu = 0$ 140

6.10 A suitable contour of integration for $k_1 > k_2$ 141

6.11 Value of the infinite sum and the truncated sum for $N = 5, 8, 11$ of Eq. 6.47 for y =4 142

6.12 Value of the infinite sum and the truncated sum for $N = 5, 8, 11$ of Eq. 6.47 for y =10 142

7.1 The four contours for the case $N = 1$ corresponding to the four different ways of "combing" the branch cuts. 152

7.2 $\tilde{\omega}(s,t)$ against t for $\ln s = 23$ 154

7.3 $\tilde{\omega}(s,t)$ against $\ln s$ for $t = 40$ 155

Abstract

UNIVERSITY OF MANCHESTER

ABSTRACT OF THESIS submitted by **Agustín Sabio Vera** for the Degree of Doctor of Philosophy and entitled **High Energy Scattering in Quantum Chromodynamics**

Month and Year of Submission: September 2000

The purpose of this thesis is to study the treatment of semihard processes within the Balitsky-Fadin-Kuraev-Lipatov (BFKL) formalism.

An introduction to the broad issue of perturbative Quantum Chromodynamics (QCD) is presented in the first chapter with special emphasis on the concepts of asymptotic freedom, factorization theorems and evolution equations for parton distributions in the high energy regime of small Bjorken x. The BFKL equation is sketched and the experimental processes where it can be tested are discussed.

The second chapter shows a diagrammatic derivation of the leading-order BFKL equation where terms of the form $(\alpha_s \ln 1/x)^n$ are resummed making use of the reggeization of the gluon and ladder exchanges. The solution for the case of forward scattering is explicitly derived.

In chapter 3 the phenomenon of QCD coherence is used to make physical predictions for gluon jet rates in deep inelastic scattering (DIS). An extensive introduction to coherence in Quantum Electrodynamics (QED) and QCD together with an analysis of the consequences of its application in the description of DIS final states is provided. The original work in this chapter has been published in [75] and [79].

The arrival of the BFKL next-to-leading order corrections resumming $\alpha_s(\alpha_s \ln 1/x)^n$ terms had a big impact in the scientific community. We sketch the derivation of these complicated corrections in chapter 4 where the NLO kernel is presented for the first time. Its analysis is deferred to chapter 5.

In chapter 5 we explain some of the serious complications which appeared when the analysis of these terms was first performed. The physical predictions taking them into account gave non-physical results setting confusion over the whole BFKL program. In simple terms we explain a possible way out in this situation by appealing to higher order terms in the perturbative expansion. The effect of these new corrections is to drastically improve the behaviour of the kernel.

In chapter 6 we set the question of self-consistency of this approach by suppressing gluon emissions which are nearby in rapidity in the parton cascade. We prove that the new scheme is consistent with multi-regge-kinematics (used to derive the BFKL equation) and we also show that the effect of the higher order corrections should be to reduce the importance of this region of the gluon phase space. This work has been published in [114].

In chapter 7 we describe a formalism to solve the BFKL equation with running coupling. We make the assumption that the QCD coupling stops running at a certain infrared scale and then show how the transition from the fixed coupling solution to the running coupling one takes place. This method has been accepted for publication in [119].

Finally, in chapter 8, we conclude with a summary of the main results of this thesis and indicate the directions for future research.

Declaration

No portion of the work referred to in this thesis has been submitted in support of an application for another degree or qualification of this or any other university or other institution of learning.

Copyright and Ownership of Intellectual Property Rights

Dedication

Dedicated to the memory of

José Rosique Cuenca

(1932-2000)

"...y ahora seremos una piña con Darío al frente"

Acknowledgements

These years in Manchester have been a fantastic experience. All the work in this thesis would have been impossible without the support of many people.

Having a family which helps you and believe in you as I have is a privilege. My deepest thanks go with all my love to my mum, Blanca Vera Flores (gracias por tantos esfuerzos y por creer en mí por encima de todo), to José Rosique Cuenca, who was like a father and sadly passed away this summer (nunca olvidaré cada consejo que me dió y sus ganas de vivir, gracias José) and to my brother Guillermo.

This year would not have been the same without the company, love and support of Sarah Louise Hill, a very especial person, thank you for so many lovely moments, especially the parchis/salsa ones!

It is not easy to find people like Jeff Forshaw, his wise advice, encouragement, support and, above everything, his friendship, have been fundamental in the completion of this work. I will never forget the summer in Annecy, the time at CERN, the climbing lessons and all the good moments working together in Manchester, thanks for all your help Jeff.

It has been a pleasure to work with Douglas Ross, his warm character and sense of humour makes you realize that it is possible to be a great physicist and laugh at it at the same time.

From my very first day in Manchester Sandy Donnachie has been a source of great support, encouragement and motivation. I tried to follow his advise, "the best way of making life interesting is keeping yourself busy"...

Special thanks go to Graham Shaw for his continuous support, Bryan Webber, Gavin Salam and Dimitri Colferai for their interest and help in my work, Martin McDermott and José Casado for so many conversations about physics and life, and Sasha Kvinikhidze for being such an especial character. Thanks also to Gail Bradbrook, Ioannis Michos, Marcelo De Francia and Stephane Pepin.

Thanks to all my fellow students at the department: Norman Evanson, Ross Davidson, Janis Gravelis, Scott Jones, George Kerley, Anahita New, Keith Richardson, Nikos Savvas and Adolfo Zamora, and to Sue Neesham and Joyce Smith who were absolutely perfect helping me in anything I needed during my time in Manchester.

It was a pleasure to share office with Nicholas Petropoulos, I am very proud of having such a good friend. He has always been close to me in the good and bad moments. I will never forget the Greek lessons and the "dental hospital"...

Thank you to my friends from "Owens Park" with whom I have had so many good moments: Francis K L Chan, Ali Fikirkoca, Julie Freeman, Inma Pérez Gómez and Kenneth K C Wong.

Thank you to my team mates at the University of Manchester and Chorlton Basketball Clubs, Eric Echangeat and Mark K Le-Goff, with whom I won the Greater Manchester League in the season 1999/2000.

Thank you to my friend in London, Antonio Filippi, for his help in the distance.

Thank you to Annabella Rauscher, especially for her warm welcome when I went to Heidelberg, and to Adrian Campbell-Smith and Gennaro Corcella with whom I shared office during my stay at CERN.

And very especial thanks to all my friends in Spain who did their best to keep in touch with me: Jorge Sánchez Solano, Gonzalo Violero, Carmen Blanco Gómez, Javier Rodriguez Pacheco, Belén Paredes Ariza and to my very best friend Luis Aznar García (gracias por no fallarme nunca Luis).

Finally I would like to thank the UK "Particle Physics and Astronomy Research Council" for financial support and the "CERN theoretical division" for my stay during the 1999 summer.

The Author

Agustín Sabio Vera graduated with a *Licenciatura en Física Teórica* from the *Universidad Autónoma de Madrid*. He also studied for a Mathematics degree and took postgraduate courses in Theoretical Physics at the same University. In September 1996 he took a year of postgraduate courses at the University of Manchester under the ERASMUS program. In September 1997 he started this thesis at the Department of Theoretical Physics of the University of Manchester.

> *"Io stimo più il trovare un vero, benchè di cosa leggiera, che disputare lungamente delle massime questioni senza conseguir verità nissuna."*
>
> *Galileo Galilei*

> *"You should realize what the universe is and what you are yourself. To know yourself is to know the universe."*
>
> *Morihei Ueshiba*

Chapter 1

Introduction

1.1 QCD

Quantum Chromodynamics (QCD) is nowadays well established as the correct theoretical framework to describe the strong interactions. At present energies it is probably the most complex component of the Standard Model because the asymptotic states detected at the experiments, hadrons, are different from the fundamental fields present in the Lagrangian, quarks and gluons. QCD evolves from a theory of free quarks and gluons at asymptotically small distances to a confining theory of hadrons at large distances. This theory is based on the $SU(3)$ colour gauge group. Historically the colour degree of freedom appeared as the solution to the problem of how to construct the wave function for the doubly charged Δ^{++} baryon. The spin of this baryon is $3/2$ and is obtained by combining three identical quarks in their ground state. The Δ^{++} wave function is then symmetric in space, spin and flavour ($SU(3)_f$) but, at the same time, as the quark constituents have half integral spin, the Fermi-Dirac statistics necessitates an anti-symmetric wave function. This conflict was solved by making the wave function totally antisymmetric in the colour degree of freedom. As coloured states are not detected in experiments it was required to add the extra constraint that only colour singlet states can exist in nature.

The idea of colour has been checked in many experiments involving high energy interactions of hadrons with hadrons, leptons with hadrons and leptons with leptons. The correct calculation of the rate for the decay $\pi^0 \to \gamma\gamma$ or the ratio of the e^+e^- hadronic total cross section to the cross section for the production of a muon pair were some of the early successes of the theory. The existence of point-like constituents inside the hadrons was clear after the deep inelastic scattering experiments carried out at SLAC. These constituents were named as *partons* and today we identify them as quarks and gluons.

In this introduction we wish to recall the key concepts for the success of QCD as the theory of the strong interaction. A crucial result is that of *asymptotic freedom*. We will devote the next few lines to explain this very important concept in the successful phenomenology of QCD.

1.1.1 Asymptotic freedom

Let us first introduce the expression for the Lagrangian in Quantum Chromodynamics, it can be written as

$$\mathcal{L} = \bar{\psi} i \partial\!\!\!/ \psi - \frac{1}{4} F^a_{\mu\nu} F^{\mu\nu}_a + g \bar{\psi} A\!\!\!/ \psi + \mathcal{L}_{\text{gauge fixing}} + \mathcal{L}_{\text{ghost}}. \tag{1.1}$$

For simplicity we have considered massless quarks. The fields for quarks and gluons are represented by ψ and A respectively. $F^a_{\mu\nu}$ is the field strength tensor derived from the gluon field

$$F^a_{\mu\nu} = \partial_\mu A^a_\nu - \partial_\nu A^a_\mu - g f^{abc} A^b_\mu A^c_\nu, \tag{1.2}$$

where $a = 1, ..., N_c^2 - 1$ is the colour index indicating the number of gluons, f^{abc} are the $SU(N_c)$ group structure constants and N_c is the number of colours in the theory. For our purposes in this section we do not need to discuss the gauge fixing part of the Lagrangian or the part corresponding to ghost degrees of freedom, unphysical scalars with Fermi-Dirac statistics, needed to cancel the contributions of non-transverse degrees of freedom which arise when working in non-physical gauges.

If we apply the Feynman rules to this Lagrangian as it stands to calculate an observable we will get ill-defined results due to the presence of infinities better known as *ultraviolet* divergences. They typically arise when one of the momenta in the loop integrals goes to infinity. An alternative to deal with these divergences would be to introduce a momentum cutoff to regularize the infinite integrals and then absorb the divergent terms into a redefinition of fields or parameters. This is known as the *renormalization* procedure. The final results should not depend on the regularization prescription.

It is more convenient to regularize the integrals analytically continuing them in the number of space-time dimensions from 4 to $D = 4 - 2\epsilon$. This transforms the divergent parts of the integrals into poles in ϵ which can be removed on introducing a subtraction scale μ^2 usually referred to as the *renormalization scale*. After regulating the divergences they can be eliminated by adding counterterms to the Lagrangian [1]. These new terms can be interpreted as a renormalization of the strong coupling and the quark and gluon wave functions.

We could apply this method only to the divergent integrals but it is easier if we transform the dimension of the whole theory. The dimension of the Lagrangian is $4-2\epsilon$, the quark field has $3/2-\epsilon$, the gluon $1-\epsilon$ and the coupling is ϵ dimensional. The introduction of the counterterms can be done by replacing the bare fields and coupling with the renormalized ones

$$\begin{aligned} \psi_{\text{bare}} &= Z_2^{\frac{1}{2}}\psi_{\text{R}}, \\ A^\mu_{\text{bare}} &= Z_3^{\frac{1}{2}}A^\mu_{\text{R}}, \\ g_{\text{bare}} &= Z_{\text{g}}\mu^\epsilon g_{\text{R}}. \end{aligned} \tag{1.3}$$

The renormalization scale μ has been introduced to make the renormalized coupling g_{R} explicitly dimensionless. Making the substitutions

$$\begin{aligned} Z_1 &= Z_{\text{g}}Z_2Z_3^{\frac{1}{2}}, \\ Z_{\text{n}} &= 1+\delta_{\text{n}}, \end{aligned} \tag{1.4}$$

the Lagrangian in terms of the renormalized quantities reads *

$$\mathcal{L} = \bar{\psi}i\partial\!\!\!/\psi - \frac{1}{4}F^a_{\mu\nu}F^{\mu\nu}_a + \mu^\epsilon g\bar{\psi}A\!\!\!/\psi + \delta_2\bar{\psi}i\partial\!\!\!/\psi - \frac{1}{4}\delta_3F^a_{\mu\nu}F^{\mu\nu}_a + \delta_1\mu^\epsilon g\bar{\psi}A\!\!\!/\psi. \tag{1.5}$$

The counterterms can be chosen such that the one loop Green's functions in the theory are finite. The counterterms needed in the general case when we include the ghost fields can be fixed using local gauge invariance in such a way that all the divergent amplitudes of the theory are eliminated leaving a renormalizable and therefore a finite predictive theory. The one loop order is especially simple and here we are only interested in the renormalization of the strong coupling constant so we focus on Z_{g} which is

$$Z_{\text{g}} = \frac{Z_1}{Z_2Z_3^{\frac{1}{2}}} = 1 - \frac{b\alpha_s}{2\epsilon}, \tag{1.6}$$

*We drop the index R, from now on all fields and couplings in $\mathcal{L}$ are renormalized.

with b defined as

$$b \equiv \frac{1}{2\pi}\left[\frac{11}{6}C_{\rm A} - \frac{2}{3}n_f T_{\rm F}\right]. \tag{1.7}$$

n_f is the number of quark flavours and α_s is the notation for $g^2/4\pi$. $C_{\rm A} = N_{\rm c}$ and $T_{\rm F} = 1/2$ are Casimir operators, i.e. they commute with all the generators of the $SU(N_{\rm c})$ group.

It is important to realize that bare quantities should be independent of the renormalization scale μ. In particular, for the coupling we can write

$$\frac{dg_{\rm bare}}{d\mu} = \frac{d}{d\mu}(Z_{\rm g}\mu^{\epsilon}g) = 0. \tag{1.8}$$

From Eq. 1.6 we know that $Z_{\rm g}$ depends on μ through α_s, therefore, squaring g and differentiating with respect to μ^2 we obtain

$$\mu^2\frac{d\alpha_s}{d\mu^2}\left(1 + 2\alpha_s\frac{1}{Z_{\rm g}}\frac{dZ_{\rm g}}{d\alpha_s}\right) + \epsilon\alpha_s = 0. \tag{1.9}$$

Expanding in powers of α_s we obtain

$$\mu^2\frac{d\alpha_s}{d\mu^2} \simeq -\epsilon\alpha_s(2\epsilon - \alpha_s)\left(\frac{1}{2\epsilon} + \frac{3}{4}\frac{b}{\epsilon^2}\alpha_s\right) \simeq -b\alpha_s^2. \tag{1.10}$$

This equation can be easily solved

$$\alpha_s^{-1}(\mu^2) = b\ln\mu^2 + \mathcal{C}, \tag{1.11}$$

the constant $\mathcal{C}$ can be fixed by introducing the scale Λ defined as the scale where the coupling goes to infinity, i.e.

$$\alpha_s(\mu^2) = \frac{1}{b\ln\frac{\mu^2}{\Lambda^2}}. \tag{1.12}$$

This result is known as the *running of the coupling* and in QCD it indicates that quarks and gluons can be considered as *asymptotically free* fields at very small distances because there the coupling between them tends to zero. It is crucial that the constant b is positive. This is different to QED where it has a negative sign and is a direct consequence of the fact that gluons carry colour charge and can interact among themselves.

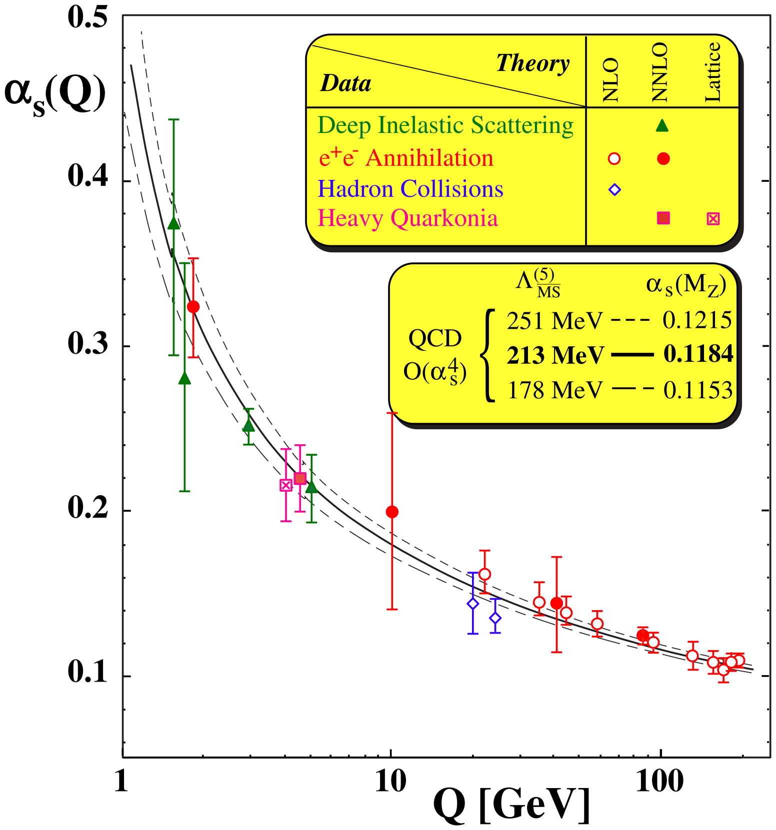

Figure 1.1: Experimental tests of the QCD running coupling

The running of the strong coupling has been tested in many experiments as is shown in Fig 1.1. The present world average for the coupling at the Z^0 mass is

$$\alpha_s(\mathrm{M_Z}) = 0.118 \pm 0.002, \tag{1.13}$$

implying that

$$\Lambda^{\overline{\mathrm{MS}}}_{\mathrm{QCD}} = 208^{+25}_{-23} \text{ MeV}, \tag{1.14}$$

for five active flavours [2]. For an extensive review of various determinations of α_s we refer the reader to [3].

The fact that the coupling is very small at large momentum scales is the starting point for perturbative QCD. We will show now how predictions for physical observables can be made using perturbative expansions in powers of α_s.

1.1.2 Factorization

There are a few observables, like jet cross sections in e^+e^- annihilation or the total width of the Z boson, which can be calculated directly in perturbation theory because they are free of nonperturbative dependence (modulo terms suppressed by powers of energy).

Unfortunately there are not many cross sections of this type and the predictions for processes like, for example, hard-scattering cross sections with hadrons in the initial state are more complicated to calculate. Nevertheless in some cases we can still apply the so called *QCD factorization theorems* [4] to express the cross section under study as a convolution of an infrared finite cross section for a short distance process which is calculable in perturbative theory, with a nonperturbative function which is universal to many different processes but non-calculable from first principles in perturbation theory. The separation between low momentum and high momentum physics is done at an arbitrary factorization scale μ_{F}. This is possible because the scattering process can be characterised by two time scales. A short time scale, of order of the largest momentum in the scattering Q which defines the hard scattering and is calculable in perturbation theory, and a long time scale, of the order of the hadron size which includes the binding and recombination of the constituents and, therefore, of nonperturbative origin.

For example, in deep inelastic scattering (DIS) schematically we can write

$$\sigma(Q^2, m^2)_{\mathrm{measurable}} = \hat{\sigma}\left(\alpha_s(\mu_{\mathrm{F}}^2), \frac{Q^2}{\mu_{\mathrm{F}}^2}\right)_{\mathrm{perturbative}} \otimes f(\mu_{\mathrm{F}}^2, m^2)_{\mathrm{non-perturbative}}, \qquad (1.15)$$

where μ_{F} defines the limit between the short-distance dynamics, present in $\hat{\sigma}(\frac{Q^2}{\mu_{\mathrm{F}}^2})$, and the long-distance dynamics at the scale of the parameter m, included in $f(\mu_{\mathrm{F}}^2, m^2)$. The convolution $\otimes$ is expressed in terms of the fractional momentum of the parton which gives origin to the scattering and includes a sum over all types of partons.

The variable μ_{F} is only constrained by the fact that we need a small parameter in the perturbative expansion, this role is played by the coupling constant, $\alpha_s(\mu_{\mathrm{F}}^2) \ll 1$, and therefore the factorization scale must be hard, i.e. $\mu_{\mathrm{F}}^2 \gg \Lambda_{\mathrm{QCD}}^2$. With this we ensure that the expansion

$$\hat{\sigma}\left(\alpha_s(\mu_{\mathrm{F}}^2), \frac{Q^2}{\mu_{\mathrm{F}}^2}\right) = \sum_n \alpha_s^n(\mu_{\mathrm{F}}^2)\ \mathcal{C}_n\left(\frac{Q^2}{\mu_{\mathrm{F}}^2}\right) \tag{1.16}$$

makes sense. As μ_{F} is an artificial variable the physical observables should be independent of it. This allow us to find the evolution of $f(\mu_{\mathrm{F}}^2, m^2)$ with the scale μ_{F} setting the ground for building the so called *evolution equations*. In order to introduce this subject in the next section we explain the concept of *renormalization scale invariance* needed to understand the perturbative calculation of hard cross sections.

1.1.3 Renormalization scale invariance

As the coupling is not an observable it can depend on the renormalization scale μ, Eq. 1.12. This is not the case for a general observable which can be calculated in QCD perturbation theory in terms of the renormalized coupling constant $\alpha_s(\mu)$ [5], i.e.

$$\mathcal{R}[\alpha_s(\mu^2), \frac{Q^2}{\mu^2}] = \sum_{n=0}^{\infty} \alpha_s^n(\mu^2)\ \mathcal{C}_n(\frac{Q^2}{\mu^2}). \tag{1.17}$$

The structure of the functions $\mathcal{C}_n$ is not arbitrary because it is determined by the renormalization scale invariance

$$\mu^2\frac{d\mathcal{R}}{d\mu^2} = \left[\mu^2\frac{\partial}{\partial\mu^2} + \mu^2\frac{d\alpha_s}{d\mu^2}\frac{\partial}{\partial\alpha_s}\right]\mathcal{R}[\alpha_s(\mu^2), \frac{Q^2}{\mu^2}] = 0. \tag{1.18}$$

Let us work to order α_s^2 in this section. The results can be generalized to any power in the coupling. The differential equation Eq. 1.18 can be written as

$$\begin{aligned}\left[\mu^2\frac{\partial}{\partial\mu^2} - b\alpha_s^2\frac{\partial}{\partial\alpha_s}\right]\left(1 + \alpha_s\mathcal{C}_1(\frac{Q^2}{\mu^2}) + \alpha_s^2\mathcal{C}_2(\frac{Q^2}{\mu^2}) + \cdots\right) \simeq \\ \alpha_s\left(\mu^2\frac{\partial}{\partial\mu^2}\mathcal{C}_1\right) + \alpha_s^2\left(\mu^2\frac{\partial}{\partial\mu^2}\mathcal{C}_2 - b\ \mathcal{C}_1\right) + \cdots = 0.\end{aligned} \tag{1.19}$$

This implies that

$$\frac{\partial}{\partial\mu^2}\mathcal{C}_1 = 0, \tag{1.20}$$

therefore $\mathcal{C}_1$ is equal to a constant $\mathcal{A}_1$. At second order we have

$$\mu^2\frac{\partial}{\partial\mu^2}\mathcal{C}_2(\frac{Q^2}{\mu^2}) - b\ \mathcal{A}_1 = 0, \tag{1.21}$$

giving a result up to an integration constant, $\mathcal{A}_2$, which reads

$$\mathcal{C}_2(\frac{Q^2}{\mu^2}) = b\mathcal{A}_1 \ln \frac{\mu^2}{Q^2} + \mathcal{A}_2. \tag{1.22}$$

Consequently the observable R at order α_s^2 can be written as

$$\mathcal{R}[\alpha_s(\mu^2), \frac{Q^2}{\mu^2}] = 1 + \alpha_s(\mu^2)\mathcal{A}_1 + \alpha_s^2(\mu^2)\mathcal{A}_1 b \ln \frac{\mu^2}{Q^2} + \alpha_s^2(\mu^2)\mathcal{A}_2 + \cdots. \tag{1.23}$$

It is very interesting that we can obtain the coefficient of the two loops logarithm without having to calculate the whole two loop calculation. Although the coupling is small it can be compensated by large logarithms when the scale Q^2 is very large. To make a correct physical prediction in this limit we should be able to resum all these logarithms to all orders. The general term for $n > 0$ in the expansion of Eq. 1.17 is

$$\mathcal{C}_n(\frac{Q^2}{\mu^2}) = \mathcal{A}_1 \left(b \ln \frac{\mu^2}{Q^2}\right)^{n-1} + \cdots. \tag{1.24}$$

Therefore we can write the observable R with the explicit expansion

$$\begin{aligned} \mathcal{R}[\alpha_s(\mu^2), \frac{Q^2}{\mu^2}] &= 1 + \mathcal{A}_1\alpha_s(\mu^2) \sum_{n=1}^{\infty} \left(b\alpha_s(\mu^2) \ln \frac{\mu^2}{Q^2}\right)^{n-1} + \mathcal{A}_2\alpha_s^2(\mu^2) + \cdots \\ &= 1 + \mathcal{A}_1 \frac{\alpha_s(\mu^2)}{1 - b\alpha_s(\mu^2) \ln \frac{\mu^2}{Q^2}} + \mathcal{A}_2\alpha_s^2(\mu^2) + \cdots. \end{aligned} \tag{1.25}$$

This result is revealing because we can introduce the parameter Λ of expression 1.12 and write

$$\frac{\alpha_s(\mu^2)}{1 - b\alpha_s(\mu^2) \ln \frac{\mu^2}{Q^2}} = \frac{1}{\alpha_s^{-1}(\mu^2) - b \ln \frac{\mu^2}{Q^2}} = \frac{1}{b \ln \frac{Q^2}{\Lambda^2}} = \alpha_s(Q^2). \tag{1.26}$$

Hence

$$\mathcal{R}[\alpha_s(\mu^2), \frac{Q^2}{\mu^2}] = 1 + \mathcal{A}_1\alpha_s(Q^2) + \mathcal{A}_2\alpha_s^2(\mu^2) + \cdots \tag{1.27}$$

which can be extended to higher order terms so that

$$\mathcal{R}[\alpha_s(\mu^2), \frac{Q^2}{\mu^2}] = 1 + \mathcal{A}_1\alpha_s(Q^2) + \mathcal{A}_2\alpha_s^2(Q^2) + \mathcal{A}_3\alpha_s^3(Q^2) + \cdots \tag{1.28}$$

and all the higher order terms can be resummed by setting the scale of the coupling to Q^2. The coefficients $\mathcal{A}_n$ have to be determined for each different observable through an explicit calculation and now the truncation at a given order n is reliable because the higher order terms are not larger than the leading order ones.

1.2 Deep inelastic scattering

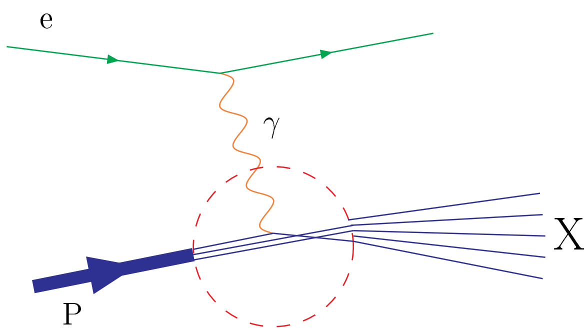

Figure 1.2: Electron-proton deep inelastic scattering

In deep inelastic electron-proton scattering $ep \to eX$ the proton is broken into hadrons due to the exchange of a very energetic virtual photon or Z^0 with large transverse momentum squared, Fig. 1.2. In this context we can apply the so called *impulse approximation* [6]. In the electron-proton centre-of-mass frame the proton momentum, $\vec{P}$, is large for high energy collisions, the momentum for the incoming electron is $(|\vec{P}|, -\vec{P})$ and the exchanged boson has $(q^0, \vec{q})$. We can consider that the proton fluctuates into a virtual state with two components: a parton with momentum $x\vec{P}$ and mass m_1, and a group of partons with total momentum $(1-x)\vec{P}$ and invariant mass m_2. In this case the difference in energy between the virtual state and the proton, ΔE, is

$$\begin{aligned} \Delta E &= \sqrt{x^2\vec{P}^2 + m_1^2} + \sqrt{(1-x)^2\vec{P}^2 + m_2^2} - \sqrt{\vec{P}^2 + M_{\text{proton}}^2} \\ &\simeq \frac{1}{|\vec{P}|}\left[\frac{m_1^2}{2x} + \frac{m_2^2}{2(1-x)} - \frac{M_{\text{proton}}^2}{2}\right]. \end{aligned} \tag{1.29}$$

The inverse of this quantity, using the uncertainty principle, gives the lifetime of the virtual state, i.e. $\tau_{\text{virtual}} \sim 1/\Delta E$. Similarly, the duration of the scattering of the boson with the proton is $\tau_{\text{collision}} \sim 1/q^0$. We can use the expression

$$q^0 = \frac{2P\cdot q + q^2}{2(\sqrt{\vec{P}^2 + M_{\text{proton}}^2} + |\vec{P}|)} \sim \frac{2M_{\text{proton}}\nu - Q^2}{4|\vec{P}|}, \tag{1.30}$$

where we have made use of the standard notation for the Lorentz invariants

$$\begin{aligned} Q^2 &\equiv -q^2, \\ \nu &\equiv \frac{P\cdot q}{M_{\text{proton}}}, \end{aligned} \tag{1.31}$$

and of the mass shell condition for the final electron (considering its mass to be zero). The impulse approximation means that we can treat the partons as free during the collision if the ratio of the time scales

$$\frac{\tau_{\text{collision}}}{\tau_{\text{virtual}}} \sim 2\frac{\frac{m_1^2}{x} + \frac{m_2^2}{(1-x)} - M_{\text{proton}}^2}{2M_{\text{proton}}\nu - Q^2} \tag{1.32}$$

is small. In deep inelastic scattering both $2M_{\text{proton}}\nu$ and Q^2 are larger than M_{proton}^2 so the approximation is correct provided we assume that x is not too close to 0 or 1. Processes where soft partons are important are not properly described by this simple picture, known as the *naive parton model*.

We can think of the proton as moving with very high momentum P. In this frame the proton is Lorentz contracted in the longitudinal direction by a factor M/P with respect to its size in the rest frame. Those partons which do not have small x are also Lorentz contracted and therefore distributed on the disk defined by the proton transverse area, in this disk the number of partons per unit of rapidity (see expression 1.100) is small. The situation for partons with very small values of x, known as *wee partons*, is different because they are not confined to the disk. Their longitudinal size can be estimated using the uncertainty principle

$$\Delta z \simeq \frac{1}{xP}. \tag{1.33}$$

In the following we define some of the quantities which allow us to obtain experimental information about these partons.

The general structure of the inclusive spin-averaged cross section in deep inelastic lepton-hadron scattering can be expressed in terms of two gauge invariant functions which characterize the structure of the target, they are known as the F_1 and F_2 *structure functions*. For charged lepton scattering the scattering is mediated by the exchange of a virtual photon and in the limit when $Q^2 \ll M_Z^2$ we can write

$$\frac{d^2\sigma^{lh}}{dxdQ^2} = \frac{4\pi\alpha^2}{xQ^4}\left[xy^2F_1(x,Q^2) + (1-y)F_2(x,Q^2)\right], \tag{1.34}$$

where we have neglected the mass of the proton. α is the electromagnetic coupling constant and y is the inelasticity because in the rest frame of the target proton it can be written as $y = 1 - E'/E$ with $E,\ E'$ being the initial and final electron energies, respectively. We give now a discussion of these structure functions in perturbation theory.

1.2.1 The Altarelli-Parisi evolution equations

In the following we would like to show how to obtain predictions for the DIS structure functions within QCD. We will explicitly calculate the contributions to each order in the coupling coming from the relevant Feynman diagrams.

At leading order the only contributing process is $\gamma^* q \to q'$ and the form of the structure functions is

$$2F_1(x,Q^2) = \frac{1}{x}F_2(x,Q^2) = \sum_q e_q^2 \int d\omega\ q(\omega)\delta(x-\omega) = \sum_q e_q^2 q(x), \tag{1.35}$$

where ω is the momentum fraction carried by the struck parton and $q(\omega)$ is a bare quark distribution. At this order we can see that the structure functions depend only on x, this fact is known as *Bjorken scaling* and we show it in Fig. 1.3. The relation between both structure functions is the *Callan-Gross relation*.

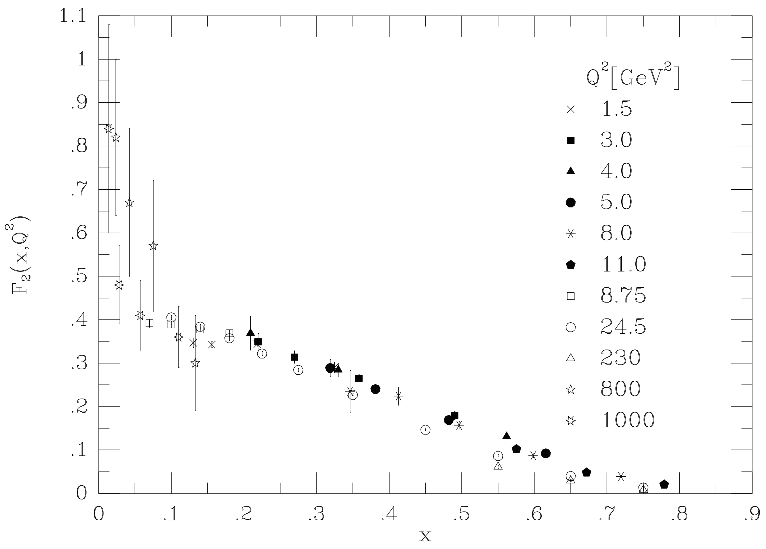

Figure 1.3: Scaling of the F_2 structure function [14]

We will explain now how the presence of gluon radiation determines the pattern of violation of Bjorken scaling. The next order includes gluon emission, $\gamma^*(q)+q(p) \rightarrow q(p')+g(k)$, see Fig. 1.4, and therefore now we must consider the gluon coupling, g_s, its polarization and the $SU(3)$ colour factors. As we will see, when extracting the

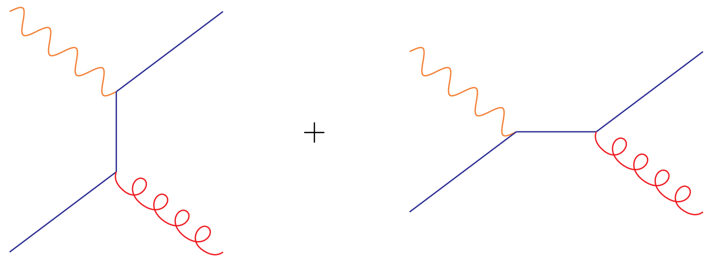

Figure 1.4: Gluon radiation in photon-quark interaction

structure functions from the hadronic vertex a Q^2 dependence is found and it is more convenient to work in terms of the Q^2 dependent parton densities $q(\omega, Q^2)$:

$$\frac{1}{x}F_2(x,Q^2) \equiv \sum_q e_q^2 q(x,Q^2). \tag{1.36}$$

From now on F_2 is no longer equal to $2xF_1$ and we will be interested only in the former. Its expression taking into account the graphs in Fig. 1.4 can be found to be

$$\frac{1}{x}F_2(x,Q^2) = \sum_q \frac{e_q^2\alpha_s}{2\pi}\int_x^1 \frac{dz}{z} q\left(\frac{x}{z}\right)\int_0^{\frac{Q^2}{z}} d(-\hat{t})\frac{4}{3}\left[\frac{1}{-\hat{t}}\frac{1+z^2}{1-z} - \frac{z^2(\hat{t}+2Q^2)}{(1-z)Q^4}\right]. \tag{1.37}$$

We have introduced the variable z as

$$z = \frac{x}{\omega} = \frac{Q^2}{2p\cdot q} = \frac{Q^2}{\hat{s}+Q^2} \tag{1.38}$$

where variables with a hat indicate that we are considering a process at the partonic level and x is the usual Bjorken variable.

It is important to note that this expression has several singularities. There is an *infrared soft singularity* at $z=1$ which corresponds to the limit

$$\hat{s} = Q^2\frac{1-z}{z} = 0 \tag{1.39}$$

at the physical threshold with emitted gluon momentum $k = 0$. These types of singularities emerge in theories which contain a massless gauge field like the photon in QED or the gluon in QCD. It will cancel when considering contributions from one loop vertex corrections, for the time being we regularize it with a cut off at $z_{\text{soft}} < 1$. The other singularity corresponds to a so called *mass* or *collinear singularity* at $\hat{t} = 0$ corresponding to the incident quark emitting a collinear gluon while itself stays on mass shell. These divergences take place when a massless field couples to other massless fields, like in the case of massless quarks in QCD, or with itself, as is the case of the gluons in QCD through the trilinear and quadrilinear gluon couplings †. We will regularize them with another cut off at $\hat{t} = -\mu^2_{\text{coll}}$ which will be absorbed later into the definition of the bare quark distribution. With all this in mind and keeping only the leading logarithms $\ln Q^2/\mu^2_{\text{coll}}$ we obtain the following expression for the structure function F_2

$$\frac{1}{x}F_2(x, Q^2) = \sum_q \frac{e_q^2 \alpha_s}{2\pi} \int_x^{z_{\text{soft}}} \frac{dz}{z} q\left(\frac{x}{z}\right) P_{qq}(z) \ln\left(\frac{Q^2}{\mu^2_{\text{coll}}}\right). \tag{1.40}$$

In the integrand there are, in general, also non-logarithmic terms which can be shifted by $P_{qq}(z) \ln(\mu^2/\mu^2_{\text{coll}})$ if we change the collinear cutoff to a different scale μ. At large Q^2 the effect of these terms is suppressed. We make use of this freedom in the choice of scale and define μ as the renormalization scale at which the coupling is defined, i.e. the Eq. 1.40 will be

$$\frac{1}{x}F_2(x, Q^2) = \sum_q \frac{e_q^2 \alpha_s(\mu^2)}{2\pi} \int_x^{z_{\text{soft}}} \frac{dz}{z} q\left(\frac{x}{z}\right) P_{qq}(z) \ln\left(\frac{Q^2}{\mu^2}\right). \tag{1.41}$$

We have introduced a function P_{qq} which is known as the *quark-quark splitting function* with a value

$$P_{qq}(z) = \frac{4}{3}\left(\frac{1+z^2}{1-z}\right). \tag{1.42}$$

†Soft and collinear singularities are generally called infrared divergences. In any observed process there is emission of an indefinite number of soft photons or gluons. Experimentally the final state of a charged particle cannot be completely specified because there are soft photons impossible to detect. In QED the Bloch-Nordsieck [7] theorem ensures that the infrared divergences cancel out after summation over all possible final states compatible with experimental detection. In QCD the situation is more complicated due to the effect of the three gluon vertex. Nevertheless the Kinoshita-Lee-Nauenberg theorem [8, 9] ensures the lack of infrared divergences after summation over initial and final degenerate states.

This function is independent of the regularization prescription and universal for different processes where a quark turns into a quark with radiation of a gluon.

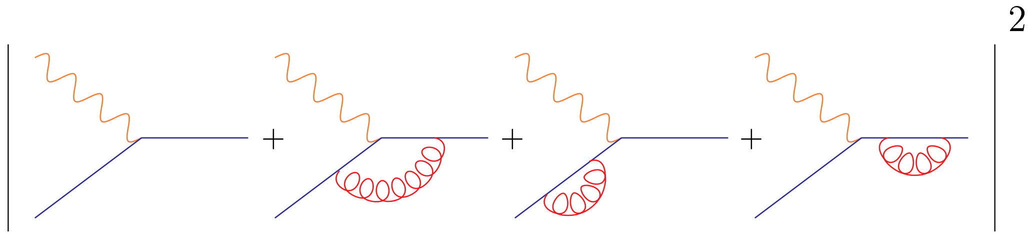

Figure 1.5: Contributions to F_2 from vertex diagrams and external wave function renormalization

The cancellation of soft divergences can be realized using dimensional regularization (see Section 1.1.1), originally introduced by 't Hooft and Veltman, where Feynman diagrams are calculated in $4-2\epsilon$ dimensions and the singularities are extracted as poles in ϵ. It is mandatory to introduce the interference of the lowest order vertex with the virtual gluon vertex diagram and the external quark wave function renormalizations, Fig. 1.5. The sum of the Born term and the virtual gluon contributions reads

$$\frac{1}{x}F_2(x,Q^2) = \tag{1.43}$$
$$\sum_q e_q^2 \int_x^1 \frac{dz}{z} q\left(\frac{x}{z}\right)\left\{\delta(1-z) + \frac{\alpha_s(\mu^2)}{2\pi}P_{qq}(z)\left[\ln\left(\frac{Q^2}{\mu^2}\right) - \frac{1}{\epsilon}\right] + \alpha_s(\mu^2)f(z)\right\}.$$

Finite non-leading logarithmic terms have been included in the function $f(z)$. Soft singularities have been cancelled by the virtual corrections with the only consequence that the splitting function has been modified to remove its original singularity, i.e.

$$P_{qq}(z) = \frac{4}{3}\frac{1+z^2}{(1-z)_+} + 2\delta(1-z), \tag{1.44}$$

where the + plus prescription means that

$$\int_0^1 dz \frac{g(z)}{(1-z)_+} \equiv \int_0^1 dz \frac{g(z)-g(1)}{1-z}. \tag{1.45}$$

The remaining singularities are all collinear and show up in the ϵ^{-1} term. We can now proceed to absorb these collinear singularities in a redefinition of the bare quark distribution as

$$q_{\mathcal{R}}(x) \equiv q(x) + \int_x^1 \frac{dz}{z} q\left(\frac{x}{z}\right) \left[\alpha_s(\mu^2) f(z) - \frac{\alpha_s(\mu^2)}{2\pi} P_{qq}(z) \frac{1}{\epsilon}\right]. \tag{1.46}$$

From now on we will use $q_{\mathcal{R}}$ but, for convenience, we will keep the notation q.

Finally, combining the results obtained so far we have the following expression for the structure function F_2

$$\frac{1}{x} F_2(x, Q^2) = \sum_q e_q^2 \int \frac{d\omega}{\omega} q(\omega) \left[\delta\left(1 - \frac{x}{\omega}\right) + \frac{\alpha_s(\mu^2)}{2\pi} P_{qq}\left(\frac{x}{\omega}\right) \ln\left(\frac{Q^2}{\mu^2}\right)\right]. \tag{1.47}$$

This expression suggests the redefinition of the quark density at high Q^2 as

$$\frac{1}{x} F_2(x, Q^2) = \sum_q e_q^2 q(x, Q^2) = \sum_q e_q^2 [q(x) + \delta q(x, Q^2)], \tag{1.48}$$

with

$$\delta q(x, Q^2) = \frac{\alpha_s(\mu^2)}{2\pi} \ln\left(\frac{Q^2}{\mu^2}\right) \int \frac{d\omega}{\omega} q(\omega) P_{qq}\left(\frac{x}{\omega}\right). \tag{1.49}$$

The effect of higher orders in the expansion will give us the resummation of terms of order $\sim [\alpha_s(\mu) \ln Q^2/\mu^2]^n$ which are the relevant ones at high Q^2 (see Section 1.1.3). This resummation can be done in the form of a differential equation derived from Eq. 1.49

$$\frac{\partial q(x, Q^2)}{\partial \ln Q^2} = \frac{\alpha_s(\mu^2)}{2\pi} \int_x^1 \frac{d\omega}{\omega} q(\omega, Q^2) P_{qq}\left(\frac{x}{\omega}\right) + \mathcal{O}(\alpha_s^2(\mu^2) \ln Q^2). \tag{1.50}$$

This takes into account the *ladder diagrams* of Fig. 1.6 resumming the contributions to the quark distribution coming from the emission of n collinear gluons.

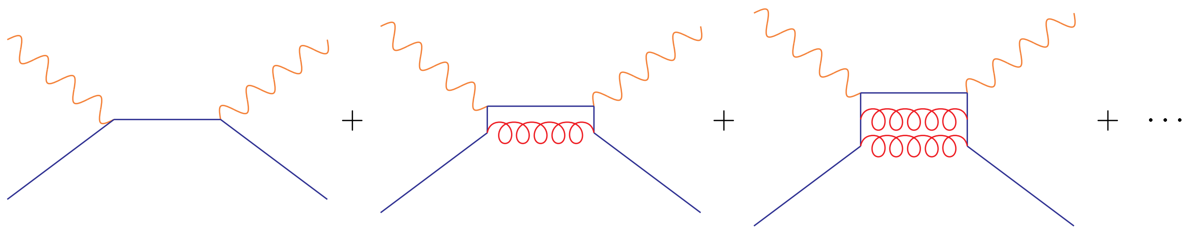

Figure 1.6: Quark-quark ladder diagrams

So far we have used the coupling at a fixed renormalization scale μ^2. From now on we will use $\alpha_s(Q^2)$ which is the correct one when we add the leading log contributions from vertex and propagator insertions in the ladder graphs (see Section 1.1.3). Therefore, for high Q^2, we get

$$\frac{\partial q(x,Q^2)}{\partial \ln Q^2} = \frac{\alpha_s(Q^2)}{2\pi}\int_x^1 \frac{d\omega}{\omega} q(\omega,Q^2) P_{qq}\left(\frac{x}{\omega}\right). \tag{1.51}$$

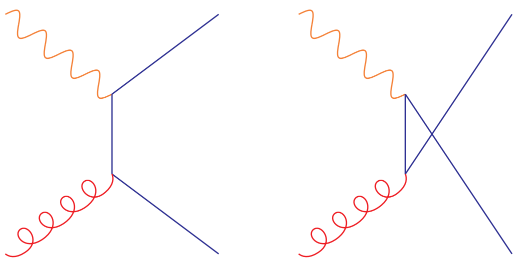

Figure 1.7: Struck quark coming from a gluon parent

This evolution equation considers the case when the photon is absorbed by a quark coming from a quark parent with momentum fraction $\omega > x$. To include the possibility of this quark having its origin in a gluon we consider graphs as Fig. 1.7. The corresponding gluon-quark splitting function is

$$P_{qg} = \frac{1}{2}[z^2 + (1-z)^2]. \tag{1.52}$$

The quark evolution then becomes

$$\frac{\partial q_i(x,Q^2)}{\partial \ln Q^2} = \frac{\alpha_s(Q^2)}{2\pi}\int_x^1 \frac{d\omega}{\omega}\left[q_i(\omega,Q^2)P_{qq}\left(\frac{x}{\omega}\right) + g(\omega,Q^2)P_{qg}\left(\frac{x}{\omega}\right)\right], \tag{1.53}$$

where a ϵ^{-1} collinear singularity has been absorbed into the bare gluon distribution as in the quark case. This evolution is valid for any massless quark and antiquark q_i.

The final component of the so called Dokshitzer-Gribov-Lipatov-Altarelli -Parisi (DGLAP) [10, 11, 12, 13] equations includes corresponding physics for the gluon distribution and reads

$$\frac{\partial g(x,Q^2)}{\partial \ln Q^2} = \frac{\alpha_s(Q^2)}{2\pi}\int_x^1 \frac{d\omega}{\omega}\left[\sum_i q_i(\omega,Q^2)P_{gq}\left(\frac{x}{\omega}\right) + g(\omega,Q^2)P_{gg}\left(\frac{x}{\omega}\right)\right], \tag{1.54}$$

with the sum running for quarks and antiquarks and the quark-gluon and gluon-gluon splitting functions being

$$
\begin{aligned}
P_{gq}(z) &= \frac{4}{3}\frac{1+(1-z)^2}{z}, \\
P_{gg}(z) &= 6\left[\frac{z}{(1-z)_+} + \frac{1-z}{z} + z(1-z) + \left(\frac{11}{12} - \frac{n_f}{18}\right)\delta(1-z)\right], \qquad (1.55)
\end{aligned}
$$

where n_f is the number of quark flavours.

The derivation shown in this section is the one for leading order DGLAP. The splitting functions can be obtained as a perturbative expansion in α_s ‡

$$P_{ab}(x, Q^2) = P_{ab}^{\mathrm{LO}}(x) + \alpha_s(Q^2) P_{ab}^{\mathrm{NLO}}(x) + \cdots . \qquad (1.56)$$

The truncation after the first two terms defines the next to leading order DGLAP evolution. Beyond leading order (LO) the splitting functions depend on the factorization scale and the definition of the parton distributions is no longer unique. At next-to-leading order (NLO) the Callan-Gross relation does not hold and we can define the so called longitudinal structure function

$$F_L(x, Q^2) = \left(1 + \frac{4M^2x^2}{Q^2}\right) F_2(x, Q^2) - 2xF_1(x, Q^2), \qquad (1.57)$$

with M being the mass of the proton. F_L equals the difference $F_2 - 2xF_1$ when $Q^2 \to \infty$. The fact that $F_L \ll F_2$ is a confirmation of the spin-$\frac{1}{2}$ property of quarks.

1.2.2 Solution to the DGLAP equations

Now we would like to solve the set of coupled equations 1.53-1.54. If we can achieve this we will know how the parton distributions change with Q^2 provided we know their value at some starting point Q_0^2 large enough to make perturbation theory reliable, i.e. $Q_0^2 >> \Lambda^2$, the Landau pole for QCD. Recall the meaning of this scale (see Eq. 1.12):

$$\alpha_s(Q^2) = \frac{1}{b \ln \frac{Q^2}{\Lambda^2}} \equiv \frac{1}{bt}. \qquad (1.58)$$

‡This expansion is the realization of the Eq. 1.28 in the case of electron-proton cross sections when folded into the evolution equations 1.53-1.54.

We have introduced t as the variable to use instead of Q and b is given in Eq. 1.7 so that, with the further notation

$$P_{qq} \otimes q_i \equiv \int_x^1 \frac{d\omega}{\omega} P_{qq}\left(\frac{x}{\omega}\right) q_i(\omega, t), \tag{1.59}$$

the DGLAP equations look like

$$\begin{aligned} \frac{dq_i(x,t)}{dt} &= \frac{\alpha_s(t)}{2\pi}[P_{qq} \otimes q_i + P_{qg} \otimes g], \\ \frac{dg(x,t)}{dt} &= \frac{\alpha_s(t)}{2\pi}[P_{gq} \otimes \sum_i q_i + P_{gg} \otimes g]. \end{aligned} \tag{1.60}$$

We can simplify these equations by working with SU(n_f) flavour symmetry singlet and non-singlet combinations of the parton distributions [14]. A singlet would be

$$q^{\mathrm{S}}(x,t) = \sum_i (q_i(x,t) + \bar{q}_i(x,t)), \tag{1.61}$$

summing over all active flavours. Non-singlet combinations, $q^{NS}(x,t)$, are of the form $u - \bar{u},\ d - \bar{d}, ...$ They satisfy the equations

$$\begin{aligned} \frac{dq^{\mathrm{NS}}(x,t)}{dt} &= \frac{\alpha_s(t)}{2\pi} P_{qq} \otimes q^{\mathrm{NS}}, \\ \frac{dq^{\mathrm{S}}(x,t)}{dt} &= \frac{\alpha_s(t)}{2\pi}[P_{qq} \otimes q^{\mathrm{S}} + 2n_f P_{qg} \otimes g], \\ \frac{dg(x,t)}{dt} &= \frac{\alpha_s(t)}{2\pi}[P_{gq} \otimes q^{\mathrm{S}} + P_{gg} \otimes g]. \end{aligned} \tag{1.62}$$

A convenient transformation is to take moments of the parton distributions and splitting functions, i.e.

$$\begin{aligned} q_j(t) &= \int_0^1 dx\ x^{j-1}\ q(x,t), \\ \gamma_j &= \int_0^1 dx\ x^{j-1}\ P(x), \end{aligned} \tag{1.63}$$

the latter are known as *anomalous dimensions*.

In this way the equations can be expressed as products of moments

$$\begin{aligned} \frac{dq_j^{\mathrm{NS}}}{dt} &= \frac{1}{2\pi bt} \gamma_j^{qq} q_j^{\mathrm{NS}}, \\ \frac{dq_j^S}{dt} &= \frac{1}{2\pi bt}[\gamma_j^{qq} q_j^S + 2n_f \gamma_j^{qg} g_j], \\ \frac{dg_j}{dt} &= \frac{1}{2\pi bt}[\gamma_j^{gq} q_j^S + \gamma_j^{gg} g_j]. \end{aligned} \tag{1.64}$$

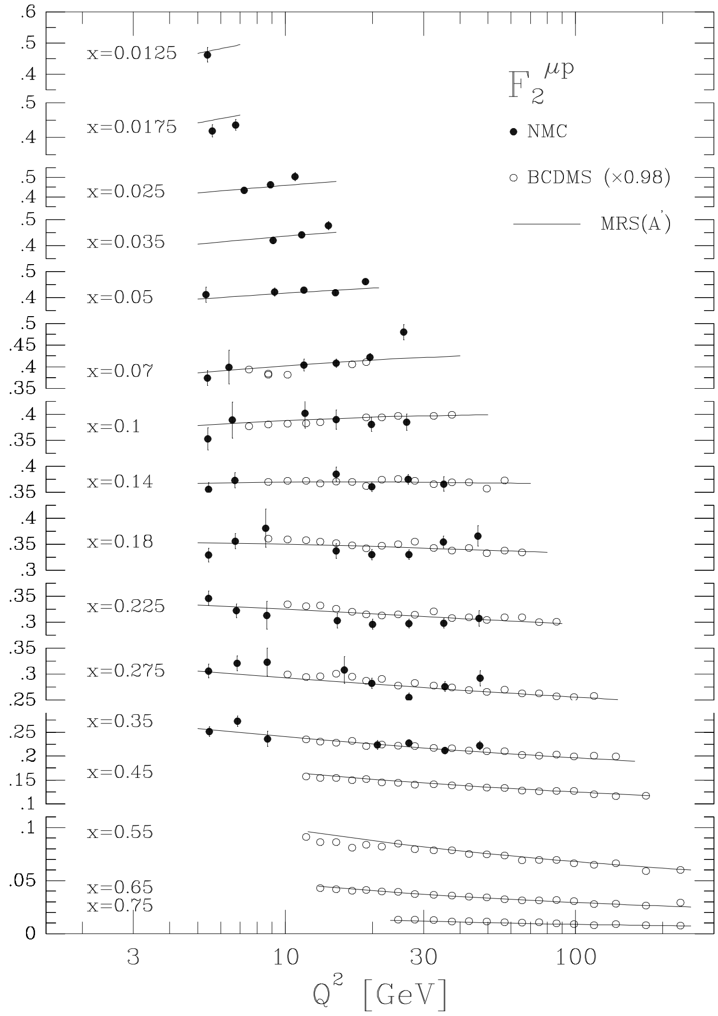

Figure 1.8: QCD fits to muon-proton DIS F_2 [14]

The solution for the non-singlet moments is straightforward

$$q_j^{\rm NS}(t) = q_j^{\rm NS}(t_0)\left(\frac{\alpha_s(t_0)}{\alpha_s(t)}\right)^{\frac{\gamma_j^{qq}}{2\pi b}}. \tag{1.65}$$

To obtain the distribution in x space we use the inverse Mellin transform integral

$$q^{\rm NS}(x,t) = \frac{1}{2\pi i}\int_C dj x^{-j} q_j^{\rm NS}(t), \tag{1.66}$$

with the contour of integration in the complex j plane being parallel to the imaginary axis and to the right of the singularities of the integrand. The singlet moments can

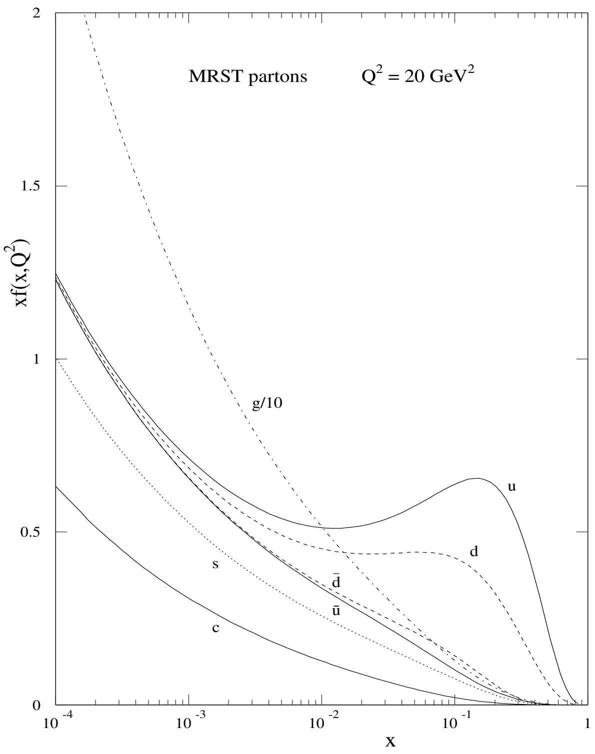

Figure 1.9: Parton density distributions as functions of x for $Q^2 = 20$ GeV^2 [15]

be solved with a similar matrix solution [14]. This allows us to make fits to the data such as those shown in Fig. 1.8.

To obtain the parton distributions from the data we assume a given structure in the x variable for different parton distributions at a low Q_0^2. Then we use the DGLAP equations to evolve the parton distributions to any higher Q^2 where observables exist. By fitting the calculations to the data we select those initial parameters which produce the best fit. An example of such a procedure is given in Fig. 1.9 where the parton distributions are given at a scale of $Q^2 = 20$ GeV^2. At large x the u and d quarks dominate. The sea quark contribution rises for small x but the dominant one comes from the gluon. At $x = 10^{-4}$ there are more than 20 gluons per unit of rapidity (see expression 1.100).

We recall that solving the DGLAP equations we have collected all the contributions proportional to

$$\left[\alpha_s(Q^2)\ln\left(\frac{Q^2}{Q_0^2}\right)\right]^n, \tag{1.67}$$

corresponding to the *leading logarithmic* approximation valid in the limit

$$\alpha_s(Q^2)\ln\left(\frac{1}{x}\right) \ll \alpha_s(Q^2)\ln\left(\frac{Q^2}{Q_0^2}\right) < 1. \tag{1.68}$$

1.2.3 Solution to the DGLAP equations at small x

One of the aims of this thesis is to study the low-x behaviour of the structure functions and to present recent theoretical advances in the formulation of small-x dynamics. The understanding of the strong interaction in the small x regime remains as a major challenge for QCD.

DIS is a process with a single scale which allows us to obtain the structure functions in the small x region and to study the transition between the non-perturbative and the perturbative regimes. We have seen that making use of factorization theorems and the DGLAP evolution equations for parton distributions we get a good description of the physics of scaling violations. Is this description modified when we enter the small x regime? At which x does the DGLAP picture for the evolution of the structure functions start to be inaccurate?

If we have a look at the available data, Fig. 1.10, we can see that F_2 rises towards $x = 0$, and this rise is much steeper as we increase Q^2. Is it possible to understand this behaviour in terms of QCD?

As we have already shown the splitting functions are calculable as power series expansions in the coupling constant (see Eq. 1.56). We have calculated the LO order term but they are known up to NLO accuracy. The gluon-gluon splitting function $P_{gg}(x, \alpha_s(Q^2))$ at fixed-order has a singularity at small x (see Eq. 1.55) and behaves like $\sim \alpha_s/x$. This singularity leads to the rise of F_2 for small x. What is the dynamics of this growth? Let us study a simplified version of the evolution equation in order to

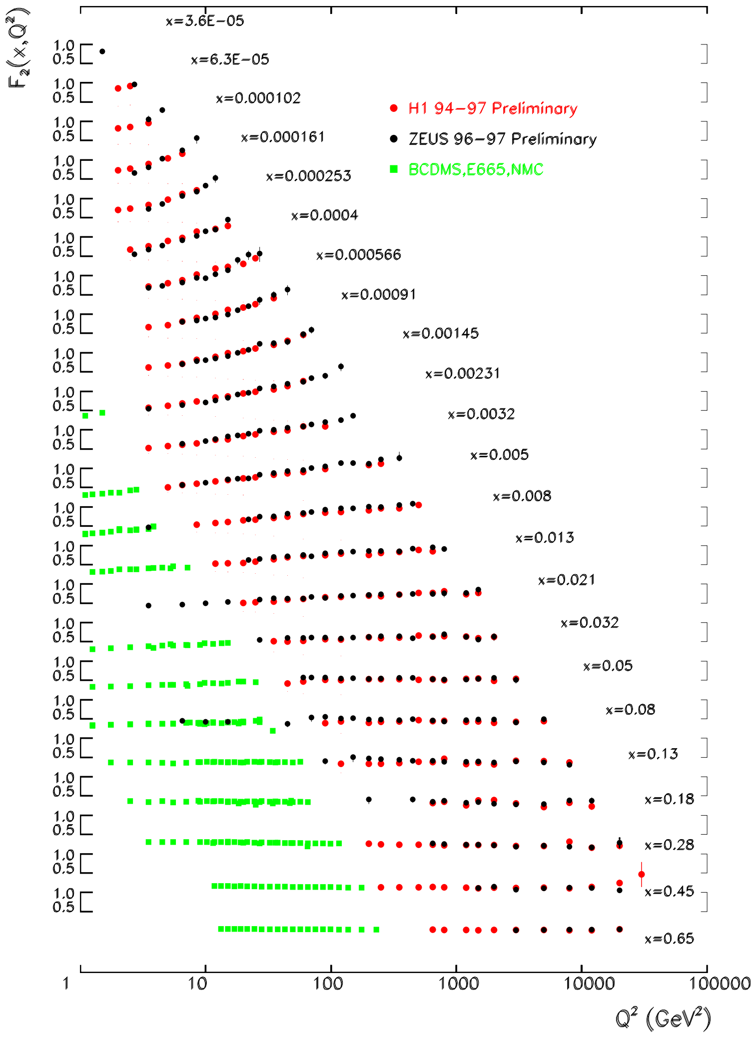

Figure 1.10: The proton structure function F_2 as a function of Q^2 for fixed x

answer this question. We will only consider the evolution for the gluonic distribution and the singular term in P_{gg} for Eq. 1.64,

$$\frac{dg_j}{dt} = \frac{\alpha_s(t)}{2\pi}\gamma_j^{gg} g_j. \tag{1.69}$$

The $x \to 0$ limit of the parton distributions is determined by the behaviour of the anomalous dimensions γ_j^{gg} at $j \sim 1$ where it goes like

$$\gamma_j^{gg} \simeq \frac{2N_c}{j-1}, \tag{1.70}$$

with N_c being the number of colours. In this limit the solution for the moments of the gluon distribution is

$$g_j(t) = g_j(t_0) \exp \frac{N_c \eta(t)}{j-1}, \tag{1.71}$$

with η given by

$$\eta(t) = \int_{t_0}^{t} dt' \; \alpha_s(t'). \tag{1.72}$$

To go back to x space we need to perform the inverse Mellin transform, Eq.1.66,

$$\begin{aligned} g(x,t) &= \frac{1}{2\pi i} \int dj \; x^{-j} \; g_j(t) \\ &= \frac{1}{2\pi i} \int dj \; g_j(t_0) \;\; \exp\left(j \ln \frac{1}{x} + \frac{N_c \eta(t)}{j-1} \right). \end{aligned} \tag{1.73}$$

In the limit when Q^2 is large and x is small, i.e. $\ln(1/x)\ln(Q^2/Q_0^2) \gg 1^{\S}$, we can estimate the integral by expanding about the saddle point of the exponential, j_{saddle}

$$j_{\text{saddle}} = 1 + \sqrt{\frac{N_c \eta(t)}{\ln \frac{1}{x}}}. \tag{1.74}$$

Therefore, the solution expressed in the original variables yields [16]

$$g(x, Q^2) \sim \frac{1}{x} \exp \sqrt{\frac{N_c}{\pi b} \ln \frac{\ln \frac{Q^2}{\Lambda^2}}{\ln \frac{Q_0^2}{\Lambda^2}} \ln \frac{1}{x}}. \tag{1.75}$$

This result corresponds to the *double leading logarithmic* approximation where the resumed logarithms are of the form

$$\left[\alpha_s(Q^2) \ln \left(\frac{Q^2}{Q_0^2} \right) \ln \left(\frac{1}{x} \right) \right]^n. \tag{1.76}$$

The solution in Eq. 1.75 is valid when we use a flat initial distribution. In this case the asymptotic x-dependence is dominated by the perturbative splitting function. What happens if we choose a steep initial dependence for the evolution, for example

$$g(x, t_0) = \mathcal{C} x^{-j_0}? \tag{1.77}$$

In this case we have to be more careful because now there are singularities to the right of the saddle point

$$g_j(t_0) = \frac{\mathcal{C}}{j - j_0}. \tag{1.78}$$

§It is important to compare this limit with the leading logarithm limit of the inequality 1.68.

The solution can be found at small x by closing the contour of integration about the pole of the initial distribution. The value of the integral is then

$$g(x,t) = \mathcal{C} x^{-j_0} \exp \frac{N\eta(t)}{j_0 - 1}, \tag{1.79}$$

and the original x behaviour remains after the Q^2 evolution. The asymptotic behaviour depends on the non-perturbative parameter j_0. The presence of this non-perturbative term means that if we pick a too steep starting distribution the room for perturbative evolution is suppressed because we do not have enough fast gluons to produce the slower ones which build up the perturbative rise at small x.

1.2.4 BFKL formalism in deep inelastic scattering

For processes where x is small, but Q^2 is not large enough as to make the *double logarithmic* approximation valid, the Balitsky-Fadin-Kuraev-Lipatov (BFKL) equation [17, 18, 19] has been proposed as the correct description. In this scheme the partonic branching in the ladder is strongly ordered in longitudinal momentum while there is no ordering on transverse scales. This formalism is applicable in the limit when

$$\alpha_s(Q^2) \ln \left(\frac{Q^2}{Q_0^2} \right) \ll \alpha_s(Q^2) \ln \left(\frac{1}{x} \right) < 1, \tag{1.80}$$

and resums the terms

$$\left[\alpha_s(Q^2) \ln \left(\frac{1}{x} \right) \right]^n \tag{1.81}$$

in the so called *leading log(1/x)* approximation. The BFKL equation is better expressed in terms of the unintegrated gluon density $f(x, \mathbf{k}^2)$ (from now on bolded variables will represent transverse momenta) related to the usual gluon density by

$$xg(x, Q^2) = \int_0^{Q^2} d\mathbf{k}^2 \frac{f(x, \mathbf{k}^2)}{\mathbf{k}^2}. \tag{1.82}$$

A representation of this equation, whose derivation we will explain in the next chapter, is

$$\frac{\partial f(x, \mathbf{k}^2)}{\partial \ln (1/x)} = \frac{3\alpha_s}{\pi} \int_0^\infty d\mathbf{l}^2 \frac{\mathbf{k}^2}{\mathbf{l}^2} \left(\frac{f(x, \mathbf{l}^2) - f(x, \mathbf{k}^2)}{|\mathbf{l}^2 - \mathbf{k}^2|} + \frac{f(x, \mathbf{k}^2)}{\sqrt{4\mathbf{l}^4 + \mathbf{k}^4}} \right). \tag{1.83}$$

We will show how to solve it analytically for fixed α_s but for the time being we would like to indicate that the solution is proportional to

$$f(x, \mathbf{k}^2) \sim \left(\frac{x}{x_0}\right)^{-\lambda}, \tag{1.84}$$

with

$$\lambda = \frac{\alpha_s N_c}{\pi} 4 \ln 2 \simeq 0.5, \text{ for } N_c = 3 \text{ and } \alpha_s = 0.19. \tag{1.85}$$

In this formalism the rise of the gluon density is faster than the double logarithmic prediction of Eq. 1.75, namely

$$g(x, Q^2) \sim x^{-\lambda - 1}. \tag{1.86}$$

We would like to indicate that the BFKL equation for DIS does not contradict DGLAP, what it does is to pick up the terms which produce leading logarithms of $1/x$ to all orders in α_s from the DGLAP kernel. At small x these logarithmic terms should be important and they affect the perturbative expansion of the splitting functions.

The DGLAP approach has been compared with structure function data during the last few years. The next-to-leading order DGLAP equations describe very well the *ep* DIS data at HERA for $2 \cdot 10^{-5} < x < 0.65$ and $1 < Q^2 < 3 \cdot 10^4$ GeV^2 as can be seen in Fig. 1.11. This could indicate that the BFKL is not needed to obtain a correct phenomenological picture in the HERA kinematic region. But if we compare the LO and NLO DGLAP results we can see that at LO and NLO we get stable predictions for F_2 but we have to change the gluon density in absolute normalization and in x shape as well. This can be explained if we study the quark splitting function

$$P_{qg}(\alpha_s, x) \simeq \alpha_s P_{qg}^{\mathrm{LO}}(x) \left[1 + 2.2 \frac{C_A}{\pi} \frac{1}{x}\right], \tag{1.87}$$

which is responsible, convoluted with the gluon distribution, for scaling violations. $P_{qg}^{\mathrm{LO}}(x)$ is flat at small x but the NLO correction is steep. To get a stable evolution in the structure function the gluon density has to be less steep at NLO than at LO. Therefore we must be careful because in the fixed order DGLAP analysis of F_2 possible large NLO perturbative corrections at small x can be easily hidden by a change in the

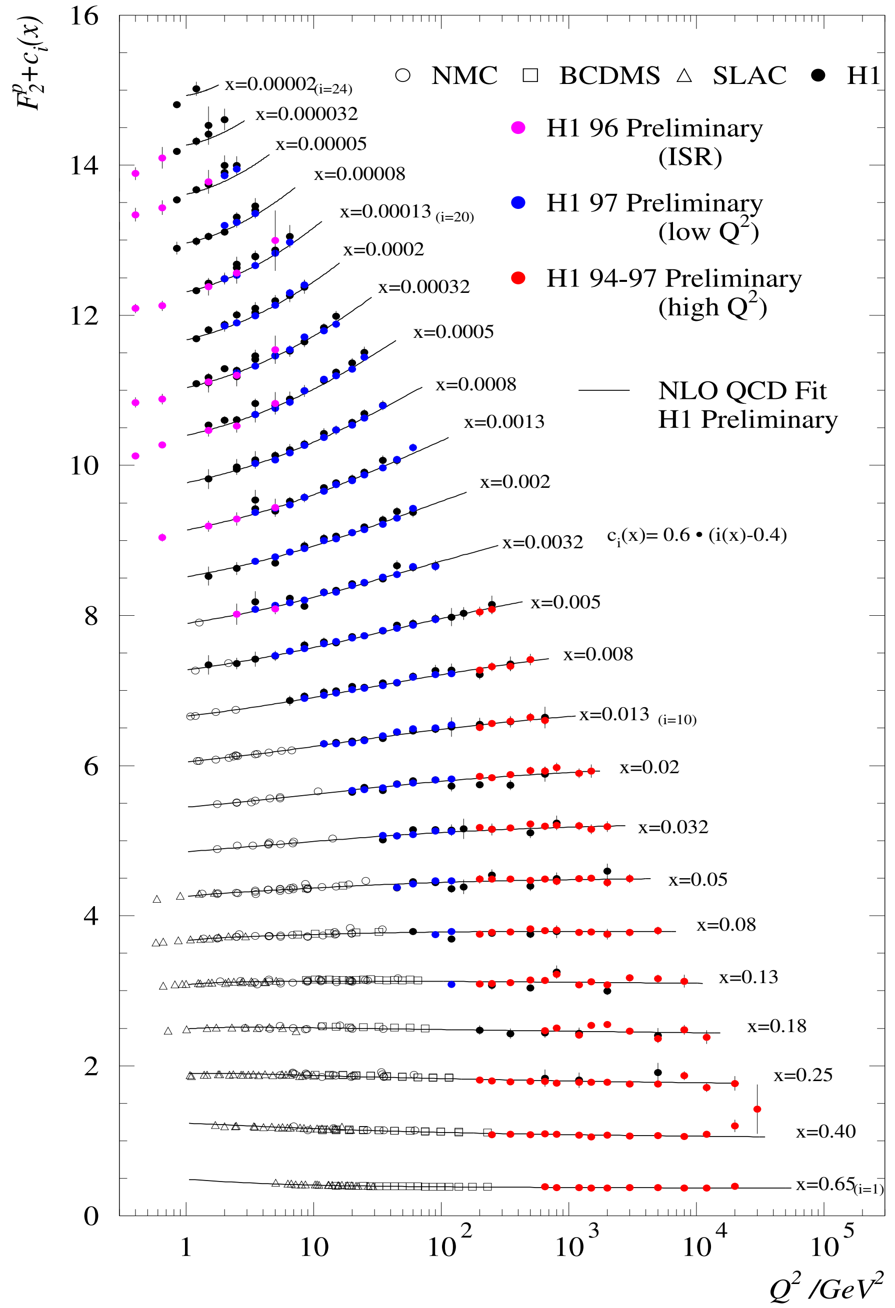

Figure 1.11: A global NLO DGLAP fit to the measurements of F_2 by the H1 and fixed target collaborations.

parton density parameterizations. We need more data to determine the importance of BFKL effects. Measurements of other structure functions such as F_L can help us to determine the correlation between P_{qg} and $g(x, Q^2)$.

There is an alternative to the treatment of the gluon ladder based on angular ordering along the gluon chain. It is the so called Catani-Ciafaloni-Fiorani-Marchesini (CCFM) equation [20, 21, 22]. This equation reproduces BFKL at small x and the conventional DGLAP evolution at large x. We will study it in more detail in the third chapter of this work.

1.2.5 Parton saturation

We have seen how the parton distributions have a fast rise when we approach the small x region. Due to the finite size of the proton this rise cannot be infinite. When the number of partons within the proton is too large they cannot be considered as free fields any longer because their wave functions start to overlap and recombination effects should be taken into account. It is expected that these effects, generally known as *parton saturation*, should limit the growth of the distributions. A rough estimate can be done of the regime where this new phenomenon should appear. Unitarity (see Eq. 1.95) forces the DIS cross section to approach a constant value modulo logarithms in the centre-of-mass energy when this energy is asymptotically large. This limit essentially corresponds to the size of the hadron. In terms of the structure function F_2 we can write [23]

$$\frac{1}{Q^2} F_2(x, Q^2) \simeq \frac{1}{Q^2} \alpha_s g(x, Q^2) \lesssim \pi R^2, \tag{1.88}$$

with R being the proton radius and we have made use of the fact that the gluon distribution function is dominant at small x. Obviously this condition is violated by both DGLAP and BFKL at small values of x. The reason is that these equations have not included the physics of parton rescattering or parton recombination processes. The effect of this physics is to introduce higher twist terms in the factorization formula 1.15. These are difficult to implement and some models have been proposed in the literature [24] which take them into account.

1.3 Small x processes at HERA

HERA is an accelerator where a beam of 27.5 GeV electrons collides with a beam of 820 GeV protons with a centre of mass energy of 300 GeV. The available kinematic (x, Q^2) plane [25] covering the range $Q^2 \sim 0.2 - 10^4$ GeV^2 and $x \sim 10^{-5} - 10^{-1}$ can be seen in Fig. 1.12. The two experiments dedicated to the study of the HERA physics are known as H1 and ZEUS.

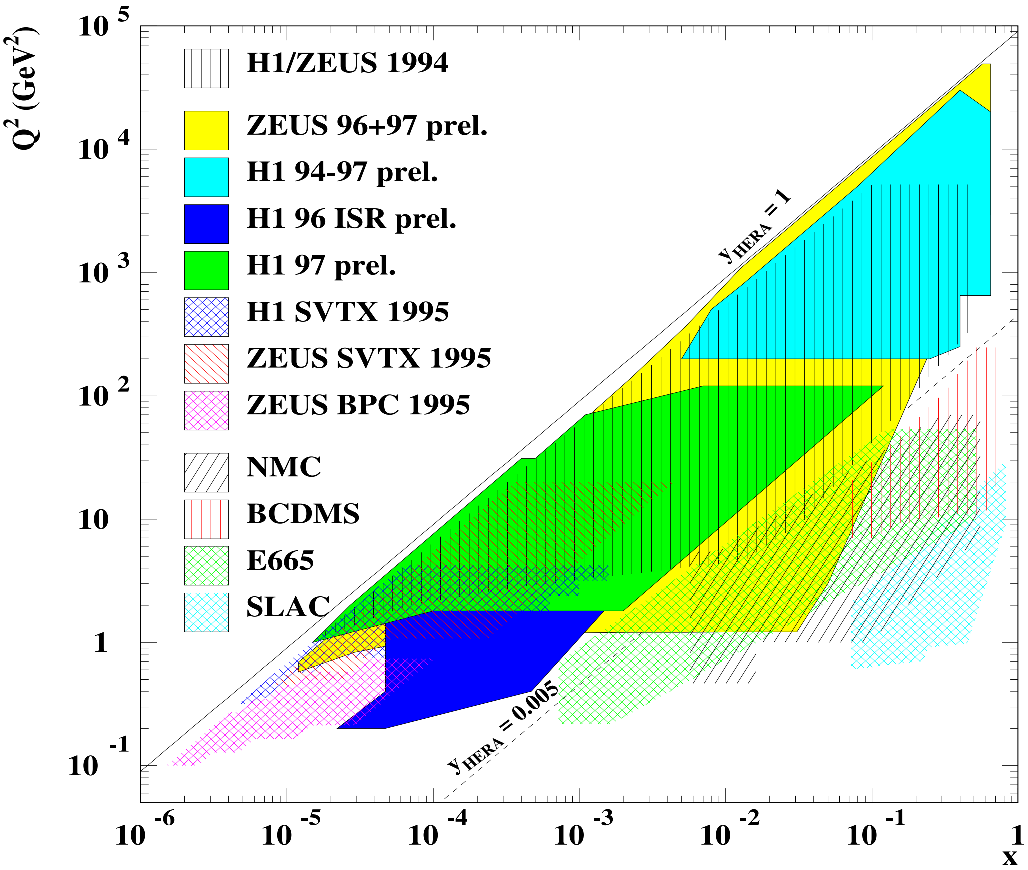

Figure 1.12: The (x, Q^2) kinematic plane of some of the fixed target and of the HERA collider DIS experiments

This collider enables us to test regions of very low Bjorken x allowing the study of the dependence of the proton structure function F_2 as a function of this variable. In Fig. 1.13 F_2 is shown as a function of x for three different values of Q^2.

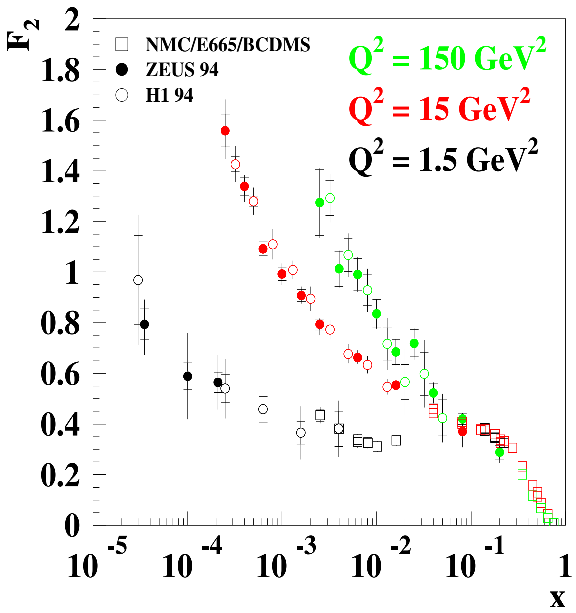

Figure 1.13: The proton structure function as a function of x for three Q^2 values

The first results coming from HERA were very interesting. In the DIS regime it was found that the number of slow partons increases steadily with decreasing x [26, 27]. As we have seen this result was expected from perturbative QCD predictions. In Fig. 1.14 we show how the NLO DGLAP equations seem to give a good description of the data down to Q^2 of 1.5 GeV^2. There is a strong rise of the structure function F_2 with decreasing x in all Q^2 bins. As Q^2 gets smaller this rise is less steep. Further studies have shown that this increase is still observed at so low values of Q^2 as 1 GeV^2 [28]. This behaviour can be understood through the formula (see also Eq. 1.34)

$$F_2 \sim \frac{Q^2}{4\pi^2\alpha}\sigma_{tot}^{\gamma^* p} \tag{1.89}$$

which is valid for small x. Regge theory (see below) provides a good description of the rise of the total cross section with the squared centre-of-mass energy s

$$\sigma_{\text{total}} \sim s^{\alpha(0)-1}, \tag{1.90}$$

with $\alpha(0)$ being the intercept of the leading trajectory. In the limit of small x the relation between W, the $\gamma^* p$ centre of mass energy, and x, is

$$W^2 \simeq \frac{Q^2}{x}. \tag{1.91}$$

Therefore the rise in the structure function at fixed Q^2 can be interpreted as a rising of the $\gamma^* p$ cross section with increasing W^2

$$F_2 \simeq x^{-\lambda}, \tag{1.92}$$

with $\lambda = \alpha(0) - 1$. A measurement of the Q^2 dependence of the exponent λ can be found in Fig. 1.15.

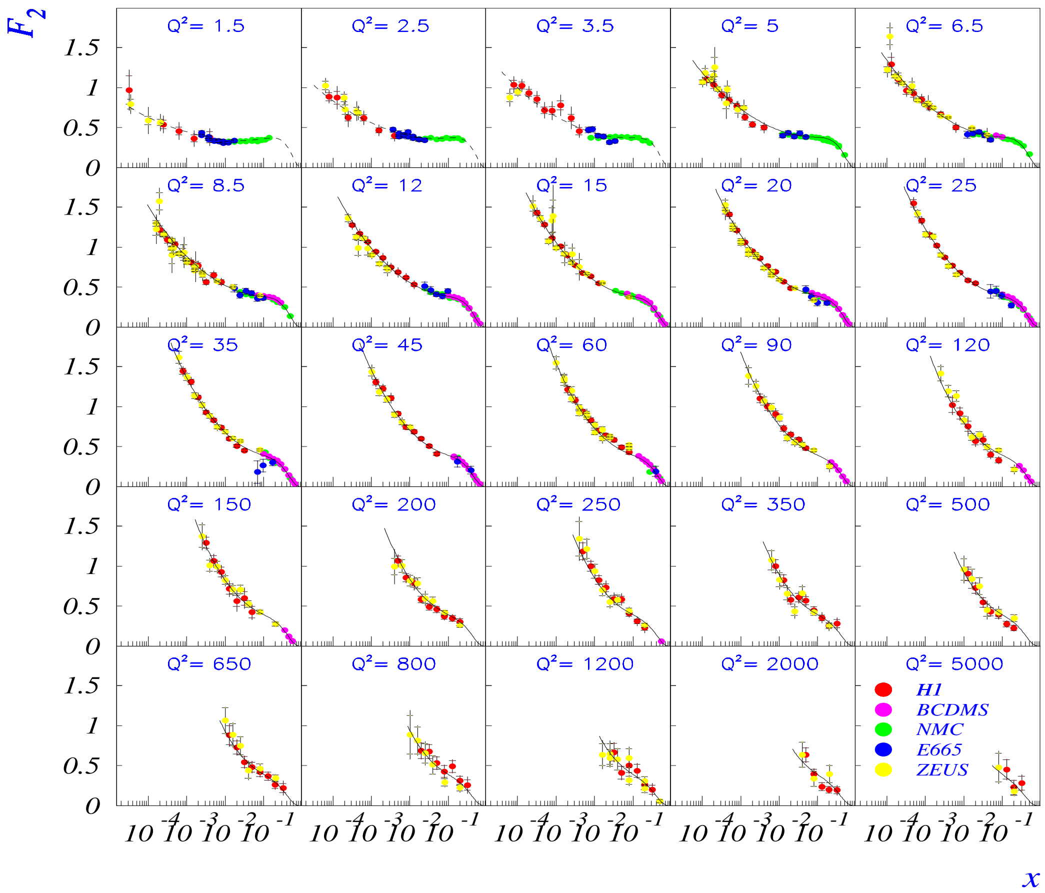

Figure 1.14: A NLO QCD fit to F_2 as function of x for fixed Q^2 values (in GeV^2)

The high value of lambda measured at high Q^2 may be consistent with the BFKL

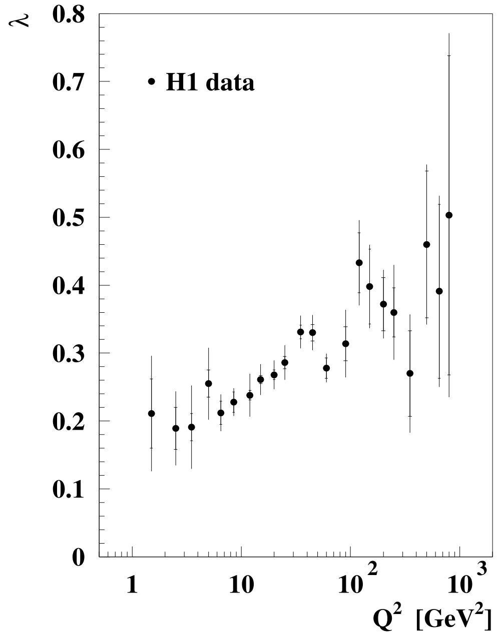

Figure 1.15: $\lambda(Q^2)$ from fits of the form $F_2 \sim x^{-\lambda}$ at fixed Q^2 and x <0.1 [29]

interpretation of the x evolution for the structure function but, as we have seen, it is also compatible with a DGLAP-type evolution.

From the total photoproduction cross section (see below) we know that $\lambda(Q^2 = 0) = 0.08$. The region where λ goes from 0.08 to ~0.15 in Fig. 1.15 is very interesting because it shows the interplay between soft and hard physics.

The transition to lower values of Q^2 can be understood introducing the concept of structure of the photon. It is well known that when the photon interacts with hadrons its behaviour is similar to that of a hadron (*vector dominance model* [31]). The photon can fluctuate into a $q\bar{q}$ pair and if the fluctuation time is larger than the interaction time with the target the photon will have a hadronic behaviour. This is the case for real photons but not for highly virtual ones. Therefore for real photons we can also define structure functions which can be studied at the HERA collider. This can be done by selecting those processes at very low Q^2 where the photon becomes quasi-real. The probe can be a high transverse momentum parton coming from the proton. As the virtuality of the emitted photon is

$$Q^2 = 2EE'(1 - \cos\theta), \tag{1.93}$$

with E, E' the energies of the incoming and outgoing electrons, and θ the scattering angle of the outgoing one, to get low Q^2 we only have to measure the outgoing electrons at very small angles. This can be achieved at the two experiments H1 and ZEUS. To understand the hadronic structure of the photon it is interesting to compare the total photoproduction cross section $\sigma_{\rm tot}^{\gamma p}$ with the total hadron-hadron cross sections.

1.4 Total cross-sections

The behaviour of total hadron-hadron cross sections can be described by Regge theory [30] which emerged in potential scattering studies through the analyticity properties of the scattering amplitude. In the Regge pole model the scattering amplitude has the limit

$$\mathcal{A}(s,t) \simeq \sum_i \beta_i(t) \frac{1 + \xi_i e^{-i\pi\alpha_i(t)}}{\sin\left[\pi\alpha_i(t)\right]} \left(\frac{s}{s_0}\right)^{\alpha_i(t)} \tag{1.94}$$

when $s \to \infty$ and the momentum transfer t is fixed. $\xi_i = \pm 1$ is called the signature of the Regge pole. The analytic functions $\alpha_i(t)$ are the Regge trajectories and the $\beta_i(t)$ are the residues of the poles. Each of these poles represents the exchange of a whole family of particles belonging to the same Regge trajectory $\alpha_i(t)$. When t takes the value of the mass squared of a particle the trajectory $\alpha_i(t)$ equals its spin. This takes into account the collective effect of all the exchanged particles in the trajectory. There is a constraint on these trajectories coming from the Froissart bound [32]

$$\sigma_{\rm tot} \leq C \ln^2 \frac{s}{s_0}, \tag{1.95}$$

i.e. for physical (negative) values of t the trajectories have to be smaller than unity if the rise of the total cross section is bound to be lower than $\ln^2 s$.

The Regge poles are classified into different families according to their quantum numbers. The Regge poles with quantum numbers of mesons form linear trajectories in the (mass^2, spin) plane. An example of these Reggeon trajectories [33] is shown in Fig. 1.16. The continuation of the trajectory to negative m^2 leads to a trajectory of

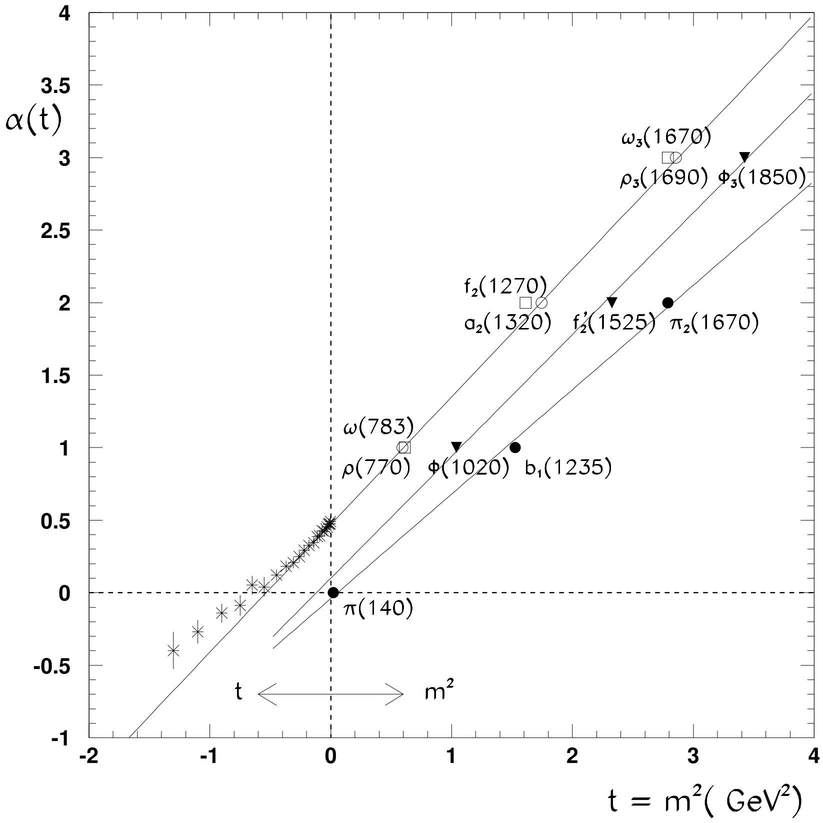

Figure 1.16: The ρ ($\circ$), ω ($\square$), ϕ ($\triangle$) and π ($\bullet$) trajectories. The ρ trajectory has been continued as measured in $\pi^- p \to \eta n$ [34]

the form

$$\alpha(t) = \alpha_0 + \alpha' \cdot t, \tag{1.96}$$

α_0 is the intercept and α' the slope. There is a family of Regge poles associated with the exchange of the quantum numbers of the vacuum, i.e. charge conjugation $C = +$, positive parity $P = +$ and zero isospin $I = 0$, called the Pomeron trajectory. There are no known hadronic bound states on this trajectory but it is believed to be populated by glue-balls. Its explanation in terms of QCD remains unknown [35]. It has been determined experimentally to be [36, 37, 38]

$$\alpha_{\mathcal{P}}(t) = 1.08 + 0.25t. \tag{1.97}$$

This trajectory is believed to determine the properties of hadron-hadron cross sections at high energies. In the limit $s \gg -t$ the amplitude for elastic scattering goes like $\mathcal{A}(s,t) \sim s^{\alpha_{\mathcal{P}}(t)}$. This translates through the optical theorem to

$$\sigma_{\text{tot}} = \frac{1}{s}\mathcal{I}m\mathcal{A}(s,t=0) \sim s^{\alpha_{\mathcal{P}}(0)-1}. \tag{1.98}$$

Donnachie and Landshoff [38] succeeded to describe all available $\bar{p}p$, pp, $K^{\pm}p$, and $\pi^{\pm}p$ total cross section data with a simple Regge motivated parameterization of the form

$$\sigma_{\text{tot}} = Xs^{0.0808} + Ys^{-0.4525}, \tag{1.99}$$

where X and Y are parameters process depended. Due to the Pomeranchuk theorem [39] X is the same for particle and antiparticle beams. The power of the first term is the Pomeron intercept and the second term corresponds to the intercept of a Reggeon with $\alpha_{\mathcal{R}}(0) = 0.5475$. The data and the parameterizations are shown in Fig. 1.17. A similar parameterization holds for photoproduction, Fig. 1.18, indicating the hadronic-like behaviour of the photon.

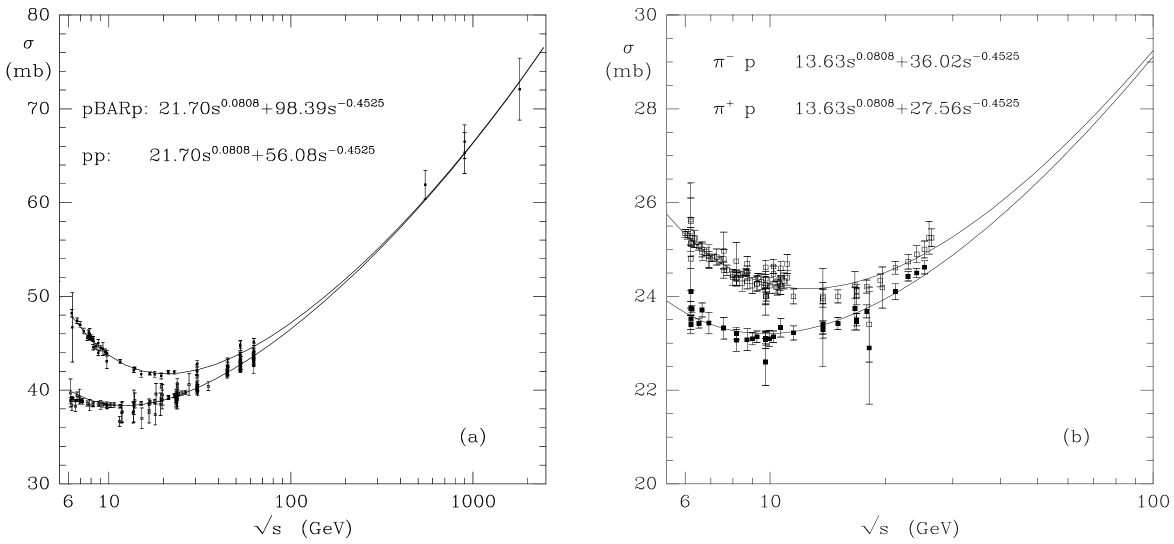

Figure 1.17: The total cross section data and parameterization of $\bar{p}p$, pp and $\pi^{\pm}p$ as function of $\sqrt{s}$

There are two further types of processes that are well described by Pomeron exchange: elastic and diffractive scattering. Elastic processes allow the determination of the Pomeron slope. They are characterized by a very small momentum transfer

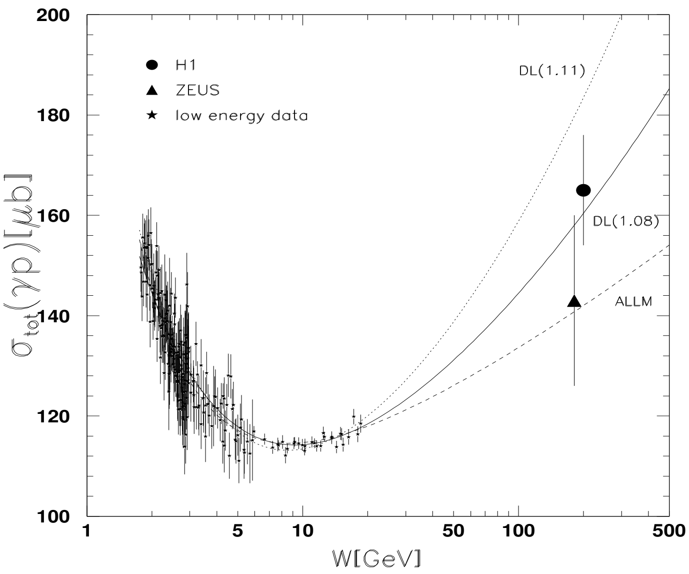

Figure 1.18: The total photoproduction cross section data as function of W. The full line and the dotted line are the Donnachie-Landshoff parameterization predictions for $\alpha_{\mathcal{P}}$=1.08 and 1.1. ALLM is a different parameterization.

between the interacting hadrons and the only effect on these is a deviation from their original trajectory. In diffractive processes the momentum transfer is usually also small but one or both hadrons can be excited into a state of finite mass which will decay afterwards giving place to single or double diffractive dissociation, respectively. It is remarkable that about a 40% of the photoproduction events at HERA energies are diffractive processes.

The characteristic signal for diffraction at high energies is the presence of large rapidity gaps. Let us explain the meaning of this considering the DIS reaction $A+B \to A' + X$. The rapidity of the particle A' is defined as

$$y \equiv \frac{1}{2} \ln \left(\frac{E_{A'} + k^{||}_{A'}}{E_{A'} - k^{||}_{A'}} \right), \tag{1.100}$$

with E being the energy and $k^{||}$ the component of the momentum in the direction of movement. The limit of y for high energies is called the pseudorapidity

$$\eta = -\ln \tan \frac{\theta_{A'}}{2}, \tag{1.101}$$

with $\theta_{A'}$ being the angle between the emerging struck parton and the incoming proton,

η is a good approximation to rapidity for particles with small mass. The pseudorapidity interval between the remnant of the proton and this parton can be expressed as

$$\Delta\eta = \eta_{\text{remnant}} - \eta_{\text{parton}} \sim \ln\left(\frac{W}{M_{\rm p}}\right)_{\gamma^* p} - \ln\left(\frac{xW}{M_{\rm p}}\right)_{\gamma^* parton} \sim \ln\left(\frac{1}{x}\right), \tag{1.102}$$

where x is proton momentum fraction carried by the parton.

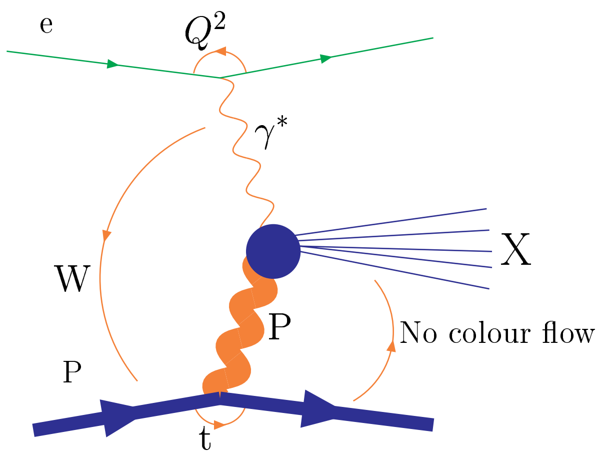

Figure 1.19: Diffractive deep inelastic scattering

In Fig. 1.19 we show the diagram corresponding to diffractive DIS, $ep \to epX$, where the final state is formed by the scattered electron and the hadrons in the photon fragmentation region. The proton only suffers a small change in its trajectory. In the $\gamma^* p$ centre of mass system and in the limit $M_X \ll W$ the rapidity separation between the proton and the system X is

$$\Delta y = \ln\frac{W^2}{M_{\rm p} M_X}. \tag{1.103}$$

The system X typically fragments into hadrons occupying around three units of rapidity. The total rapidity separation for a typical scattering with $W = 200$ GeV and $M_X = 20$ GeV is $\Delta y \sim 7.7$ leaving a rapidity gap larger than four units. In the BFKL formalism the typical separation in rapidity between two emissions in the ladder should be large. This implies that only a small number of rungs should be the core of the evolution at HERA energies.

We have seen that, at the moment, it is not possible to demonstrate the relevance of the BFKL approach just using total cross section measurements only. Footprints for BFKL must be searched for in those exclusive channels where the DGLAP evolution is suppressed.

1.5 Other tests for BFKL

An important source of information about QCD dynamics has been provided by the study of *jet production* in DIS at HERA. The evolution equations derived in perturbative QCD describe inclusive quantities like the DIS cross section but they can also describe some final state properties if the influence from the radiation pattern which originated the evolution is not completely lost in the hadronization process, i.e. assuming that *parton-hadron duality* [42] is correct. The predictions for this pattern of radiation are different if we use DGLAP or BFKL. In DGLAP the strong ordering in transverse momenta relative to the proton beam implies that partons with high k_T must be radiated close to the point where the virtual photon is absorbed and partons with low k_T should be close to the proton. In other words, partons with large x have small transverse momenta. In BFKL this is not the case because there is not strong ordering in k_T and there should be a large parton activity between the current system and the proton remnant. We would expect partons with larger transverse momenta in the final state than predicted by DGLAP. In brief, for DGLAP, partons with a large fraction of the proton momentum can only have small transverse momentum and for BFKL they can also be emitted with a large one.

One of the processes where deviations from DGLAP could be found is the production of *forward jets at HERA* [43, 44, 45]. If at small x the struck quark has a transverse momentum of order $\sim Q^2$, the virtuality of the incoming photon, then the DGLAP evolution should be strongly suppressed. This quark produces a jet which lies on the forward direction because small x implies not large Q^2. The treatment of particle production in the forward direction can be complicated because in this region hadronization effects are larger. The H1 collaboration recently presented some preliminary results for this process but conclusions cannot yet be drawn because there are some theoretical uncertainties related to how compare the data to DGLAP [46].

It would be desirable to find processes where the available x is smaller than that for forward jets. This can be achieved if we look for production of very energetic forward π^0s with the further advantage that the use of a single forward particle reduces the uncertainty due to jet finding algorithms. The process $e^+p \to e^+\pi^0 X$ has been studied by H1 [47] for DIS events with large π^0 energy ($x_{\pi^0} > 0.01$) and large $p_{\rm T}^{\pi^0} > 3.5$ GeV. The photon virtuality was in the range $2 < Q^2 < 70$ GeV^2. The kinematics is such that the meson is emitted close to the forward direction and is clearly separated in rapidity from the quark jet. In Fig. 1.20 we show the differential cross section $d\sigma/dx$. As expected the DGLAP picture does not work for this observable. The prediction from a modified LO BFKL calculation convoluted with π^0 fragmentation functions is good but has a large theoretical error.

Another option to ensure two similar small scales is the hard diffractive production of heavy vector mesons in DIS, $\gamma p \to V + X$ at large momentum transfer t and large centre-of-mass energy s with V being the vector meson. In [48] it is shown that a finite momentum transfer $|t| \gg \Lambda_{QCD}^2$ suppresses the diffusion into the infrared and allows a perturbative treatment of the gluon evolution.

The Tevatron hadron collider offers another possibility to study rapidity gap physics via the exchange of a colour singlet between two high energy jets with not very large and similar transverse momenta and a large rapidity separation [49, 50]. In the production of these jets the centre of mass energy can be much larger than the momentum transfer and logarithms in the ratio of both should be resummed in the cross sections. This can be done through BFKL and the prediction for the cross section goes like

$$\sigma \sim \frac{1}{Q^2}\frac{e^{2\frac{\alpha_s(Q)12\ln 2}{\pi}\Delta\eta}}{(\alpha_s\Delta\eta)^{3/2}}, \tag{1.104}$$

where in the power of the exponential we have included the leading-order BFKL Pomeron intercept and $\Delta\eta \geq 0$ is the difference in pseudorapities between the two

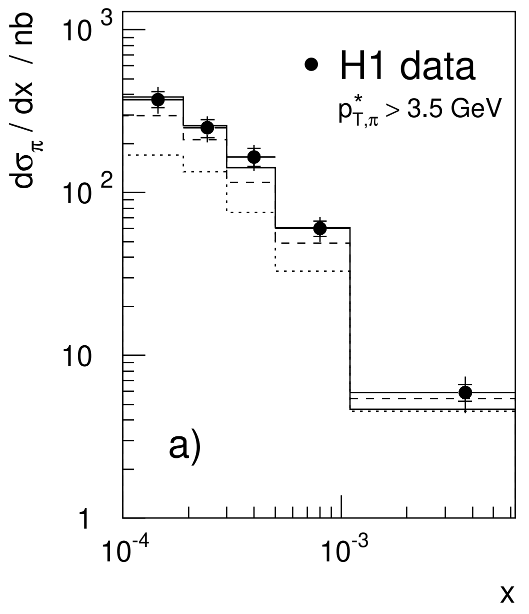

Figure 1.20: The differential cross section as a function of x for forward π^0s for $2 < Q^2 < 70$ GeV^2, $x_{\pi^0} > 0.01$ and the angle between the proton and pion between 5 and 25 degrees. The dotted line is a prediction calculated with DGLAP. The solid line is a modified LO BFKL calculation.

jets. In this relation the test of the BFKL evolution is provided by the $\Delta\eta$ dependence of the cross section. The D0 collaboration [51] measured the ratio of the cross sections for two different beam energies with $\sqrt{s} = 1800$ and 630 GeV and for different values of difference in rapidity between jets. The measurements gave

$$R_{1800/630} = 2.9 \pm 0.3(\text{stat.}) \pm 0.3(\text{syst.}) \tag{1.105}$$

for $\Delta\eta_{630} = 2.6$ and $\Delta\eta_{1800} = 4.7$. This result is in accord with BFKL [52, 53].

A recent proposal [54, 55, 56] to understand the BFKL dynamics is to study the number of associated "mini-jets" in Higgs boson production at the Large Hadron Collider (LHC). For mini-jets it is meant jets with transverse momenta larger than some resolution scale much smaller than the hard scale Q characterizing the process. The mini-jet multiplicity can be calculated assuming that the dominant production mechanism is gluon-gluon fusion and it turns out to be rather insensitive to the Higgs

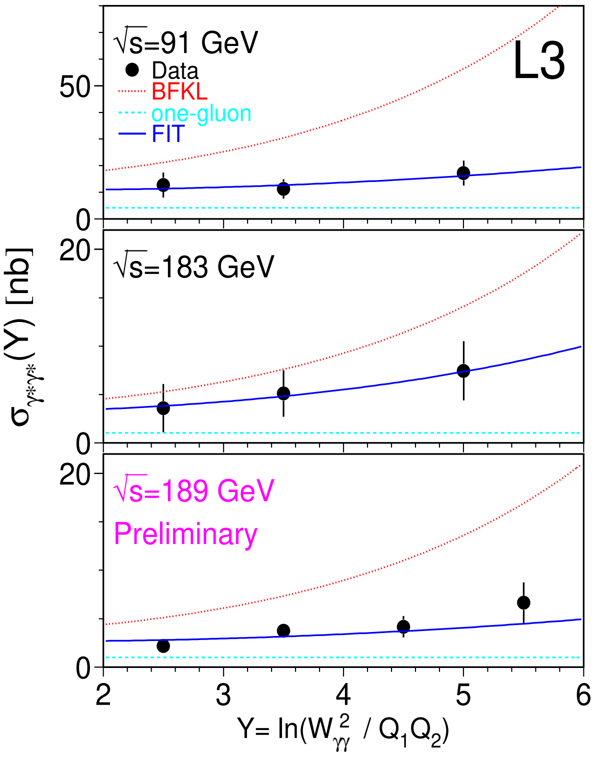

Figure 1.21: $\gamma^*\gamma^*$ cross section for Q^2 values of 3.5, 14 and 14.5 GeV^2 [111]

mass at the energy of the LHC.

Another typical process for the study of the BFKL dynamics is high energy $\gamma^*\gamma^*$ scattering at LEP2. These collisions have been recently measured by the L3 and OPAL collaborations [57]. The data can be seen in picture 1.21. The LO BFKL predictions are too high. The growth of the cross section with high energy has a power of 0.29 ± 0.025 for scales in the range of 3.5 and 14.5 GeV^2 [58, 59].

Possible future photon colliders could provide novel possibilities to test the high energy limit of QCD. There are some processes which could be useful tools to test the QCD Pomeron in high energy $e\gamma$ and $\gamma\gamma$ collisions [60]. The processes would be the natural extension of the ones already analyzed, this includes production of forward jets with $k_t^2 \sim Q^2$ and diffractive production of vector mesons, both in deep inelastic $e\gamma$ scattering, or the diffractive production of heavy vector mesons in $\gamma\gamma$ collisions. One advantage of these colliders is that they would give access to regions of very small x.

From the experimental evidence we have so far no conclusive remarks can be made about the finding of deviations from DGLAP evolution. More experiments and precision data have to be obtained in order to make definite conclusions about the dynamics of the physics at small x. This kinematic region is of fundamental importance not only for a deeper understanding of QCD but also to interpret the data which will be available from future colliders, in particular the large hadron collider (LHC). These studies are also of importance to help disentangle the backgrounds present in signals of new physics.

Chapter 2

The BFKL equation at leading order

In the following we will show how to construct the leading order BFKL equation. We will resum all the terms which give contributions of the form $(\alpha_S \ln \frac{s}{t})^n$ in the kinematic region where the square of the centre of mass energy is much larger than any of the scales in the scattering process. This is the so called *Regge limit* $(s \gg -t)$.

To build the equation we will need two essential ingredients; the *reggeized gluon* and the *effective vertex*. We explain and derive these concepts in the next few sections.

2.1 The reggeization of the gluon

We are interested in the calculation of scattering amplitudes in the asymptotic regime of very high centre-of-mass energy, s. We consider that a particle 'reggeizes' if the amplitude has the behaviour

$$\mathcal{A} \sim s^{\alpha(t)} \tag{2.1}$$

when its quantum numbers are exchanged in the t-channel [61, 62, 63, 64]. $\alpha(t)$ is known as the *trajectory* and it is equal to the spin of the particle if t has the same value as its squared mass.

In the following we are going to show a derivation of the reggeization of the gluon to all orders in perturbation theory keeping the leading $\ln s$ terms at each order [65, 66, 17, 67, 68, 69]. We will select the diagrams in which the exchanged quantum numbers in the t-channel are spin-1 and colour octet, corresponding to gluon exchange.

2.1.1 Tree level

Let us consider quark-quark scattering in the Regge limit [70]. The tree level amplitude is represented in Fig. 2.1 where p_1 and p_2 are the momenta of the incoming quarks; q is the exchanged momenta due to the strong interaction; λ and λ' are the helicities of the Dirac spinors; i, j, l and m $(= 1, 2, 3)$ are the quark colour indices; a and b $(= 1, \ldots, 8)$ are the gluon colour indices and, finally, μ and ν are Lorentz indicators.

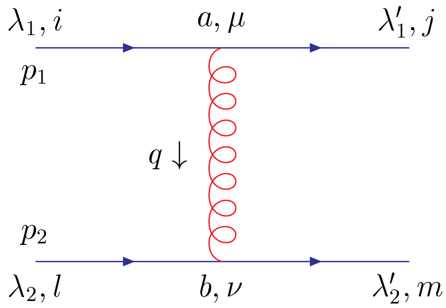

Figure 2.1: Simplest diagram contributing to leading order octet exchange

For simplicity we will use the Feynman gauge for gluon propagators. The amplitude at tree level then reads

$$\begin{aligned} \mathcal{A}^{(0)}_{2\to 2} &= \bar{u}_{\lambda'_1}(p_1 - q)\left(-ig_s\gamma^\mu \mathbf{T}^a_{ij}\right)u_{\lambda_1}(p_1) \\ &\quad \left(\frac{-i\delta_{ab}g_{\mu\nu}}{q^2}\right)\bar{u}_{\lambda'_2}(p_2 + q)\left(-ig_s\gamma^\nu \mathbf{T}^b_{lm}\right)u_{\lambda_2}(p_2), \end{aligned} \tag{2.2}$$

where $\mathbf{T}^a_{ij}$ are the $SU(N_c)$ colour matrices in the fundamental representation.

Now, as we are interested in the kinematic region where $s \gg -t$, we can simplify this amplitude. First, we want to work in the centre-of-mass frame and we choose our coordinates such that p_1 and p_2 lie on the z-axis

$$\begin{aligned} p_1 &= \frac{\sqrt{s}}{2}(1, \mathbf{0}, 1), \\ p_2 &= \frac{\sqrt{s}}{2}(1, \mathbf{0}, -1). \end{aligned}$$

Second, we express the momentum carried by the gluon propagator, q, in its Sudakov representation

$$q^\mu = zp_1^\mu + \bar{z}p_2^\mu + \mathbf{q}^\mu = \left(\frac{\sqrt{s}}{2}(z + \bar{z}), \mathbf{q}, \frac{\sqrt{s}}{2}(z - \bar{z})\right).$$

Notice how the momentum transferred, q, is related to the Lorentz invariant Mandelstam variable t

$$t = q^2 = z\bar{z}s - \mathbf{q}^2.$$

This and the on-mass-shell constraint for the outgoing quarks allows us to write

$$(p_1 - q)^2 = t - s\bar{z} = 0,$$

$$(p_2 + q)^2 = t + sz = 0,$$

leading to

$$q^\mu = -\frac{t}{s}(p_1^\mu - p_2^\mu) + \mathbf{q}^\mu \;\simeq\; \mathbf{q}^\mu$$

in the Regge limit. The third ingredient is the *eikonal approximation* which states that the components of the exchanged gauge particle momentum are small compared with the ones from the emitting parton ('soft emission'). In our case this means that the incoming quarks do not suffer any appreciable recoil after emitting and absorbing the various exchanged particles. With this in mind we can write

$$\mathcal{A}^{(0)}_{2\to 2} = i g_s^2 \frac{1}{q^2}\left(\bar{u}_{\lambda_1'}(p_1)\gamma^\mu u_{\lambda_1}(p_1)\right)\left(\bar{u}_{\lambda_2'}(p_2)\gamma_\mu u_{\lambda_2}(p_2)\right)\mathbf{T}^a_{ij}\mathbf{T}^a_{lm}. \tag{2.3}$$

Now, using the normalisation

$$\bar{u}_\alpha(p)u_\beta(p) = 2m\delta_{\alpha\beta}$$

and the Dirac equation for on-mass-shell spinors

$$(\not{p} - m)u = 0,$$

we have

$$\bar{u}_\alpha(p)\gamma^\mu u_\beta(p) = \frac{m}{p_\mu}\bar{u}_\alpha(p)u_\beta(p) = 2p^\mu\delta_{\alpha\beta}.$$

Finally, neglecting the masses of the quarks and setting $\alpha_s = g_s^2/4\pi$, the expression for the amplitude is

$$\mathcal{A}^{(0)}_{2\to 2} = i 8\pi\alpha_s \frac{s}{t}\delta_{\lambda_1\lambda_1'}\delta_{\lambda_2\lambda_2'}\mathbf{T}^a_{ij}\mathbf{T}^a_{lm}. \tag{2.4}$$

This result is gauge invariant within our eikonal approximation.

2.1.2 One-loop

At leading order approximation and in covariant gauges the one-loop contributions come from those Feynman diagrams without corrections to vertices or propagators. In the following we calculate the amplitude for the graph in Fig. 2.2.

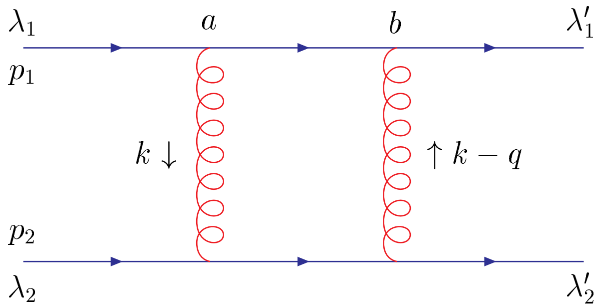

Figure 2.2: First graph contributing to one-loop corrections

A direct way of obtaining this amplitude is to apply the Feynman rules and to calculate the loop-momentum integral with the technology of the Feynman parameters. Instead we will use the *Cutkosky rules* which are more convenient, especially for higher order corrections. These rules allow us to write the imaginary part of our amplitude in terms of the one calculated at tree level

$$\begin{aligned}
\mathrm{Im}\mathcal{A}^{(1)(2.2)}_{2\to 2} &= \frac{1}{2(2\pi)^2}\int d^4k\ \delta\left((p_1-k)^2\right)\delta\left((p_2+k)^2\right)\mathcal{A}^{(0)}_{2\to 2}(k)\mathcal{A}^{(0)\dagger}_{2\to 2}(k-q)\\
&= 4\alpha_s^2 s\ \delta_{\lambda_1\lambda_1'}\delta_{\lambda_2\lambda_2'}(\mathbf{T}^b\mathbf{T}^a\otimes\mathbf{T}^b\mathbf{T}^a)\\
&\qquad\int dz\ d\bar{z}\ d\mathbf{k}\ \delta\left(\bar{z}(z-1)s+\mathbf{k}^2\right)\delta\left(z(\bar{z}+1)s-\mathbf{k}^2\right)\frac{1}{\mathbf{k}^2}\frac{1}{(\mathbf{k}-\mathbf{q})^2}\\
&= 4\alpha_s^2 s\ \delta_{\lambda_1\lambda_1'}\delta_{\lambda_2\lambda_2'}(\mathbf{T}^b\mathbf{T}^a\otimes\mathbf{T}^b\mathbf{T}^a)\int d\mathbf{k}\ \frac{1}{\mathbf{k}^2}\frac{1}{(\mathbf{k}-\mathbf{q})^2},
\end{aligned}\tag{2.5}$$

where, as before, we have used a Sudakov decomposition of the variable k

$$k^\mu = zp_1^\mu + \bar{z}p_2^\mu + \mathbf{k}^\mu,$$

for which

$$d^4k = \frac{s}{2}\ dz\ d\bar{z}\ d\mathbf{k}.$$

Taking into account that we are looking for the leading logarithm $\ln(s/t)$ in the amplitude and that s/t is negative we can write

$$\mathcal{A} = \mathrm{Re}\mathcal{A} + i\ \mathrm{Im}\mathcal{A} = \mathcal{C}\ln\frac{s}{t} + \cdots = \mathcal{C}\ln\left|\frac{s}{t}\right| - i\ \pi\ \mathcal{C},$$

so that

$$\mathrm{Re}\mathcal{A} = -\frac{1}{\pi}\mathrm{Im}\mathcal{A}\ln\left|\frac{s}{t}\right|.$$

In our particular problem

$$\mathrm{Re}\mathcal{A}^{(1)(2.2)}_{2\to 2} = -\frac{4}{\pi}\alpha_s^2 s\ \delta_{\lambda_1\lambda_1'}\delta_{\lambda_2\lambda_2'}(\mathbf{T}^b\mathbf{T}^a\otimes\mathbf{T}^b\mathbf{T}^a)\int d\mathbf{k}\ \frac{1}{\mathbf{k}^2}\frac{1}{(\mathbf{k}-\mathbf{q})^2}\ln\left|\frac{s}{t}\right|. \quad (2.6)$$

There is another contribution to consider coming from the 'crossed' diagram of Fig. 2.3. This one is easy to calculate because it corresponds to interchanging s by u in the previous amplitude and calculating a new colour factor, i.e.

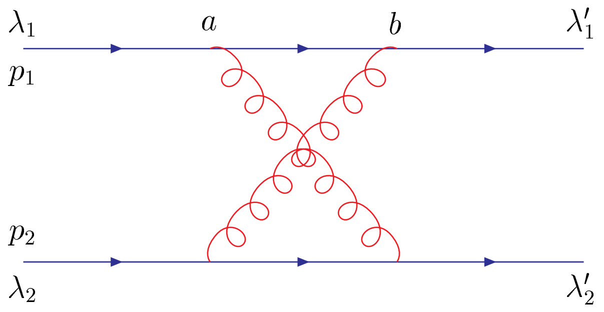

Figure 2.3: Second graph contributing to one-loop corrections

$$\mathrm{Re}\mathcal{A}^{(1)(2.3)}_{2\to 2} = -\frac{4}{\pi}\alpha_s^2 u\ \delta_{\lambda_1\lambda_1'}\delta_{\lambda_2\lambda_2'}(\mathbf{T}^b\mathbf{T}^a\otimes\mathbf{T}^a\mathbf{T}^b)\int d\mathbf{k}\ \frac{1}{\mathbf{k}^2}\frac{1}{(\mathbf{k}-\mathbf{q})^2}\ln\left|\frac{u}{t}\right|. \quad (2.7)$$

In the Regge limit u can be approximated by $-s$ so we can write for the whole amplitude

$$\begin{aligned}\mathrm{Re}\mathcal{A}^{(1)}_{2\to 2} &= \mathrm{Re}\mathcal{A}^{(1)(2.2)}_{2\to 2} + \mathrm{Re}\mathcal{A}^{(1)(2.3)}_{2\to 2}\\ &= \frac{4}{\pi}\alpha_s^2 s\ \delta_{\lambda_1\lambda_1'}\delta_{\lambda_2\lambda_2'}\int d\mathbf{k}\ \frac{1}{\mathbf{k}^2}\frac{1}{(\mathbf{k}-\mathbf{q})^2}\ln\left|\frac{s}{t}\right|\left(\mathbf{T}^b\mathbf{T}^a\otimes\left[\mathbf{T}^a,\mathbf{T}^b\right]\right). \quad (2.8)\end{aligned}$$

The colour factor is pure octet, i.e. it can be related to the tree level one by

$$\mathbf{T}^b\mathbf{T}^a\otimes\left[\mathbf{T}^a,\mathbf{T}^b\right] = -\frac{i^2}{2}f_{bac}f_{bad}\mathbf{T}^d\otimes\mathbf{T}^c = -i^2\frac{N_c}{2}\delta_{cd}\mathbf{T}^d\otimes\mathbf{T}^c = \frac{N_c}{2}\mathbf{T}^d\otimes\mathbf{T}^d,$$

therefore

$$\mathrm{Re}\mathcal{A}^{(1)}_{2\to 2} = \frac{2}{\pi}N_c\ \alpha_s^2\ s\ \delta_{\lambda_1\lambda_1'}\delta_{\lambda_2\lambda_2'}\int d\mathbf{k}\ \frac{1}{\mathbf{k}^2}\frac{1}{(\mathbf{k}-\mathbf{q})^2}\ln\left|\frac{s}{t}\right|\mathbf{T}^a\otimes\mathbf{T}^a. \quad (2.9)$$

Finally, we can write the one-loop amplitude in terms of the tree level result as

$$\mathcal{A}^{(1)}_{2\to 2} = \frac{N_c\ \alpha_s}{4\pi^2}\int d\mathbf{k}\ \frac{t}{\mathbf{k}^2(\mathbf{k}-\mathbf{q})^2}\ln\left(\frac{s}{t}\right)\mathcal{A}^{(0)}_{2\to 2}, \quad (2.10)$$

which we rewrite as

$$\mathcal{A}^{(1)}_{2\to 2} = \epsilon(t)\ln\left(\frac{s}{t}\right)\mathcal{A}^{(0)}_{2\to 2}, \tag{2.11}$$

for convenience in future sections.

2.1.3 Two-loops

Once again in leading accuracy we do not need to consider diagrams with corrections to vertices or with self-energy insertions. With the graphs in Fig. 2.4 we will be able to partially reconstruct the imaginary part of the amplitude. This will be fully built if we add the other contributions coming from those diagrams in Fig. 2.5.

For the first set of diagrams (Fig. 2.4) we can now proceed in the same way as in the previous section using the Sudakov parametrisation

$$k_i^\mu = z_i p_1^\mu + \bar{z}_i p_2^\mu + \mathbf{k}_i^\mu$$

for the internal gluon momenta and restricting ourselves to the leading logarithm region

$$z_2 \ll z_1 \ll 1$$
$$|\bar{z}_1| \ll |\bar{z}_2| \ll 1,$$

we get the following expression for the amplitude

$$\begin{aligned}\mathcal{A}^{(2)2.4\mu}_{2\to 3} &= -\frac{2isg^3}{\mathbf{k}_1^2\mathbf{k}_2^2}\,\delta_{\lambda_1\lambda_1'}\delta_{\lambda_2\lambda_2'}\left[\left(z_1+\frac{2\mathbf{k}_1^2}{\bar{z}_2 s}\right)p_1^\mu\right.\\ &\quad\left.+\left(\bar{z}_2+\frac{2\mathbf{k}_2^2}{z_1 s}\right)p_2^\mu-(\mathbf{k}_1+\mathbf{k}_2)^\mu\right]f_{abc}\mathbf{T}^a\otimes\mathbf{T}^b,\end{aligned} \tag{2.12}$$

which carries a Lorentz index corresponding to the gluon with one end not attached to any propagator. This amplitude can be written in a very revealing way using the fact that $s = 2p_1^\alpha p_{2\alpha}$, i.e.

$$\mathcal{A}^{(2)2.4\mu}_{2\to 3} = -\frac{4ig^3p_1^\alpha p_2^\beta}{\mathbf{k}_1^2\mathbf{k}_2^2}\,\delta_{\lambda_1\lambda_1'}\delta_{\lambda_2\lambda_2'}\Lambda^\mu_{\alpha\beta}(\mathbf{k}_1,\mathbf{k}_2)f_{abc}\mathbf{T}^a\otimes\mathbf{T}^b, \tag{2.13}$$

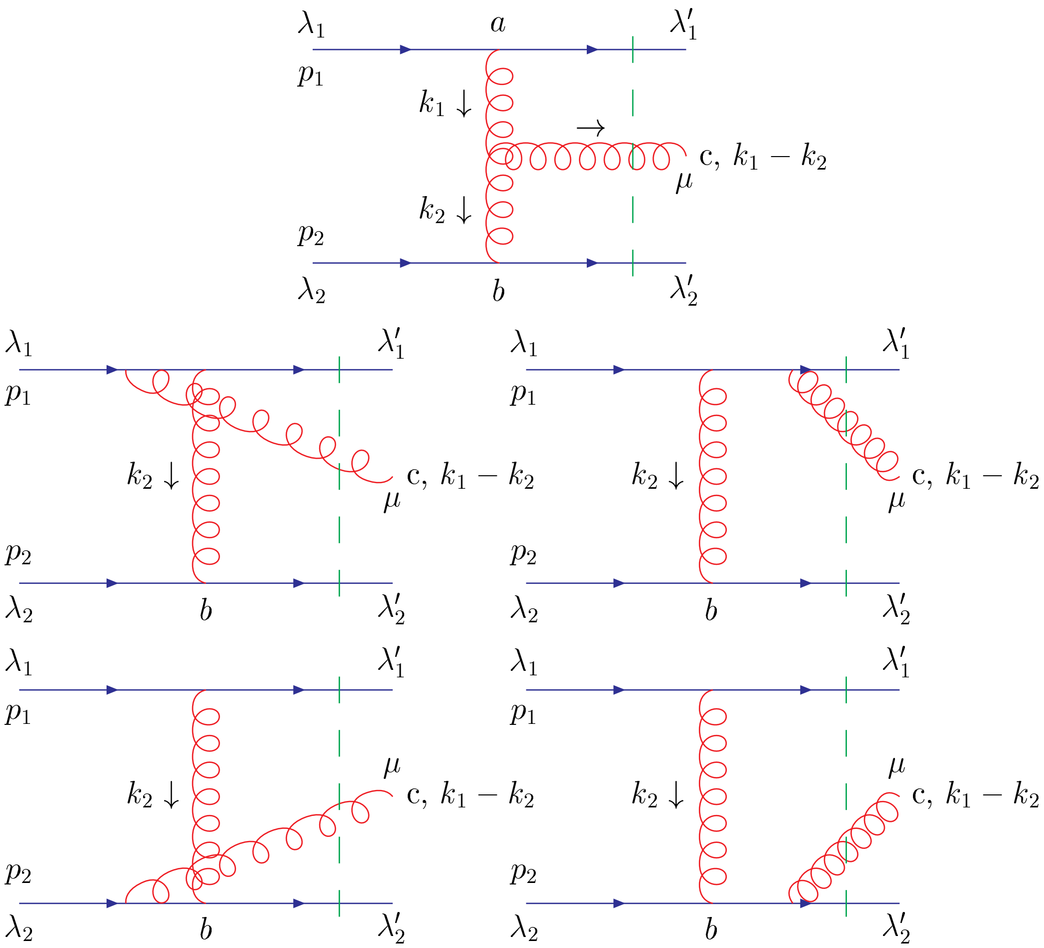

Figure 2.4: Contributions to $\mathrm{Im}\mathcal{A}^{(2)}_{2\to 2}$ at leading order

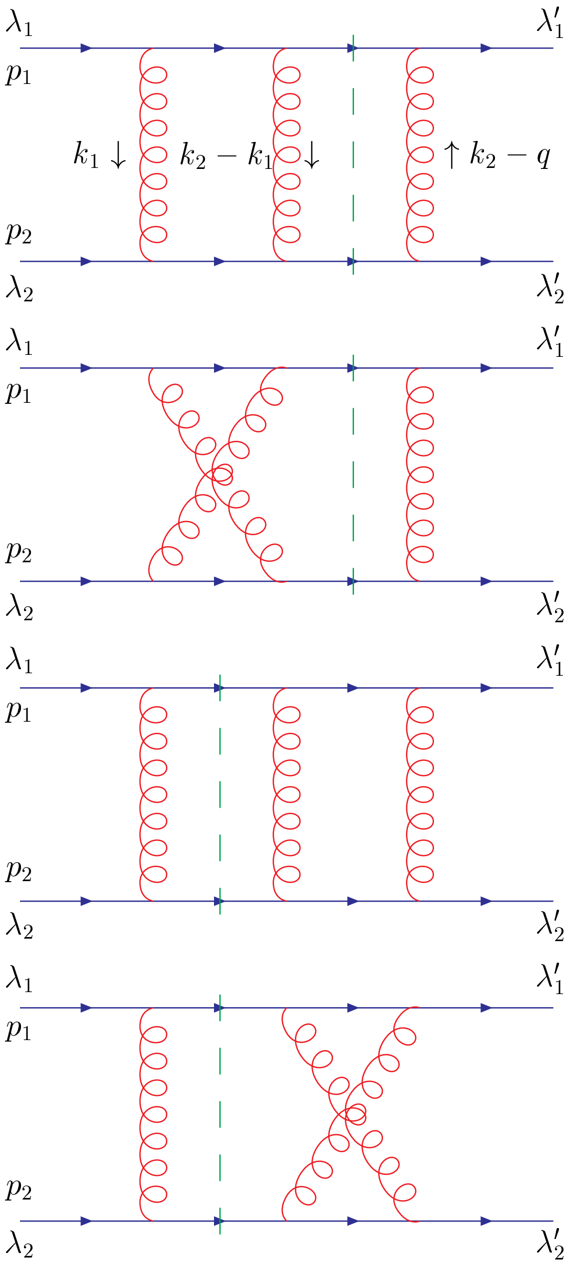

Figure 2.5: Contributions to $\mathrm{Im}\mathcal{A}^{(2)}_{2\to2}$ at leading order

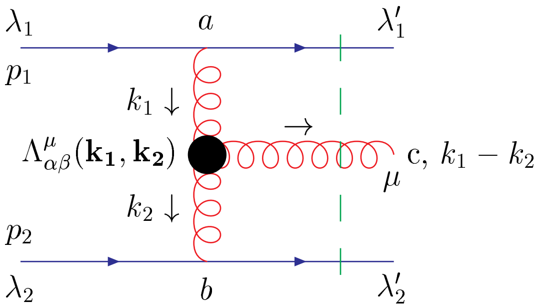

Figure 2.6: Effective vertex in the leading logarithm approximation

with

$$\Lambda^\mu_{\alpha\beta}(\mathbf{k}_1, \mathbf{k}_2) \quad = \quad \frac{2p_{1\alpha}p_{2\beta}}{s}\left[\left(z_1 + \frac{2k_1^2}{\bar{z}_2 s}\right)p_1^\mu + \left(\bar{z}_2 + \frac{2k_2^2}{z_1 s}\right)p_2^\mu - (\mathbf{k}_1 + \mathbf{k}_2)^\mu\right]$$

playing the role of an effective vertex. It can be proved that it is gauge invariant in the leading logarithm approximation and it will be represented as in Fig. 2.6.

Now we are in good shape to calculate the contribution to the imaginary part of the total amplitude from the graphs in Fig. 2.4 just by multiplying the $\mathcal{A}^{(2)2.4\mu}_{2\to3}$ amplitudes times their hermitian conjugates, summing over all possible polarisations (μ) of the intermediate gluon and integrating over the Sudakov three-body phase space with the corresponding on-shell conditions at the cut lines.

$$\begin{aligned}\mathrm{Im}\mathcal{A}^{(2)2.4}_{2\to2} \quad &= \quad -\frac{1}{2}\int\frac{1}{(2\pi)^5}\left(\frac{s}{2}\right)^2 dz_1\; dz_2\; d\bar{z}_1\; d\bar{z}_2\; d\mathbf{k}_1\; d\mathbf{k}_2 \\ &\quad \delta(-\bar{z}_1 s - \mathbf{k}_1^2)\;\delta(z_2 s - \mathbf{k}_2^2)\;\delta(-z_1\bar{z}_2 s - (\mathbf{k}_1 - \mathbf{k}_2)^2) \\ &\quad \mathcal{A}^{(2)2.4\mu}_{2\to3}(\mathbf{k}_1, \mathbf{k}_2)\;\mathcal{A}^{\dagger(2)2.4}_{2\to3\mu}(\mathbf{k}_1 - q, \mathbf{k}_2 - q).\end{aligned} \tag{2.14}$$

In the delta functions we set

$$\mathbf{k}_1^2 = \mathbf{k}_2^2 = (\mathbf{k}_1 - \mathbf{k}_2)^2 = s_0 \tag{2.15}$$

where s_0 will scale s in the terms with $\ln s$. At leading logarithm order the choice of this scale is arbitrary. The correct way of scaling s will be determined by the higher order corrections and it will be discussed later in this thesis.

After some algebra with the colour factors, integrating over the Sudakov variables and operating with the propagators we obtain

$$\begin{aligned}\mathrm{Im}\mathcal{A}^{(2)2.4}_{2\to 2} &= -\frac{N_c^2\alpha_s^2}{32\pi^3}\mathcal{A}^{(0)}_{2\to 2}\,\mathbf{q}^2\int_{s_0/s}^{1}\frac{dz_1}{z_1}d\mathbf{k}_1\,d\mathbf{k}_2\left[\frac{\mathbf{q}^2}{\mathbf{k}_1^2\mathbf{k}_2^2(\mathbf{k}_1-\mathbf{q})^2(\mathbf{k}_2-\mathbf{q})^2}\right.\\ &\left.-\frac{1}{\mathbf{k}_1^2(\mathbf{k}_1-\mathbf{k}_2)^2(\mathbf{k}_2-\mathbf{q})^2}-\frac{1}{\mathbf{k}_2^2(\mathbf{k}_1-\mathbf{k}_2)^2(\mathbf{k}_1-\mathbf{q})^2}\right].\end{aligned}\tag{2.16}$$

It is interesting to notice that the contribution from the four graphs in Fig. 2.5 is

$$\begin{aligned}\mathrm{Im}\mathcal{A}^{(2)2.5}_{2\to 2} &= -\frac{N_c^2\alpha_s^2}{32\pi^3}\mathcal{A}^{(0)}_{2\to 2}\,\mathbf{q}^2\int d\mathbf{k}_1\,d\mathbf{k}_2\\ &\left[\frac{1}{\mathbf{k}_1^2(\mathbf{k}_1-\mathbf{k}_2)^2(\mathbf{k}_2-\mathbf{q})^2}+\frac{1}{\mathbf{k}_2^2(\mathbf{k}_1-\mathbf{k}_2)^2(\mathbf{k}_1-\mathbf{q})^2}\right]\ln\frac{s}{s_0},\end{aligned}\tag{2.17}$$

because when we add both results the expression for the imaginary part of the amplitude simplifies to

$$\begin{aligned}\mathrm{Im}\mathcal{A}^{(2)}_{2\to 2} &= \mathrm{Im}\mathcal{A}^{(2)2.4}_{2\to 2}+\mathrm{Im}\mathcal{A}^{(2)2.5}_{2\to 2}\\ &= -\frac{N_c^2\alpha_s^2}{32\pi^3}\mathcal{A}^{(0)}_{2\to 2}\,(\mathbf{q}^2)^2\int\frac{d\mathbf{k}_1}{\mathbf{k}_1^2(\mathbf{k}_1-\mathbf{q})^2}\frac{d\mathbf{k}_2}{\mathbf{k}_2^2(\mathbf{k}_2-\mathbf{q})^2}\ln\frac{s}{s_0}\end{aligned}\tag{2.18}$$

which, in our notation of Eq. 2.11, can be written as

$$\mathrm{Im}\mathcal{A}^{(2)}_{2\to 2} = -\frac{\pi}{2}\mathcal{A}^{(0)}_{2\to 2}\epsilon^2(t)\ln\frac{s}{s_0}.\tag{2.19}$$

Therefore, the corresponding real part reads

$$\mathrm{Re}\mathcal{A}^{(2)}_{2\to 2} = \frac{1}{4}\mathcal{A}^{(0)}_{2\to 2}\epsilon^2(t)\ln^2\frac{s}{s_0},\tag{2.20}$$

and the total amplitude up to two loops when adding the crossed diagrams is

$$\mathcal{A}_{2\to 2} = \mathcal{A}^{(0)}_{2\to 2}\left(1+\epsilon(t)\ln\frac{s}{s_0}+\frac{1}{2}\epsilon^2(t)\ln^2\frac{s}{s_0}+\cdots\right).\tag{2.21}$$

2.1.4 All-loops

This last result is encouraging because it looks like the first three terms in the Taylor expansion of $\mathcal{A}^{(0)}_{2\to 2}s^{\epsilon(t)}$. We will show now that this in fact the case. We are going to skip many of the technical details but it is natural to think that to calculate the all-loops amplitude we can use the effective vertex derived in Eq. 2.13. Iterating as shown

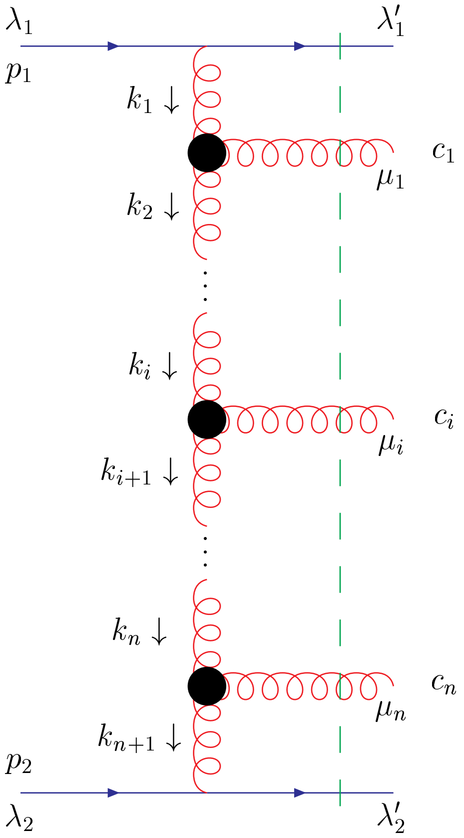

Figure 2.7: $q+q \to q+q+n$ gluons amplitude in the leading logarithm approximation at tree level

in Fig. 2.7 we can get the amplitude for octet exchange in $q+q \to q+q+n$ gluons. The extra ingredients are the propagators for the vertical gluons and the generalisation of the leading order kinematic inequalities

$$\frac{s_0}{s} \ll z_{i+1} \ll z_i \ll 1$$
$$\frac{s_0}{s} \ll |\bar{z}_i| \ll |\bar{z}_{i+1}| \ll 1.$$

The result for the amplitude in Fig. 2.7 is

$$\begin{aligned}\mathcal{A}^{(n)\mu_1\cdots\mu_n}_{2\to 2+n} &= -2sg_s^{2+n}\,\delta_{\lambda_1\lambda'_1}\delta_{\lambda_2\lambda'_2}\frac{1}{\mathbf{k}_1^2}\prod_{i=1}^{n} f_{a_i a_{i+1} c_i}\mathbf{T}^{a_1}\otimes\mathbf{T}^{a_{n+1}} \\ &\quad \prod_{j=1}^{n}\left[\frac{2p_1^{\alpha_j}p_2^{\beta_{j+1}}}{s}\Lambda^{\mu_j}_{\alpha_j\beta_{j+1}}(k_j,k_{j+1})\frac{i}{\mathbf{k}_{j+1}^2}\right],\end{aligned} \tag{2.22}$$

with c_i being the colour indices of the s-channel gluons.

In order to get the imaginary part of the octet exchange amplitude we should proceed as usual multiplying the last result by the hermitian conjugate and integrating over momenta. But before that we should not forget the generalisation of those terms in Fig. 2.5. The effect of these terms to all orders is to modify the propagators of the ith vertical gluons in the following way (in Feynman gauge)

$$\frac{ig_{\mu\nu}}{\mathbf{k}_i^2} \to \frac{ig_{\mu\nu}}{\mathbf{k}_i^2}\left(\frac{z_{i-1}}{z_i}\right)^{\epsilon(k_i^2)}.$$

The best method to prove this result is by induction. We will assume that this modification of the propagator is valid to all orders and we will arrive at an integral equation. The solution to this equation will prove to be self-consistent with the initial assumption. This guess is known as *reggeization* of the gluon propagator and the whole procedure as a *bootstrap* method.

Our amplitude then reads

$$\begin{aligned}\mathcal{A}_{2\to 2+n}^{(n)\mu_1\cdots\mu_n} &= -2sg_s^{2+n}\;\delta_{\lambda_1\lambda_1'}\delta_{\lambda_2\lambda_2'}\frac{1}{\mathbf{k}_1^2}\left(\frac{1}{z_1}\right)^{\epsilon(k_1^2)}\prod_{i=1}^{n} f_{a_ia_{i+1}c_i}\mathbf{T}^{a_1}\otimes\mathbf{T}^{a_{n+1}}\\ &\quad\prod_{j=1}^{n}\left[\frac{2p_1^{\alpha_j}p_2^{\beta_{j+1}}}{s}\Lambda^{\mu_j}_{\alpha_j\beta_{j+1}}(k_j,k_{j+1})\frac{i}{\mathbf{k}_{j+1}^2}\left(\frac{z_j}{z_{j+1}}\right)^{\epsilon(k_{j+1}^2)}\right],\end{aligned} \tag{2.23}$$

and is known as *multi-Regge exchange* amplitude.

Finally, the imaginary part of the amplitude to all orders is

$$\begin{aligned}\mathrm{Im}\mathcal{A}_{2\to 2}^{\mathrm{Octet}} &= \frac{1}{2}\sum_{n=0}^{\infty}(-1)^n\frac{1}{2^{4n+3}\pi^{3n+2}}\prod_{i=1}^{n}\int_{z_i+1}^{1}\frac{dz_i}{z_i}\prod_{j=1}^{n+1}d^2\mathbf{k}_j dz_{n+1}\delta(sz_{n+1}-s_0)\\ &\quad\mathcal{A}_{2\to 2+n}^{(n)\mu_1\cdots\mu_n}(\mathbf{k}_1,\ldots,\mathbf{k}_n)\;\mathcal{A}^{\dagger(n)}_{2\to 2+n\;\mu_1\cdots\mu_n}(\mathbf{k}_1-\mathbf{q},\ldots,\mathbf{k}_n-\mathbf{q}).\end{aligned} \tag{2.24}$$

It is possible to express this result as an integral equation if we perform a Mellin transform with respect to s/s_0. The solution can be found and reads

$$\mathrm{Im}\mathcal{A}_{2\to 2}^{\mathrm{Octet}} = -\frac{\pi}{2}\epsilon(t)\left(\frac{s}{s_0}\right)^{\epsilon(t)}\mathcal{A}_{2\to 2}^{(0)}. \tag{2.25}$$

The last step is to add the crossed diagrams and we arrived at

$$\mathcal{A}_{2\to 2}^{\mathrm{Octet}} = 8\pi\alpha_s\frac{s_0}{t}\mathbf{T}^a\otimes\mathbf{T}^a\;\delta_{\lambda_1\lambda_1'}\delta_{\lambda_2\lambda_2'}\left(\frac{s}{s_0}\right)^{1+\epsilon(t)}\frac{1-e^{i\pi(1+\epsilon(t))}}{2}. \tag{2.26}$$

This result proves the consistency of the bootstrap condition and shows the reggeization of the gluon as in the expression 2.1 with

$$\alpha(t) = 1 + \epsilon(t) \tag{2.27}$$

the gluon trajectory.

2.2 The BFKL equation

Given that we have been able to prove the reggeization of the gluon would it be possible to find a particle with the quantum numbers of the vacuum that reggeizes? This would give us the Pomeron trajectory. The answer is that, as we need a colour singlet exchange, there are no basic constituents in QCD to solve our problem.

A way out is to build singlet exchanges with at least two gluons exchanged in the t-channel. The advantage of this model is that we have all the calculations done from the previous section, the octet exchange, the only differences come from the colour factors. At the end of this section we will obtain an integral equation for the Pomeron amplitude which is known as the Balitsky, Fadin, Kuraev, Lipatov (BFKL) equation. Again the calculations will be performed in the leading logarithm approximation.

2.2.1 One-loop

For a singlet exchange the lowest order diagrams are those in Fig. 2.2 and Fig. 2.3. The amplitude is very similar to that in Eq. 2.5 but changing the colour factor, i.e.

$$\mathrm{Im}\mathcal{A}_{2\to 2}^{(1)(2.2)} + \mathrm{Im}\mathcal{A}_{2\to 2}^{(1)(2.3)} = 4\alpha_s^2 s\; \delta_{\lambda_1\lambda_1'}\delta_{\lambda_2\lambda_2'}(\frac{N_c^2-1}{4N_c^2})\int d\mathbf{k}\;\frac{1}{\mathbf{k}^2}\frac{1}{(\mathbf{k}-\mathbf{q})^2}. \tag{2.28}$$

From Eq. 2.6 and Eq. 2.7 it can be seen that the real part of this amplitude turns out to be zero leaving a purely imaginary one-loop amplitude

$$\mathcal{A}_{2\to 2}^{(1)} \;=\; i4\alpha_s^2 s\; \delta_{\lambda_1\lambda_1'}\delta_{\lambda_2\lambda_2'}(\frac{N_c^2-1}{4N_c^2})\int d\mathbf{k}\;\frac{1}{\mathbf{k}^2}\frac{1}{(\mathbf{k}-\mathbf{q})^2}. \tag{2.29}$$

2.2.2 Two-loops

The next order of perturbation theory requires to add those contributions from diagrams 2.4 and 2.5. Their amplitudes are

$$\mathcal{A}^{(2)2.4}_{2\to2} = -i\frac{2N_c\alpha_s^3 s}{\pi^2}\,\delta_{\lambda_1\lambda_1'}\delta_{\lambda_2\lambda_2'}(\frac{N_c^2-1}{4N_c^2})\ \ln\frac{s}{s_0}\int d\mathbf{k}_1\ d\mathbf{k}_2\left[\frac{\mathbf{q}^2}{\mathbf{k}_1^2\mathbf{k}_2^2(\mathbf{k}_1-\mathbf{q})^2(\mathbf{k}_2-\mathbf{q})^2}\right.$$
$$\left.-\frac{1}{\mathbf{k}_1^2(\mathbf{k}_1-\mathbf{k}_2)^2(\mathbf{k}_2-\mathbf{q})^2}-\frac{1}{\mathbf{k}_2^2(\mathbf{k}_1-\mathbf{k}_2)^2(\mathbf{k}_1-\mathbf{q})^2}\right], \tag{2.30}$$

and

$$\mathcal{A}^{(2)2.5}_{2\to2} = -i\frac{N_c\alpha_s^3 s}{\pi^2}\,\delta_{\lambda_1\lambda_1'}\delta_{\lambda_2\lambda_2'}(\frac{N_c^2-1}{4N_c^2})\ \ln\frac{s}{s_0}\int d\mathbf{k}_1\ d\mathbf{k}_2$$
$$\left[\frac{1}{\mathbf{k}_1^2(\mathbf{k}_1-\mathbf{k}_2)^2(\mathbf{k}_2-\mathbf{q})^2}+\frac{1}{\mathbf{k}_2^2(\mathbf{k}_1-\mathbf{k}_2)^2(\mathbf{k}_1-\mathbf{q})^2}\right]. \tag{2.31}$$

Unfortunately in this case we do not get a very simplified expression for the imaginary part of the amplitude to order α_s^3

$$\mathrm{Im}\mathcal{A}^{(2)}_{2\to2} = -\frac{2N_c\alpha_s^3 s}{\pi^2}\,\delta_{\lambda_1\lambda_1'}\delta_{\lambda_2\lambda_2'}(\frac{N_c^2-1}{4N_c^2})\ \ln\frac{s}{s_0}\int d\mathbf{k}_1\ d\mathbf{k}_2\left[\frac{\mathbf{q}^2}{\mathbf{k}_1^2\mathbf{k}_2^2(\mathbf{k}_1-\mathbf{q})^2(\mathbf{k}_2-\mathbf{q})^2}\right.$$
$$\left.-\frac{1}{2\mathbf{k}_1^2(\mathbf{k}_1-\mathbf{k}_2)^2(\mathbf{k}_2-\mathbf{q})^2}-\frac{1}{2\mathbf{k}_2^2(\mathbf{k}_1-\mathbf{k}_2)^2(\mathbf{k}_1-\mathbf{q})^2}\right]. \tag{2.32}$$

2.2.3 All-loops

Before going to the all orders derivation it is easier if we work in the Mellin space. Let us define $f_\omega(\mathbf{k}_1,\mathbf{k}_2,\mathbf{q})$ as

$$\int_1^\infty d\left(\frac{s}{s_0}\right)\ \left(\frac{s}{s_0}\right)^{-\omega-1}\frac{\mathcal{A}(s,t)}{s} =$$
$$i4\alpha_s^2\,\delta_{\lambda_1\lambda_1'}\delta_{\lambda_2\lambda_2'}(\frac{N_c^2-1}{4N_c^2})\int d\mathbf{k}_1\ d\mathbf{k}_2\frac{f_\omega(\mathbf{k}_1,\mathbf{k}_2,\mathbf{q})}{\mathbf{k}_2^2(\mathbf{k}_1-\mathbf{q})^2} \tag{2.33}$$

the Mellin transform of a general amplitude $\mathcal{A}(s,t)$.

Hence, for our one-loop amplitude we have

$$f^{(1)}_\omega(\mathbf{k}_1,\mathbf{k}_2,\mathbf{q}) = \frac{1}{\omega}\delta^2(\mathbf{k}_1-\mathbf{k}_2), \tag{2.34}$$

and for the one at two-loops

$$f_\omega^{(2)}(\mathbf{k}_1,\mathbf{k}_2,\mathbf{q}) = -\frac{N_c\alpha_s}{2\pi^2\omega^2}\left[\frac{\mathbf{q}^2}{\mathbf{k}_1^2(\mathbf{k}_2-\mathbf{q})^2} - \frac{1}{2(\mathbf{k}_1-\mathbf{k}_2)^2}\left(1+\frac{\mathbf{k}_2^2(\mathbf{k}_1-\mathbf{q})^2}{\mathbf{k}_1^2(\mathbf{k}_2-\mathbf{q})^2}\right)\right]. \quad (2.35)$$

With this information in our hands we can create our all-loops ladder with reggeized gluons in the vertical propagators and their couplings to the gluons in the s-channel as our effective vertices of the previous section. With these elements we build the integral equation for $f_\omega(\mathbf{k}_1,\mathbf{k}_2,\mathbf{q})$, the so called BFKL equation

$$\begin{aligned}\omega f_\omega(\mathbf{k}_1,\mathbf{k}_2,\mathbf{q}) &= \delta^2(\mathbf{k}_1-\mathbf{k}_2)\\ &+\frac{\bar{\alpha}_s}{2\pi}\int d\mathbf{l}\left\{\frac{-\mathbf{q}^2}{(\mathbf{l}-\mathbf{q})^2\mathbf{k}_1^2}\,f_\omega(\mathbf{l},\mathbf{k}_2,\mathbf{q}) + \frac{1}{(\mathbf{l}-\mathbf{k}_1)^2}\left(f_\omega(\mathbf{l},\mathbf{k}_2,\mathbf{q}) - \frac{\mathbf{k}_1^2\,f_\omega(\mathbf{k}_1,\mathbf{k}_2,\mathbf{q})}{\mathbf{l}^2+(\mathbf{k}_1-\mathbf{l})^2}\right.\right.\\ &\left.\left.+\frac{(\mathbf{k}_1-\mathbf{q})^2\mathbf{l}^2 f_\omega(\mathbf{l},\mathbf{k}_2,\mathbf{q})}{(\mathbf{l}-\mathbf{q})^2\mathbf{k}_1^2} - \frac{(\mathbf{k}_1-\mathbf{q})^2 f_\omega(\mathbf{k}_1,\mathbf{k}_2,\mathbf{q})}{(\mathbf{l}-\mathbf{q})^2+(\mathbf{k}_1-\mathbf{l})^2}\right)\right\}, \end{aligned}\quad (2.36)$$

where we have defined $\bar{\alpha}_s = N_c\alpha_s/\pi$.

This equation has a simpler expression for zero momentum transfer ($\mathbf{q}=0$) which is the relevant one for the forward scattering amplitude and the total cross section

$$\omega f_\omega(\mathbf{k}_1,\mathbf{k}_2) = \delta^2(\mathbf{k}_1-\mathbf{k}_2) + \frac{\bar{\alpha}_s}{\pi}\int\frac{d\mathbf{l}}{(\mathbf{l}-\mathbf{k}_1)^2}\left(f_\omega(\mathbf{l},\mathbf{k}_2) - \frac{\mathbf{k}_1^2\,f_\omega(\mathbf{k}_1,\mathbf{k}_2)}{\mathbf{l}^2+(\mathbf{k}_1-\mathbf{l})^2}\right). \quad (2.37)$$

2.3 Solution to the BFKL equation at leading order for forward scattering

It is useful to write the BFKL equation for zero momentum transfer in the following way

$$\omega f_\omega(\mathbf{k}_1,\mathbf{k}_2) \;=\; \delta^2(\mathbf{k}_1-\mathbf{k}_2) + \int d\mathbf{l}\;\mathcal{K}(\mathbf{k}_1,\mathbf{l})f_\omega(\mathbf{l},\mathbf{k}_2), \quad (2.38)$$

where $\mathcal{K}(\mathbf{k},\mathbf{l})$ is the kernel of the integral equation. It can be written in terms of the contributions from real and virtual gluon emissions as

$$\mathcal{K}(\mathbf{k},\mathbf{l}) \;=\; \mathcal{K}_{\rm real}(\mathbf{k},\mathbf{l}) + \mathcal{K}_{\rm virtual}(\mathbf{k},\mathbf{l}), \quad (2.39)$$

with

$$\begin{aligned}\mathcal{K}_{\rm real}(\mathbf{k},\mathbf{l}) &= \frac{\bar{\alpha}_s}{\pi}\frac{1}{(\mathbf{k}-\mathbf{l})^2}, \\ \mathcal{K}_{\rm virtual}(\mathbf{k},\mathbf{l}) &= -\frac{\bar{\alpha}_s}{2\pi}\int\frac{d\mathbf{q}}{\mathbf{q}^2}\frac{\mathbf{k}^2}{(\mathbf{q}-\mathbf{k})^2}\delta^2(\mathbf{k}-\mathbf{l}).\end{aligned} \tag{2.40}$$

This inhomogeneous integral equation has a self-adjoint kernel and the solution to the corresponding homogeneous equation can be expressed in terms of a Fourier expansion

$$f_\omega(\mathbf{k}_1,\mathbf{k}_2) = \sum_{n=-\infty}^{\infty}\int_{-\infty}^{\infty} d\nu\; a(\nu,n)e^{i\nu(\lambda_1-\lambda_2)}e^{in(\phi_1-\phi_2)}, \tag{2.41}$$

with $\lambda_{1,2} = \ln(\mathbf{k}_{1,2}^2/s_0)$, s_0 being a scale factor, and $\phi_1-\phi_2$ the azimuthal angle between $\mathbf{k}_1$ and $\mathbf{k}_2$. Using a suitable integral representation of the inhomogeneous term (the delta function) and taking the function $\omega(\nu,n)$ as the eigenvalue of the homogeneous equation the solution can be written as

$$f_\omega(\mathbf{k}_1,\mathbf{k}_2) = \frac{1}{2\pi^2}\frac{1}{\mathbf{k}_1\mathbf{k}_2}\sum_{n=-\infty}^{\infty}\int_{-\infty}^{\infty} d\nu\frac{1}{\omega-\omega(\nu,n)}e^{i\nu(\lambda_1-\lambda_2)}e^{in(\phi_1-\phi_2)}. \tag{2.42}$$

The spectrum of eigenvalues can be found if we insert the last equation into the homogeneous expression getting the formula [71]

$$\omega(\nu,n) = \bar{\alpha}_s\left(2\mathcal{R}e\int_0^1 dx\frac{x^{\frac{|n|-1}{2}+i\nu}}{1-x} - \int_0^1 dx\frac{1}{1-x} - \int_0^1 dx\frac{1}{2x}\right), \tag{2.43}$$

with x being defined as

$$x = \frac{\mathbf{k}_1^2}{\mathbf{l}^2}\Theta(\mathbf{l}^2-\mathbf{k}_1^2) + \frac{\mathbf{l}^2}{\mathbf{k}_1^2}\Theta(\mathbf{k}_1^2-\mathbf{l}^2). \tag{2.44}$$

There are infrared divergences at $\mathbf{l}^2 = 0$ and $(\mathbf{k}_1-\mathbf{l})^2 = 0$ which can be regulated by an infrared cutoff and, by shifting the first divergence to $(\mathbf{k}_1-\mathbf{l})^2 = 0$, we obtain a well behaved spectrum

$$\omega(\nu,n) = 2\bar{\alpha}_s\left(\mathcal{R}e\int_0^1 dx\frac{x^{\frac{|n|-1}{2}+i\nu}}{1-x} - \int_0^1 dx\frac{1}{1-x}\right). \tag{2.45}$$

This can be rewritten in terms of the logarithmic derivative of the Γ function

$$\frac{d\ln\Gamma(z)}{dz} = \psi(z) = \int_0^1 dx\frac{x^{z-1}-1}{x-1} - \gamma, \tag{2.46}$$

where $\gamma = 0.577215...$ is the Euler-Mascheroni constant. The final form for the eigenvalue is

$$\omega(\nu, n) = -2\bar{\alpha}_s \mathcal{R}e \left[\psi\left(\frac{|n|+1}{2} + i\nu\right) + \gamma \right], \tag{2.47}$$

and all the infrared and ultraviolet divergences have cancelled out.

The leading logarithm behaviour can be found by taking the singularity with the largest real part in the ω-plane of the expression Eq. 2.42. The largest values of the eigenvalue 2.47 are at $|n| = 0$. In this case we can get the useful expansion for small ν

$$\omega(\nu, n=0) = 2\bar{\alpha}_s \left(2\ln 2 + \sum_{k=1}^{\infty} (-1)^k (2^{2k+1} - 1)\zeta(2k+1)\nu^{2k} \right), \tag{2.48}$$

with $\zeta(k)$ the Riemann ζ-function. Within this approximation we can write

$$f_\omega(\mathbf{k}_1, \mathbf{k}_2) \simeq \frac{1}{\pi} \frac{1}{\mathbf{k}_1 \mathbf{k}_2} \int_{-\infty}^{\infty} \frac{d\nu}{2\pi} \left(\frac{\mathbf{k}_1^2}{\mathbf{k}_2^2} \right)^{i\nu} \frac{1}{\omega - \omega_0 + a^2\nu^2}, \tag{2.49}$$

where $\omega_0 = \bar{\alpha}_s 4 \ln 2$ is the position of the branch point of the cut generated by the continuous function in ν and the constant a^2 is equal to $\bar{\alpha}_s 14\zeta(3)$. Performing the contour integration the solution reads

$$f_\omega(\mathbf{k}_1, \mathbf{k}_2) \simeq \frac{1}{2\pi a} \frac{1}{\mathbf{k}_1 \mathbf{k}_2} \left(\frac{\mathbf{k}_1 \mathbf{k}_2}{\max(\mathbf{k}_1^2, \mathbf{k}_2^2)} \right)^{\frac{\sqrt{\omega - \omega_0}}{a}} \frac{1}{\sqrt{\omega - \omega_0}}. \tag{2.50}$$

The final answer for the quark-quark forward elastic scattering amplitude is obtained using the expression 2.33 and reads

$$\begin{aligned} \frac{\mathcal{A}(s, t=0)}{s} &\simeq i4\alpha_s^2\, \delta_{\lambda_1 \lambda_1'} \delta_{\lambda_2 \lambda_2'} \left(\frac{N_c^2 - 1}{4N_c^2}\right) \\ &\int \frac{d\mathbf{k}_1}{\mathbf{k}_1^2} \frac{d\mathbf{k}_2}{\mathbf{k}_2^2} \frac{1}{\sqrt{\mathbf{k}_1^2 \mathbf{k}_2^2}} \frac{1}{2\pi a} \frac{1}{\sqrt{\pi \ln \frac{s}{s_0}}} \exp\left(-\frac{\ln^2\left(\frac{\mathbf{k}_1^2}{\mathbf{k}_2^2}\right)}{4a^2 \ln \frac{s}{s_0}} \right) \left(\frac{s}{s_0}\right)^{\omega_0}. \end{aligned} \tag{2.51}$$

Chapter 3

Coherence in QCD

3.1 Coherence in Quantum Electrodynamics

Coherence effects are present in any gauge theory, in particular they are the origin of an interesting effect in Quantum Electrodynamics (QED) [72] where the soft bremsstrahlung from electron-positron pairs is suppressed. In this section we will give an intuitive explanation of this phenomenon. It will be an introduction to the next section, where we will deal in a more formal way with the QCD case.

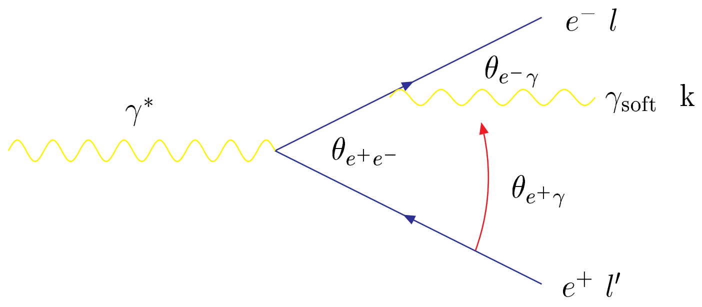

Figure 3.1: Kinematics of $\gamma^* \to e^+e^-\gamma_{\rm soft}$

We will review the study of the process $\gamma^* \to e^+e^-\gamma$ with soft bremsstrahlung from the electron line as shown in Fig. 3.1. We will assume that the opening angle $\theta_{e^+e^-}$ is smaller than $\theta_{e^-\gamma}$ and both angles are small.

In perturbation theory the virtual state consisting of an electron and a positron has different energy from the state with an electron, a positron and a soft photon. The difference in energies can be calculated as

$$\begin{aligned}
\Delta E &= (E_{e^-}(l) + E_{\rm soft\ \gamma}(k) + E_{e^+}(l')) - (E_{\rm virtual\ e^-}(l+k) + E_{e^+}(l')) \\
&= \sqrt{|\vec{l}|^2 + m^2} + |\vec{k}| - \sqrt{|\vec{l} + \vec{k}|^2 + m^2} \\
&\simeq |\vec{k}|(1 - \cos\theta_{e^-\gamma}) \qquad (3.1)
\end{aligned}$$

in the limit $|\vec{l}| \gg |\vec{k}|$. Therefore, for small $\theta_{e^-\gamma}$ angles, we have

$$\Delta E \simeq |\vec{k}|\theta^2_{e^-\gamma}. \qquad (3.2)$$

Using the uncertainty principle we can estimate how long the virtual electron state lives

$$\Delta t \sim \frac{1}{\Delta E} \sim \frac{1}{|\vec{k}|\theta^2_{e^-\gamma}} \sim \frac{\lambda_t}{\theta_{e^-\gamma}}, \tag{3.3}$$

where $\lambda_t^{-1} \sim k_t \sim k\theta_{e^-\gamma}$ is the transverse wavelength of the emitted soft photon. During this time the e^- and e^+ separate a transverse distance

$$\Delta b_{e^+e^-} \sim \theta_{e^+e^-}\Delta t = \frac{\lambda_t \theta_{e^+e^-}}{\theta_{e^-\gamma}}. \tag{3.4}$$

If $\theta_{e^-\gamma} > \theta_{e^+e^-}$ the separation between the two emitters is less than the transverse wavelength of the emitted soft photons. This implies that the photon perceives the electron-positron pair as an unresolved charge neutral object giving place to destructive interference with no radiation occurring. When $\theta_{e^-\gamma} < \theta_{e^+e^-}$ there is emission of radiation. The final scenario is one with soft photons only emitted either inside a narrow cone around the electron or inside a narrow cone around the positron.

We have explained the origin of angular ordering in QED. Now we will explain the same effect within QCD. Complications arise due to the colour charge carried by the gluons but the philosophy will be the same.

3.2 Coherence in Quantum Chromodynamics

In this section we want to give a description of the angular property of soft gluon emission characteristic of QCD [5]. First we want to start showing how to extract general Feynman rules for soft gluon emission. We consider the process $\gamma^* \to q\bar{q}g$, i.e. the $q\bar{q}$ decay of an off-shell photon as shown in Fig. 3.2. The amplitude for this process can be written as

$$\mathcal{A} = \bar{u}(l)\epsilon(k)\frac{g_s}{2l\cdot k}(\not{l} + \not{k})(-ie\gamma^\mu)v(l')\mathbf{T}^a. \tag{3.5}$$

If we add the amplitude corresponding to emission from the antiquark line we obtain

$$\mathcal{A} = g_s \mathbf{T}^a J\cdot\epsilon\ \mathcal{A}_{\text{Born}}, \tag{3.6}$$

where we have used the eikonal approximation $k \ll l, l'$ to obtain the current

$$J^\mu = \left(\frac{l^\mu}{l\cdot k} - \frac{l'^\mu}{l'\cdot k}\right) \tag{3.7}$$

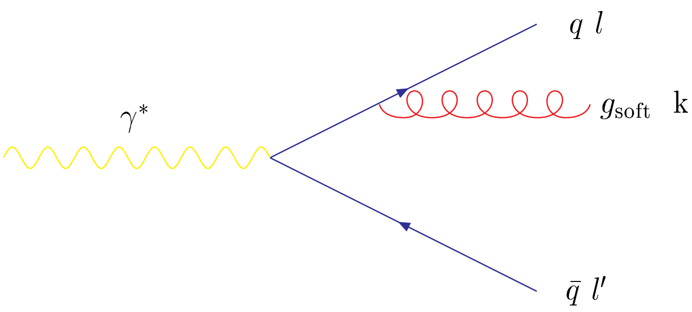

Figure 3.2: Kinematics of $\gamma^* \to q\bar{q}g_{\rm soft}$

The soft gluon emission has factorized into a product of an emission factor and the amplitude at the Born level without any soft emission. We have seen how the treatment of soft gluons is very simple due to the straightforward coupling to quark lines, as in this case, where the qqg vertex is

$$g_s \mathbf{T}^a 2p^\mu \tag{3.8}$$

and to gluon lines where the ggg vertex can be proved to simplify to

$$ig_s f^{abc} 2p^\mu g_{\alpha\beta}. \tag{3.9}$$

We can now calculate the cross section corresponding to the amplitude (3.6)

$$\begin{aligned}
d\sigma &= \sum_a |\mathcal{A}|^2 \frac{d^3k}{(2\pi)^3 2k^0} \\
&= \sum_a \mathbf{T}^a\mathbf{T}^a |\mathcal{A}_{\rm Born}|^2 J^\mu J^\nu g_s^2 \sum_{\mu\nu} \epsilon_\mu \epsilon_\nu^* \frac{d^3k}{(2\pi)^3 2k^0} \\
&= C_{\rm F} d\sigma_{\rm Born} \frac{2l\cdot l'}{l\cdot k\ l'\cdot k} g_s^2 \frac{d\phi\ k^0 dk^0}{(2\pi)8\pi^2} d\cos\theta \\
&= C_{\rm F} d\sigma_{\rm Born} \frac{1-cos\theta_{ll'}}{(1-cos\theta_{lk})(1-cos\theta_{l'k})} \alpha_s \frac{d\phi\ dk^0}{(2\pi)k^0} d\cos\theta \\
&= C_{\rm F} d\sigma_{\rm Born} \left\{\mathcal{W}_{ll'} + \mathcal{W}_{l'l}\right\} \alpha_s \frac{d\phi\ dk^0}{(2\pi)k^0} d\cos\theta,
\end{aligned} \tag{3.10}$$

where we have used θ_{ab} to identify the angle between the three momenta $\vec{a}$ and $\vec{b}$ and the functions $\mathcal{W}_{ab}$ are

$$\mathcal{W}_{ab} = \frac{1}{2}\left[\frac{\cos\theta_{bk} - \cos\theta_{ab}}{(1-\cos\theta_{ak})(1-\cos\theta_{bk})} + \frac{1}{1-\cos\theta_{ak}}\right]. \tag{3.11}$$

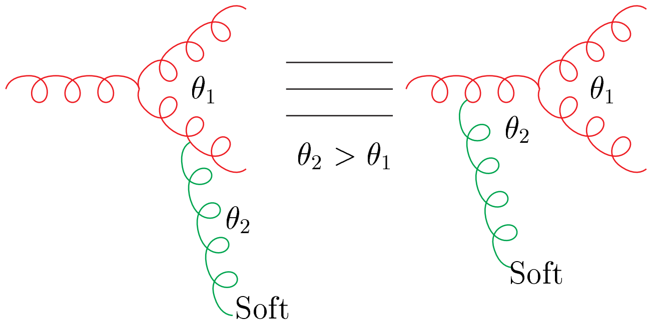

Figure 3.3: Colour coherence effect in a gluonic cascade

These functions are useful because if we integrate over the azimuthal angle in the direction of $\vec{l}$ we obtain

$$\int_0^{2\pi} \frac{d\phi_{lk}}{2\pi} \mathcal{W}_{ll'} = \frac{1}{1 - \cos\theta_{lk}} \Theta(\theta_{ll'} - \theta_{lk}), \tag{3.12}$$

i.e. the contribution from the term $\mathcal{W}_{ll'}$ ($\mathcal{W}_{l'l}$) is confined to a cone centred on the direction of line $\vec{l}$ ($\vec{l'}$) and extending in angle as far as the direction of line $\vec{l'}$ ($\vec{l}$). Inside the two cones we can consider the radiation from the emitters as independent.

In the case of the process $g \to q\bar{q}$ any soft gluon emitted with an angle from one of the fermionic lines larger than the angle of emission in the $q\bar{q}$ pair will probe only the total colour charge of the pair. This charge is the same as the one from the parent gluon. Therefore the radiation happens as if the soft gluon was emitted from the parent gluon g. We can then think of a continuous reduction of the opening angle at which successive soft gluons are emitted.

This result can be generalized to the decay hard gluon $\to$ soft gluon. This phenomenon is known as colour coherence and leads to the angular ordering of sequential gluon emissions in a cascade, i.e. if the opening angle of the ith gluon is θ_i then $\theta_i < \theta_{i-1}$ as is shown in Fig. 3.3.

3.3 Small x final states

One of the aims of this thesis is to understand the dynamics of QCD at very small values of Bjorken x in Deep Inelastic Scattering. The HERA collider provides a very powerful machine for experimental studies in this regime. From the theoretical point of view totally inclusive observables such as the structure function F_2 at small x are not sufficient to precisely describe the physics dominant in this kinematic region. It is necessary to analyse less inclusive features of the problem where different theoretical approaches give different predictions. These could teach us which is the correct mechanism responsible for the small x rise in F_2.

As we have already explained in small Bjorken x DIS at large momentum transfer Q^2 an electron is scattered through the exchange of a highly virtual (large $-q^2$) photon with a proton. After a DIS process what we measure in the detector is the scattered electron and jets of hadrons produced during the interaction of the photon with the proton. The proton is broken up and its remnants are emitted in the direction of the original proton.

When the values of Bjorken-x are as low as $x = 10^{-4}$ the logarithms in $1/x$ need to be considered and resummed. As we have stated before, this calculation is performed by the BFKL equation which resums the leading $[\alpha_S \ln 1/x]^n$ terms. The derivation of the BFKL equation relies upon the validity of the Regge kinematics. To calculate exclusive quantities, e.g. the number of gluons emitted in DIS, we should, in principle, extend this kinematics and take into account QCD coherence effects.

As we have seen the emission of soft gluons in perturbative QCD takes place into angular ordered regions. DIS at small x is an important case in which soft gluons are involved.

In DIS, suppose the $(i-1)$th emitted gluon (from the proton) has energy E_{i-1} and that it emits a gluon with a fraction $(1-z_i)$ of this energy and a transverse momentum

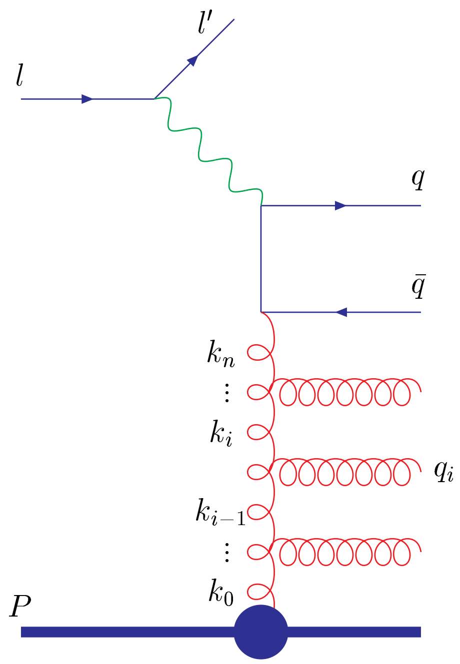

Figure 3.4: Notation for DIS momenta with soft gluon radiation

of magnitude q_i. The (small) opening angle θ_i of this emitted gluon is given by

$$\theta_i \approx \frac{q_i}{(1 - z_i)E_{i-1}}, \tag{3.13}$$

and z_i is the fraction of the energy of the $(i-1)$th gluon carried off by the ith gluon, i.e.

$$z_i = \frac{E_i}{E_{i-1}}. \tag{3.14}$$

Colour coherence leads to angular ordering with increasing opening angles towards the hard scale (the photon) so in this case we have $\theta_{i+1} > \theta_i$, which may be expressed as

$$\frac{q_{i+1}}{(1 - z_{i+1})} > \frac{z_i q_i}{(1 - z_i)}. \tag{3.15}$$

In the limit $z_i, z_{i+1} \ll 1$ this reduces to

$$q_{i+1} > z_i q_i. \tag{3.16}$$

The kinematics of the virtual graphs (which reggeize the t-channel gluons) are similarly modified and ensure the cancellation of the collinear singularities in inclusive quantities.

In Ref. [21, 22, 73, 74] the (t=0) BFKL equation for $f_\omega(\boldsymbol{k})$, the unintegrated structure function in ω-space (ω is the variable conjugate to x), was obtained in a form which is suitable for the study of more exclusive quantities

$$f_\omega(\boldsymbol{k}) = f_\omega^0(\boldsymbol{k}) + \bar{\alpha}_S \int \frac{d^2\boldsymbol{q}}{\pi q^2} \int_0^1 \frac{dz}{z} z^\omega \Delta_R(z,k)\Theta(q-\mu) f_\omega(\boldsymbol{q}+\boldsymbol{k}), \tag{3.17}$$

where μ is a collinear cutoff, $\boldsymbol{q}$ is the transverse momentum of the emitted gluon, and the gluon Regge factor which sums all the virtual contributions is

$$\Delta_R(z_i, k_i) = \exp\left[-\bar{\alpha}_S \ln\frac{1}{z_i} \ln\frac{k_i^2}{\mu^2}\right], \tag{3.18}$$

with $k_i \equiv |\boldsymbol{k}_i|$, and $\bar{\alpha}_S \equiv C_A \alpha_S/\pi$, ($C_A = 3$).

The driving term, $f_\omega^0(\boldsymbol{k})$, includes the virtual corrections which reggeize the bare gluon. This form of the BFKL equation has a kernel which, under iteration, generates real gluon emissions with all the virtual corrections summed to all orders. As such, it is suitable for the study of the final state. Since f_ω is an inclusive structure function, it includes the sum over all final states and the μ-dependence cancels between the real and virtual contributions.

In this section we wish to examine the individual contributions to the structure function of an on-shell gluon which come from the emission of r gluons, each of which is constrained to have its transverse momentum less than Q (where $\mu \ll Q$). By selecting an on-shell gluon as the target we can use the simple boundary condition

$$f_\omega^0(\boldsymbol{k}) = \delta^2(\boldsymbol{k}). \tag{3.19}$$

Since the gluon is on shell it does not pick up any corrections due to reggeization. Note that our main conclusions do not depend upon the precise nature of the target particle.

We define the structure function, $F_{0\omega}(Q,\mu)$, by integrating over all $\mu^2 \le q_i^2 \le Q^2$, i.e.

$$F_{0\omega}(Q,\mu) \equiv \Theta(Q-\mu) + \sum_{r=1}^{\infty} \int_{\mu^2}^{Q^2} \prod_{i=1}^{r} \frac{d^2\boldsymbol{q}_i}{\pi q_i^2} dz_i \frac{\bar{\alpha}_S}{z_i} z_i^\omega \Delta_R(z_i,k_i), \tag{3.20}$$

and we have isolated the contributions from i real gluon emissions by iterating the kernel explicitly.

Consider the contributions to the structure function from a fixed number r of emitted initial state gluons, $F_{0\omega}^{(r)}(Q)$, i.e.

$$F_{0\omega}(Q) = \int_0^1 dx\ x^\omega F_0(x,Q) = 1 + \sum_{r=1}^{\infty} F_{0\omega}^{(r)}(Q). \tag{3.21}$$

In this formulation (which does not include coherence) in Ref. [22] the perturbative expansion for the $F_{0\omega}^{(r)}(Q,\mu)$ was obtained. This is of the form

$$F_{0\omega}^{(r)}(Q,\mu) = \sum_{n=r}^{\infty} C_0^{(r)}(n;T)\frac{\bar{\alpha}_S^n}{\omega^n}, \tag{3.22}$$

with $T \equiv \ln(Q/\mu)$, and the inclusive structure function satisfies

$$F_{0\omega}(Q) \equiv \sum_{i=0}^{\infty} F_{0\omega}^{(i)}(Q) = \left(\frac{Q^2}{\mu^2}\right)^{\bar{\gamma}}, \tag{3.23}$$

where $\bar{\gamma}$ is the BFKL anomalous dimension.

It was pointed out in Ref. [22] that coherence effects significantly modify the individual $F_{0\omega}^{(r)}(Q)$ whilst preserving the sum $F_{0\omega}(Q)$. It can be concluded that care must be taken to account properly for coherence in the calculation of associated distributions.

Modifying the BFKL formalism to account for coherence [21, 22, 73, 74], $F_{0\omega}(Q,\mu)$ becomes

$$F_\omega(Q,\mu) = \Theta(Q-\mu) + \sum_{r=1}^{\infty}\int_0^{Q^2}\prod_{i=1}^{r}\frac{d^2\boldsymbol{q}_i}{\pi q_i^2}dz_i\frac{\bar{\alpha}_S}{z_i}z_i^\omega\Delta(z_i,q_i,k_i)\Theta(q_i - z_{i-1}q_{i-1}), \tag{3.24}$$

where $\Delta_R(z_i,k_i)$ is substituted by the coherence improved Regge factor

$$\Delta(z_i,q_i,k_i) = \exp\left[-\bar{\alpha}_S \ln\frac{1}{z_i}\ln\frac{k_i^2}{z_i q_i^2}\right]; \quad k_i > q_i, \tag{3.25}$$

and for the first emission we take $q_0 z_0 = \mu$.

The perturbative expansion of $F_\omega^{(r)}(Q)$ is now of the form

$$F_\omega^{(r)}(Q) = \sum_{n=r}^{\infty}\sum_{m=1}^{n} C^{(r)}(n,m;T)\frac{\bar{\alpha}_S^n}{\omega^{2n-m}}. \tag{3.26}$$

In the formalism with coherence no collinear cutoff is needed, except on the emission of the first gluon. This is because subsequent collinear emissions are regulated by the angular ordering constraint and it is those collinear emissions which induce the additional powers of $1/\omega$. Transforming to x-space it means that

$$\frac{\bar{\alpha}_S^n}{\omega^{n+p}} \Longleftrightarrow \frac{\bar{\alpha}_S^n}{x}\left(\ln\frac{1}{x}\right)^{n+p-1}, \; p < n,$$

i.e. coherence induces additional $\ln(1/x)$. In inclusive quantities these logarithms cancel. At a less inclusive level, such as for the associated distributions, the logarithms need not cancel any more.

3.3.1 Introducing a resolution scale

To understand the structure of the gluon emission it is very useful to introduce an extra scale in the formalism [75]. The r-gluon emission rate is not an observable quantity because in practise we can only detect emissions above some resolution scale, which from now on we call μ_R. This scale is constrained by the collinear cutoff and the virtuality of the incoming photon, $\mu \ll \mu_R \ll Q$. In this chapter we compute the r resolved-gluon emission contributions to the structure function, without restricting the number of unresolved emissions which may occur.

An implementation of a resolution scale in the BFKL equation has been studied by Lewis et al. [76]. In their work they derive a form of the BFKL equation which enables the structure of the gluon emissions to be studied in small x deep inelastic scattering. The equation incorporates the summation of the virtual and unresolved real gluon emissions. They solve the equation to calculate the number of small x deep inelastic events containing 0, 1, 2 ... resolved gluon jets. In their analysis they did not consider the possible influence of QCD coherence effects which could, in principle, have invalidated their results. The work shown in the following will prove that at least at leading order, their results are still valid.

Within the leading $\log(1/x)$ approximation, the resolved gluons can be identified as jets since any corrections arising from additional radiation are suppressed by $\mathcal{O}(\alpha_s)$.

In the following we will show the perturbative calculation of the r-jet cross-sections to order $\bar{\alpha}_S^3$, where r is the number of gluon emissions with transverse momentum bigger than μ_R.

To obtain the $\bar{\alpha}_S^3$ accuracy we expand the Regge form factor in powers of the strong coupling

$$\Delta_R(z_i,k_i) = \exp\left[-\bar{\alpha}_S \ln\frac{1}{z_i}\ln\frac{k_i^2}{\mu^2}\right] \sim 1 - \bar{\alpha}_S \ln\frac{1}{z_i}\ln\frac{k_i^2}{\mu^2} + \frac{1}{2}\bar{\alpha}_S^2 \ln^2\frac{1}{z_i}\ln^2\frac{k_i^2}{\mu^2} \tag{3.27}$$

and insert it in the expression for the structure function

$$F_{0\omega}(Q,\mu) \equiv \Theta(Q-\mu) + \sum_{r=1}^{\infty}\int_{\mu^2}^{Q^2}\prod_{i=1}^{r}\frac{d^2\boldsymbol{q}_i}{\pi q_i^2}dz_i\frac{\bar{\alpha}_S}{z_i}z_i^{\omega}\Delta_R(z_i,k_i) \tag{3.28}$$

Diagrammatically the contributions to $F_{0\omega}(Q,\mu)$ to order $\bar{\alpha}_S^3$ are indicated in the Fig 3.5. The lines with a circle represent resolved gluons.

First we calculate the contribution to $F_{0\omega}(Q,\mu)$ from any number of emitted gluons with all of them unresolved*. For the emission of a single unresolved gluon we have

$$\begin{aligned} U &= \int_0^1 dz_1 z_1^{\omega-1}\int_{\mu^2}^{\mu_R^2}\frac{d^2\boldsymbol{q}_1}{\pi q_1^2}\left[\bar{\alpha}_S - \bar{\alpha}_S^2\ln\frac{1}{z_1}\ln\frac{q_1^2}{\mu^2} + \frac{1}{2}\bar{\alpha}_S^3\ln^2\frac{1}{z_1}\ln^2\frac{q_1^2}{\mu^2}\right] + ... \\ &= \frac{(2\bar{\alpha}_S)}{\omega}S + \frac{(2\bar{\alpha}_S)^2}{\omega^2}\left[-\frac{1}{2}S^2\right] + \frac{(2\bar{\alpha}_S)^3}{\omega^3}\left[\frac{1}{3}S^3\right] + ... \end{aligned} \tag{3.29}$$

For two unresolved emissions:

$$\begin{aligned} UU &= \int_0^1 dz_1 z_1^{\omega-1}\int_0^1 dz_2 z_2^{\omega-1}\int_{\mu^2}^{\mu_R^2}\frac{d^2\boldsymbol{q}_1}{\pi q_1^2}\int_{\mu^2}^{\mu_R^2}\frac{d^2\boldsymbol{q}_2}{\pi q_2^2} \\ &\quad\times\left[\bar{\alpha}_S^2 - \bar{\alpha}_S^3\left(\ln\frac{1}{z_1}\ln\frac{q_1^2}{\mu^2} + \ln\frac{1}{z_2}\ln\frac{k_2^2}{\mu^2}\right)\right] + ... \\ &= \frac{(2\bar{\alpha}_S)^2}{\omega^2}S^2 + \frac{(2\bar{\alpha}_S)^3}{\omega^3}\left[-\frac{7}{6}S^3\right] + ... \end{aligned} \tag{3.30}$$

where $\boldsymbol{k}_i = \boldsymbol{k}_{i-1} - \boldsymbol{q}_i$, and we can write $\boldsymbol{k}_i^2 = [\sum_{n=1}^{i}\boldsymbol{q}_n]^2$. We have $\boldsymbol{k}_0 = 0$, and

$$T \equiv \ln\frac{Q}{\mu_R},\ S \equiv \ln\frac{\mu_R}{\mu}.$$

*A detailed explanation on how to deal with the integrations over the gluon phase space is given in the Appendix A.

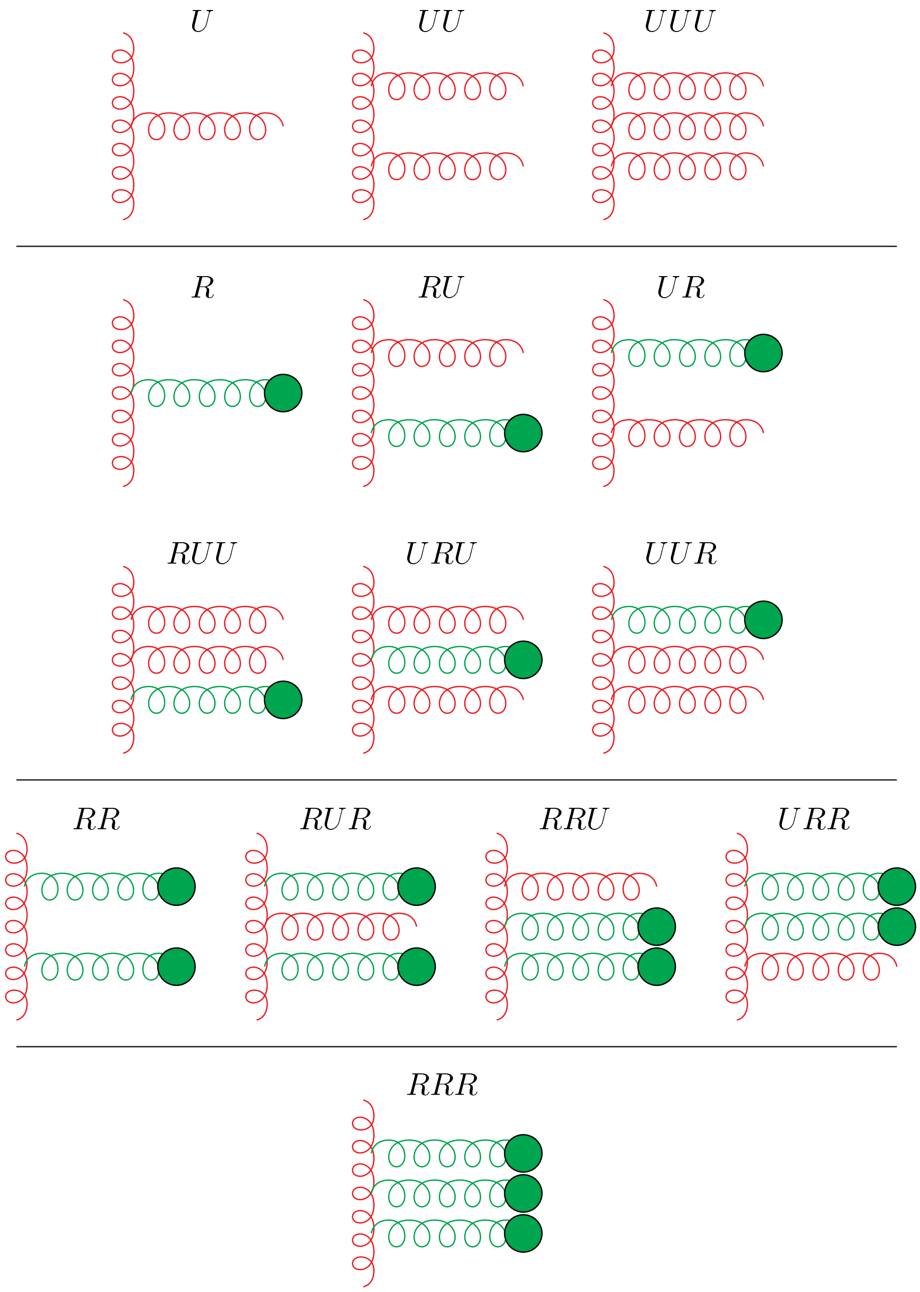

Figure 3.5: Contributions to the structure function to order $\bar{\alpha}_S^3$

The contribution from three unresolved emissions is

$$\begin{aligned} UUU &= \int_0^1 dz_1 z_1^{\omega-1} \int_0^1 dz_2 z_2^{\omega-1} \int_0^1 dz_3 z_3^{\omega-1} \int_{\mu^2}^{\mu_R^2} \frac{d^2\boldsymbol{q}_1}{\pi q_1^2} \int_{\mu^2}^{\mu_R^2} \frac{d^2\boldsymbol{q}_2}{\pi q_2^2} \int_{\mu^2}^{\mu_R^2} \frac{d^2\boldsymbol{q}_3}{\pi q_3^2} \bar{\alpha}_S^3 + \ldots \\ &= \frac{(2\bar{\alpha}_S)^3}{\omega^3} S^3 + \ldots \end{aligned} \tag{3.31}$$

Thus the 0-jet rate is

$$\begin{aligned} \text{“}0-\text{jet”} &= U + UU + UUU + \ldots \\ &= \frac{(2\bar{\alpha}_S)}{\omega} S + \frac{(2\bar{\alpha}_S)^2}{\omega^2}\left[\frac{S^2}{2}\right] + \frac{(2\bar{\alpha}_S)^3}{\omega^3}\left[\frac{S^3}{6}\right] + \ldots \end{aligned} \tag{3.32}$$

Now we concentrate on calculating the 1-jet rate. For one resolved emission:

$$\begin{aligned} R &= \int_0^1 dz_1 z_1^{\omega-1} \int_{\mu_R^2}^{Q^2} \frac{d^2\boldsymbol{q}_1}{\pi q_1^2} \left[\bar{\alpha}_S - \bar{\alpha}_S^2 \ln\frac{1}{z_1} \ln\frac{q_1^2}{\mu^2} + \frac{1}{2}\bar{\alpha}_S^3 \ln^2\frac{1}{z_1} \ln^2\frac{q_1^2}{\mu^2}\right] + \ldots \\ &= \frac{(2\bar{\alpha}_S)}{\omega} T + \frac{(2\bar{\alpha}_S)^2}{\omega^2}\left[-\frac{1}{2}T^2 - TS\right] + \frac{(2\bar{\alpha}_S)^3}{\omega^3}\left[\frac{1}{3}T^3 + T^2 S + TS^2\right] + \ldots \end{aligned} \tag{3.33}$$

When the first emission is resolved and the second unresolved:

$$\begin{aligned} RU &= \int_0^1 dz_1 z_1^{\omega-1} \int_0^1 dz_2 z_2^{\omega-1} \int_{\mu_R^2}^{Q^2} \frac{d^2\boldsymbol{q}_1}{\pi q_1^2} \int_{\mu^2}^{\mu_R^2} \frac{d^2\boldsymbol{q}_2}{\pi q_2^2} \\ &\quad \times \left[\bar{\alpha}_S^2 - \bar{\alpha}_S^3 \left(\ln\frac{1}{z_1}\ln\frac{q_1^2}{\mu^2} + \ln\frac{1}{z_2}\ln\frac{k_2^2}{\mu^2}\right)\right] + \ldots \\ &= \frac{(2\bar{\alpha}_S)^2}{\omega^2} TS + \frac{(2\bar{\alpha}_S)^3}{\omega^3}\left[-T^2 S - 2TS^2\right] + \ldots \end{aligned} \tag{3.34}$$

If the first emission is unresolved and the second resolved:

$$\begin{aligned} UR &= \int_0^1 dz_1 z_1^{\omega-1} \int_0^1 dz_2 z_2^{\omega-1} \int_{\mu^2}^{\mu_R^2} \frac{d^2\boldsymbol{q}_1}{\pi q_1^2} \int_{\mu_R^2}^{Q^2} \frac{d^2\boldsymbol{q}_2}{\pi q_2^2} \\ &\quad \times \left[\bar{\alpha}_S^2 - \bar{\alpha}_S^3 \left(\ln\frac{1}{z_1}\ln\frac{q_1^2}{\mu^2} + \ln\frac{1}{z_2}\ln\frac{k_2^2}{\mu^2}\right)\right] + \ldots \\ &= \frac{(2\bar{\alpha}_S)^2}{\omega^2} TS + \frac{(2\bar{\alpha}_S)^3}{\omega^3}\left[-\frac{3}{2}TS^2 - \frac{1}{2}T^2 S\right] + \ldots \end{aligned} \tag{3.35}$$

Similarly for three emissions with two of them unresolved:

$$\begin{aligned} RUU &= \int_0^1 dz_1 z_1^{\omega-1} \int_0^1 dz_2 z_2^{\omega-1} \int_0^1 dz_3 z_3^{\omega-1} \int_{\mu_R^2}^{Q^2} \frac{d^2\boldsymbol{q}_1}{\pi q_1^2} \int_{\mu^2}^{\mu_R^2} \frac{d^2\boldsymbol{q}_2}{\pi q_2^2} \int_{\mu^2}^{\mu_R^2} \frac{d^2\boldsymbol{q}_3}{\pi q_3^2} \bar{\alpha}_S^3 + \ldots \\ &= \frac{(2\bar{\alpha}_S)^3}{\omega^3} TS^2 + \ldots \end{aligned} \tag{3.36}$$

$$\begin{aligned}URU &= \int_0^1 dz_1 z_1^{\omega-1}\int_0^1 dz_2 z_2^{\omega-1}\int_0^1 dz_3 z_3^{\omega-1}\int_{\mu^2}^{\mu_R^2}\frac{d^2\boldsymbol{q}_1}{\pi q_1^2}\int_{\mu_R^2}^{Q^2}\frac{d^2\boldsymbol{q}_2}{\pi q_2^2}\int_{\mu^2}^{\mu_R^2}\frac{d^2\boldsymbol{q}_3}{\pi q_3^2}\bar{\alpha}_S^3+...\\ &= \frac{(2\bar{\alpha}_S)^3}{\omega^3}TS^2+... \qquad (3.37)\end{aligned}$$

$$\begin{aligned}UUR &= \int_0^1 dz_1 z_1^{\omega-1}\int_0^1 dz_2 z_2^{\omega-1}\int_0^1 dz_3 z_3^{\omega-1}\int_{\mu^2}^{\mu_R^2}\frac{d^2\boldsymbol{q}_1}{\pi q_1^2}\int_{\mu^2}^{\mu_R^2}\frac{d^2\boldsymbol{q}_2}{\pi q_2^2}\int_{\mu_R^2}^{Q^2}\frac{d^2\boldsymbol{q}_3}{\pi q_3^2}\bar{\alpha}_S^3+...\\ &= \frac{(2\bar{\alpha}_S)^3}{\omega^3}TS^2+... \qquad (3.38)\end{aligned}$$

The sum of these contributions is the 1-jet rate:

$$\text{“}1-\text{jet”} = R+RU+UR+RUU+URU+UUR+...$$

$$=\frac{(2\bar{\alpha}_S)}{\omega}T+\frac{(2\bar{\alpha}_S)^2}{\omega^2}\left[TS-\frac{1}{2}T^2\right]+\frac{(2\bar{\alpha}_S)^3}{\omega^3}\left[\frac{1}{3}T^3-\frac{1}{2}T^2S+\frac{1}{2}TS^2\right]+... \qquad (3.39)$$

Let us now focus on the 2-jet rates, i.e. two of the emitted gluons have transverse momentum bigger than our resolution scale. There are several contributions, the first one comes from the case when only two gluons are emitted and both detected

$$\begin{aligned}RR &= \int_0^1 dz_1 z_1^{\omega-1}\int_0^1 dz_2 z_2^{\omega-1}\int_{\mu_R^2}^{Q^2}\frac{d^2\boldsymbol{q}_1}{\pi q_1^2}\int_{\mu_R^2}^{Q^2}\frac{d^2\boldsymbol{q}_2}{\pi q_2^2}\\ &\quad\times\left[\bar{\alpha}_S^2-\bar{\alpha}_S^3\left(\ln\frac{1}{z_1}\ln\frac{q_1^2}{\mu^2}+\ln\frac{1}{z_2}\ln\frac{k_2^2}{\mu^2}\right)\right]+...\\ &= \frac{(2\bar{\alpha}_S)^2}{\omega^2}T^2+\frac{(2\bar{\alpha}_S)^3}{\omega^3}\left[-\frac{7}{6}T^3-2T^2S\right]+... \qquad (3.40)\end{aligned}$$

If there is an additional undetected emission we must account for three more terms:

$$\begin{aligned}RRU &= \int_0^1 dz_1 z_1^{\omega-1}\int_0^1 dz_2 z_2^{\omega-1}\int_0^1 dz_3 z_3^{\omega-1}\int_{\mu_R^2}^{Q^2}\frac{d^2\boldsymbol{q}_1}{\pi q_1^2}\int_{\mu_R^2}^{Q^2}\frac{d^2\boldsymbol{q}_2}{\pi q_2^2}\int_{\mu^2}^{\mu_R^2}\frac{d^2\boldsymbol{q}_3}{\pi q_3^2}\bar{\alpha}_S^3+...\\ &= \frac{(2\bar{\alpha}_S)^3}{\omega^3}T^2S+... \qquad (3.41)\end{aligned}$$

$$\begin{aligned}RUR &= \int_0^1 dz_1 z_1^{\omega-1}\int_0^1 dz_2 z_2^{\omega-1}\int_0^1 dz_3 z_3^{\omega-1}\int_{\mu_R^2}^{Q^2}\frac{d^2\boldsymbol{q}_1}{\pi q_1^2}\int_{\mu^2}^{\mu_R^2}\frac{d^2\boldsymbol{q}_2}{\pi q_2^2}\int_{\mu_R^2}^{Q^2}\frac{d^2\boldsymbol{q}_3}{\pi q_3^2}\bar{\alpha}_S^3+...\\ &= \frac{(2\bar{\alpha}_S)^3}{\omega^3}T^2S+... \qquad (3.42)\end{aligned}$$

$$\begin{aligned} URR &= \int_0^1 dz_1 z_1^{\omega-1} \int_0^1 dz_2 z_2^{\omega-1} \int_0^1 dz_3 z_3^{\omega-1} \int_{\mu^2}^{\mu_R^2} \frac{d^2\boldsymbol{q}_1}{\pi q_1^2} \int_{\mu_R^2}^{Q^2} \frac{d^2\boldsymbol{q}_2}{\pi q_2^2} \int_{\mu_R^2}^{Q^2} \frac{d^2\boldsymbol{q}_3}{\pi q_3^2} \bar{\alpha}_S^3 + ... \\ &= \frac{(2\bar{\alpha}_S)^3}{\omega^3} T^2 S + ... \end{aligned} \tag{3.43}$$

and so

$$\begin{aligned} \text{“}2-\text{jet”} &= RR + RRU + RUR + URR + ... \\ &= \frac{(2\bar{\alpha}_S)^2}{\omega^2}\left[T^2\right] + \frac{(2\bar{\alpha}_S)^3}{\omega^3}\left[T^2 S - \frac{7}{6}T^3\right] + ... \end{aligned} \tag{3.44}$$

We now consider the emission of three resolved gluons. There is only one term to order $\bar{\alpha}_S^3$, i.e.

$$\begin{aligned} RRR &= \int_0^1 dz_1 z_1^{\omega-1} \int_0^1 dz_2 z_2^{\omega-1} \int_0^1 dz_3 z_3^{\omega-1} \int_{\mu_R^2}^{Q^2} \frac{d^2\boldsymbol{q}_1}{\pi q_1^2} \int_{\mu_R^2}^{Q^2} \frac{d^2\boldsymbol{q}_2}{\pi q_2^2} \int_{\mu_R^2}^{Q^2} \frac{d^2\boldsymbol{q}_3}{\pi q_3^2} \bar{\alpha}_S^3 + ... \\ &= \frac{(2\bar{\alpha}_S)^3}{\omega^3} T^3 + ... = \text{“}3-\text{jet”} \end{aligned} \tag{3.45}$$

It is important to remark that the sum of the powers in T and S is always equal or smaller than the power of ω in all these terms. This is characteristic of leading order BFKL kinematics.

3.3.2 Coherence with a resolution scale

Our aim in this section is to compute the 0-, 1-, 2-, 3-jet rates accounting for coherence. We want to investigate how the predictions for these observables are modified when we introduce angular ordering in the parton cascade.

To proceed we must introduce the coherence condition $\Theta(q_i - z_{i-1}q_{i-1})$ in the definition of the structure function

$$F_\omega(Q,\mu) = \Theta(Q-\mu) + \sum_{r=1}^{\infty} \int_0^{Q^2} \prod_{i=1}^{r} \frac{d^2\boldsymbol{q}_i}{\pi q_i^2} dz_i \frac{\bar{\alpha}_S}{z_i} z_i^\omega \Delta(z_i, q_i, k_i)\Theta(q_i - z_{i-1}q_{i-1}) \tag{3.46}$$

and the Taylor expansion of the coherence improved Regge factor

$$\Delta(z_i, q_i, k_i) \sim 1 - \bar{\alpha}_S \ln\frac{1}{z_i} \ln\frac{k_i^2}{z_i q_i^2} + \frac{1}{2}\bar{\alpha}_S^2 \ln^2\frac{1}{z_i} \ln^2\frac{k_i^2}{z_i q_i^2}. \tag{3.47}$$

For unresolved emissions (with the subscript "c" indicating coherence) we have

$$\begin{aligned} U|_c &= \int_0^1 dz_1 z_1^{\omega-1} \int_{\mu^2}^{\mu_R^2} \frac{d^2\boldsymbol{q}_1}{\pi q_1^2}\left[\bar{\alpha}_S - \bar{\alpha}_S^2 \ln^2\frac{1}{z_1} + \frac{1}{2}\bar{\alpha}_S^3 \ln^4\frac{1}{z_1}\right] + ... \\ &= \frac{(2\bar{\alpha}_S)}{\omega}S + \frac{(2\bar{\alpha}_S)^2}{\omega^2}\left[-\frac{S}{\omega}\right] + \frac{(2\bar{\alpha}_S)^3}{\omega^3}\left[3\frac{S}{\omega^2}\right] + ... \end{aligned} \tag{3.48}$$

$$\begin{aligned} UU|_c &= \int_0^1 dz_1 z_1^{\omega-1}\int_0^1 dz_2 z_2^{\omega-1}\int_{\mu^2}^{\mu_R^2}\frac{d^2\boldsymbol{q}_1}{\pi q_1^2}\int_{z_1^2 q_1^2}^{\mu_R^2}\frac{d^2\boldsymbol{q}_2}{\pi q_2^2} \\ &\times\left[\bar{\alpha}_S^2 - \bar{\alpha}_S^3\left(\ln^2\frac{1}{z_1} + \ln^2\frac{1}{z_2} + \ln\frac{1}{z_2}\ln\frac{k_2^2}{q_2^2}\right)\right] + ... \\ &= \frac{(2\bar{\alpha}_S)^2}{\omega^2}\left[\frac{S}{\omega} + \frac{S^2}{2}\right] + \frac{(2\bar{\alpha}_S)^3}{\omega^3}\left[-5\frac{S}{\omega^2} - \frac{S^2}{\omega}\right] + ... \end{aligned} \tag{3.49}$$

$$\begin{aligned} UUU|_c &= \int_0^1 dz_1 z_1^{\omega-1}\int_0^1 dz_2 z_2^{\omega-1}\int_0^1 dz_3 z_3^{\omega-1}\int_{\mu^2}^{\mu_R^2}\frac{d^2\boldsymbol{q}_1}{\pi q_1^2}\int_{z_1^2 q_1^2}^{\mu_R^2}\frac{d^2\boldsymbol{q}_2}{\pi q_2^2}\int_{z_2^2 q_2^2}^{\mu_R^2}\frac{d^2\boldsymbol{q}_3}{\pi q_3^2}\bar{\alpha}_S^3 + ... \\ &= \frac{(2\bar{\alpha}_S)^3}{\omega^3}\left[2\frac{S}{\omega^2} + \frac{S^2}{\omega} + \frac{1}{6}S^3\right] + ... \end{aligned} \tag{3.50}$$

In the case of one single resolved emission, we have to consider (to order $\bar{\alpha}_S^3$) six terms:

$$\begin{aligned} R|_c &= \int_0^1 dz_1 z_1^{\omega-1} \int_{\mu_R^2}^{Q^2} \frac{d^2\boldsymbol{q}_1}{\pi q_1^2}\left[\bar{\alpha}_S - \bar{\alpha}_S^2 \ln^2\frac{1}{z_1} + \frac{1}{2}\bar{\alpha}_S^3 \ln^4\frac{1}{z_1}\right] + ... \\ &= \frac{(2\bar{\alpha}_S)}{\omega}T + \frac{(2\bar{\alpha}_S)^2}{\omega^2}\left[-\frac{T}{\omega}\right] + \frac{(2\bar{\alpha}_S)^3}{\omega^3}\left[3\frac{T}{\omega^2}\right] + ... \end{aligned} \tag{3.51}$$

$$\begin{aligned} RU|_c &= \int_0^1 dz_1 z_1^{\omega-1}\int_0^1 dz_2 z_2^{\omega-1}\int_{\mu_R^2}^{Q^2}\frac{d^2\boldsymbol{q}_1}{\pi q_1^2}\int_{z_1^2 q_1^2}^{\mu_R^2}\frac{d^2\boldsymbol{q}_2}{\pi q_2^2}\Theta(\mu_R - z_1 q_1) \\ &\times\left[\bar{\alpha}_S^2 - \bar{\alpha}_S^3\left(\ln^2\frac{1}{z_1} + \ln^2\frac{1}{z_2} + \ln\frac{1}{z_2}\ln\frac{k_2^2}{q_2^2}\right)\right] + ... \\ &= \frac{(2\bar{\alpha}_S)^2}{\omega^2}\left[\frac{T}{\omega} - \frac{1}{2}T^2\right] + \frac{(2\bar{\alpha}_S)^3}{\omega^3}\left[-5\frac{T}{\omega^2} + \frac{T^2}{\omega}\right] + ... \end{aligned} \tag{3.52}$$

$$\begin{aligned} UR|_c &= \int_0^1 dz_1 z_1^{\omega-1}\int_0^1 dz_2 z_2^{\omega-1}\int_{\mu^2}^{\mu_R^2}\frac{d^2\boldsymbol{q}_1}{\pi q_1^2}\int_{\mu_R^2}^{Q^2}\frac{d^2\boldsymbol{q}_2}{\pi q_2^2} \\ &\times\left[\bar{\alpha}_S^2 - \bar{\alpha}_S^3\left(\ln^2\frac{1}{z_1} + \ln^2\frac{1}{z_2} + \ln\frac{1}{z_2}\ln\frac{k_2^2}{q_2^2}\right)\right] + ... \\ &= \frac{(2\bar{\alpha}_S)^2}{\omega^2}TS + \frac{(2\bar{\alpha}_S)^3}{\omega^3}\left[-2\frac{TS}{\omega}\right] + ... \end{aligned} \tag{3.53}$$

$$
\begin{aligned}
RUU|_c &= \int_0^1 dz_1 z_1^{\omega-1} \int_0^1 dz_2 z_2^{\omega-1} \int_0^1 dz_3 z_3^{\omega-1} \int_{\mu_R^2}^{Q^2} \frac{d^2\boldsymbol{q}_1}{\pi q_1^2} \int_{z_1^2 q_1^2}^{\mu_R^2} \frac{d^2\boldsymbol{q}_2}{\pi q_2^2} \\
&\times \int_{z_2^2 q_2^2}^{\mu_R^2} \frac{d^2\boldsymbol{q}_3}{\pi q_3^2} \Theta(\mu_R - z_1 q_1) \bar{\alpha}_S^3 + ... \\
&= \frac{(2\bar{\alpha}_S)^3}{\omega^3} \left[2\frac{T}{\omega^2} - \frac{T^2}{\omega} + \frac{1}{3} T^3 \right] + ...
\end{aligned} \tag{3.54}
$$

$$
\begin{aligned}
URU|_c &= \int_0^1 dz_1 z_1^{\omega-1} \int_0^1 dz_2 z_2^{\omega-1} \int_0^1 dz_3 z_3^{\omega-1} \int_{\mu^2}^{\mu_R^2} \frac{d^2\boldsymbol{q}_1}{\pi q_1^2} \int_{\mu_R^2}^{Q^2} \frac{d^2\boldsymbol{q}_2}{\pi q_2^2} \\
&\times \int_{z_2^2 q_2^2}^{\mu_R^2} \frac{d^2\boldsymbol{q}_3}{\pi q_3^2} \Theta(\mu_R - z_2 q_2) \bar{\alpha}_S^3 + ... \\
&= \frac{(2\bar{\alpha}_S)^3}{\omega^3} \left[\frac{TS}{\omega} - \frac{1}{2} T^2 S \right] + ...
\end{aligned} \tag{3.55}
$$

$$
\begin{aligned}
UUR|_c &= \int_0^1 dz_1 z_1^{\omega-1} \int_0^1 dz_2 z_2^{\omega-1} \int_0^1 dz_3 z_3^{\omega-1} \int_{\mu^2}^{\mu_R^2} \frac{d^2\boldsymbol{q}_1}{\pi q_1^2} \int_{z_1^2 q_1^2}^{\mu_R^2} \frac{d^2\boldsymbol{q}_2}{\pi q_2^2} \int_{\mu_R^2}^{Q^2} \frac{d^2\boldsymbol{q}_3}{\pi q_3^2} \bar{\alpha}_S^3 + ... \\
&= \frac{(2\bar{\alpha}_S)^3}{\omega^3} \left[\frac{TS}{\omega} + \frac{1}{2} T S^2 \right] + ...
\end{aligned} \tag{3.56}
$$

In these calculations we neglect terms which are beyond leading logarithmic approximation, i.e. terms suppressed by $\sim \omega^n$, with $(n \geq 1)$. To take into account those terms we would need a better understanding of the next-to-leading order corrections to BFKL and a calculation of the form factor with coherence beyond the leading order limit. The former problem is the subject of the second part of this thesis and the latter is by no means straightforward.

Finally we consider the case when we resolve two or three of the emissions:

$$
\begin{aligned}
RR|_c &= \int_0^1 dz_1 z_1^{\omega-1} \int_0^1 dz_2 z_2^{\omega-1} \int_{\mu_R^2}^{Q^2} \frac{d^2\boldsymbol{q}_1}{\pi q_1^2} \int_{max(\mu_R^2, z_1^2 q_1^2)}^{Q^2} \frac{d^2\boldsymbol{q}_2}{\pi q_2^2} \\
&\times \left[\bar{\alpha}_S^2 - \bar{\alpha}_S^3 \left(\ln^2 \frac{1}{z_1} + \ln^2 \frac{1}{z_2} + \ln \frac{1}{z_2} \ln \frac{k_2^2}{q_2^2} \right) \right] + ... \\
&= \frac{(2\bar{\alpha}_S)^2}{\omega^2} \left[T^2 \right] + \frac{(2\bar{\alpha}_S)^3}{\omega^3} \left[-2\frac{T^2}{\omega} \right] + ...
\end{aligned} \tag{3.57}
$$

$$
\begin{aligned}
RRU|_c &= \int_0^1 dz_1 z_1^{\omega-1} \int_0^1 dz_2 z_2^{\omega-1} \int_0^1 dz_3 z_3^{\omega-1} \int_{\mu_R^2}^{Q^2} \frac{d^2\boldsymbol{q}_1}{\pi q_1^2} \int_{max(\mu_R^2, z_1^2 q_1^2)}^{Q^2} \frac{d^2\boldsymbol{q}_2}{\pi q_2^2} \\
&\times \int_{z_2^2 q_2^2}^{\mu_R^2} \frac{d^2\boldsymbol{q}_3}{\pi q_3^2} \Theta(\mu_R - z_2 q_2) \bar{\alpha}_S^3 + ... \\
&= \frac{(2\bar{\alpha}_S)^3}{\omega^3} \left[\frac{T^2}{\omega} - \frac{2}{3} T^3 \right] + ...
\end{aligned} \tag{3.58}
$$

$$
\begin{aligned}
RUR|_c &= \int_0^1 dz_1 z_1^{\omega-1} \int_0^1 dz_2 z_2^{\omega-1} \int_0^1 dz_3 z_3^{\omega-1} \int_{\mu_R^2}^{Q^2} \frac{d^2\boldsymbol{q}_1}{\pi q_1^2} \int_{z_1^2 q_1^2}^{\mu_R^2} \frac{d^2\boldsymbol{q}_2}{\pi q_2^2} \\
&\times \int_{\mu_R^2}^{Q^2} \frac{d^2\boldsymbol{q}_3}{\pi q_3^2} \Theta(\mu_R - z_1 q_1) \bar{\alpha}_S^3 + ... \\
&= \frac{(2\bar{\alpha}_S)^3}{\omega^3} \left[\frac{T^2}{\omega} - \frac{T^3}{2} \right] + ... \qquad (3.59)
\end{aligned}
$$

$$
\begin{aligned}
URR|_c &= \int_0^1 dz_1 z_1^{\omega-1} \int_0^1 dz_2 z_2^{\omega-1} \int_0^1 dz_3 z_3^{\omega-1} \int_{\mu^2}^{\mu_R^2} \frac{d^2\boldsymbol{q}_1}{\pi q_1^2} \int_{\mu_R^2}^{Q^2} \frac{d^2\boldsymbol{q}_2}{\pi q_2^2} \\
&\times \int_{max(\mu_R^2, z_2^2 q_2^2)}^{Q^2} \frac{d^2\boldsymbol{q}_3}{\pi q_3^2} \bar{\alpha}_S^3 + ... \\
&= \frac{(2\bar{\alpha}_S)^3}{\omega^3} \left[T^2 S \right] + ... \qquad (3.60)
\end{aligned}
$$

$$
\begin{aligned}
RRR|_c &= \int_0^1 dz_1 z_1^{\omega-1} \int_0^1 dz_2 z_2^{\omega-1} \int_0^1 dz_3 z_3^{\omega-1} \\
&\times \int_{\mu_R^2}^{Q^2} \frac{d^2\boldsymbol{q}_1}{\pi q_1^2} \int_{max(\mu_R^2, z_1^2 q_1^2)}^{Q^2} \frac{d^2\boldsymbol{q}_2}{\pi q_2^2} \int_{max(\mu_R^2, z_2^2 q_2^2)}^{Q^2} \frac{d^2\boldsymbol{q}_3}{\pi q_3^2} \bar{\alpha}_S^3 + ... \\
&= \frac{(2\bar{\alpha}_S)^3}{\omega^3} \left[T^3 \right] + ... \qquad (3.61)
\end{aligned}
$$

The integration limits as in, for example, Eq. 3.57, $max(\mu_R^2, z_1^2 q_1^2)$, ensure that the second emission is coherent to the previous one ($q_2^2 > z_1^2 q_1^2$) and resolved ($q_2^2 > \mu_R^2$) even when the z_1 factor goes to zero.

At first sight these results are completely different from those computed without coherence (BFKL). It is noteworthy that there exist stronger singularities ($\omega \to 0$) than occur in the BFKL approach. The presence of these new singularities may lead one to think that the calculation of exclusive quantities with the BFKL equation is destined to give incorrect expressions, and that the correct solution to the problem is to introduce coherence. However, if we calculate the 0-, 1-, 2-, 3-jet production rates with coherence we obtain the following expressions:

$$
\text{“}0-\text{jet”} = U|_c + UU|_c + UUU|_c = \frac{(2\bar{\alpha}_S)}{\omega} S + \frac{(2\bar{\alpha}_S)^2}{\omega^2} \left[\frac{S^2}{2} \right] + \frac{(2\bar{\alpha}_S)^3}{\omega^3} \left[\frac{S^3}{6} \right] \qquad (3.62)
$$

$$
\begin{aligned}
\text{“}1-\text{jet”} &= R|_c + RU|_c + UR|_c + RUU|_c + URU|_c + UUR|_c \\
&= \frac{(2\bar{\alpha}_S)}{\omega} T + \frac{(2\bar{\alpha}_S)^2}{\omega^2} \left[TS - \frac{1}{2} T^2 \right] \\
&+ \frac{(2\bar{\alpha}_S)^3}{\omega^3} \left[\frac{1}{3} T^3 - \frac{1}{2} T^2 S + \frac{1}{2} T S^2 \right] \qquad (3.63)
\end{aligned}
$$

$$\begin{aligned}\text{“}2-\text{jet”} &= RR|_c + RRU|_c + RUR|_c + URR|_c \\ &= \frac{(2\bar{\alpha}_S)^2}{\omega^2}\left[T^2\right] + \frac{(2\bar{\alpha}_S)^3}{\omega^3}\left[T^2 S - \frac{7}{6}T^3\right]\end{aligned} \tag{3.64}$$

$$\text{“}3-\text{jet”} = RRR|_c = \frac{(2\bar{\alpha}_S)^3}{\omega^3}\left[T^3\right] \tag{3.65}$$

The additional “coherence induced” logarithms cancel making these results identical to those obtained without coherence in the previous chapter.

3.3.3 Equivalence between BFKL and CCFM jet rates

Table 1: BFKL

$F_{0\omega}^{(1)} =$	$U+$	$R+$		
$F_{0\omega}^{(2)} =$	$UU+$	$RU + UR+$	RR	
$F_{0\omega}^{(3)} =$	$UUU+$	$RUU + URU + UUR+$	$RRU + RUR + URR+$	RRR
	0-jet	1-jet	2-jet	3-jet

Table 2: COHERENCE

$F_{\omega}^{(1)} =$	$U\vert_c+$	$R\vert_c+$		
$F_{\omega}^{(2)} =$	$UU\vert_c+$	$RU\vert_c + UR\vert_c+$	$RR\vert_c$	
$F_{\omega}^{(3)} =$	$UUU\vert_c+$	$RUU\vert_c + URU\vert_c + UUR\vert_c+$	$RRU\vert_c + RUR\vert_c + URR\vert_c+$	$RRR\vert_c$
	0-jet	1-jet	2-jet	3-jet

On summing the nth row in Table 1 the dependence on the resolution scale disappears and leads to $F_{0\omega}^{(n)}$ which is different from the $F_{\omega}^{(n)}$ computed by summing the corresponding row of Table 2. This is the result demonstrated in [22], i.e. for BFKL

$$U + R = \tag{3.66}$$

$$\frac{(2\bar{\alpha}_S)}{\omega}\left[T+S\right] + \frac{(2\bar{\alpha}_S)^2}{\omega^2}\left[-\frac{1}{2}(T+S)^2\right] + \frac{(2\bar{\alpha}_S)^3}{\omega^3}\left[\frac{1}{3}(T+S)^3\right] + \ldots = F_{0,\omega}^{(1)}(Q)$$

$$UU + RU + UR + RR = \tag{3.67}$$

$$\frac{(2\bar{\alpha}_S)^2}{\omega^2}\left[(T+S)^2\right] + \frac{(2\bar{\alpha}_S)^3}{\omega^3}\left[-\frac{7}{6}(T+S)^3\right] + \ldots = F_{0,\omega}^{(2)}(Q)$$

$$UUU + RUU + URU + UUR + RRU + RUR + URR + RRR = \tag{3.68}$$
$$\frac{(2\bar{\alpha}_S)^3}{\omega^3}\left[(T+S)^3\right] + ... = F^{(3)}_{0,\omega}(Q)$$

Whilst for the terms with angular ordering one finds

$$U|_c + R|_c = \tag{3.69}$$
$$\frac{(2\bar{\alpha}_S)}{\omega}[T+S] + \frac{(2\bar{\alpha}_S)^2}{\omega^2}\left[-\frac{1}{\omega}(T+S)\right] + \frac{(2\bar{\alpha}_S)^3}{\omega^3}\left[\frac{3}{\omega^2}(T+S)\right] + ... = F^{(1)}_{\omega}(Q)$$

$$UU|_c + RU|_c + UR|_c + RR|_c = \tag{3.70}$$
$$\frac{(2\bar{\alpha}_S)^2}{\omega^2}\left[\frac{1}{2}(T+S)^2 + \frac{1}{\omega}(T+S)\right] + \frac{(2\bar{\alpha}_S)^3}{\omega^3}\left[-\frac{1}{\omega}(T+S)^2 - \frac{5}{\omega^2}(T+S)\right] + ... = F^{(2)}_{\omega}(Q)$$

$$UUU|_c + RUU|_c + URU|_c + UUR|_c + RRU|_c + RUR|_c + URR|_c + RRR|_c = \tag{3.71}$$
$$\frac{(2\bar{\alpha}_S)^3}{\omega^3}\left[\frac{1}{6}(T+S)^3 + \frac{1}{\omega}(T+S)^2 + \frac{2}{\omega^2}(T+S)\right] + ... = F^{(3)}_{\omega}(Q)$$

However, summing the columns in each table, one obtains the more physical n-jet rates. In this case the BFKL and coherence results coincide. We note that this cancellation supports the work of [76, 77].

We have shown the explicit cancellation of coherence induced collinear singularities in n-jet rate calculations to order $\bar{\alpha}_S^3$ at the leading logarithm level. Nevertheless we wish to remark that this is not to say that coherence effects are always unimportant. In particular, we have neglected formally subleading terms in $F^{(r)}_{\omega}$ which are only suppressed by factors $\sim (\omega T)^n$ (with $n > 0$). Those terms are relevant if we go beyond the leading $\ln(1/x)$ approximation.

3.3.4 Jet rates to all orders and the CCFM-BFKL equivalent description of final states at leading order

So far to calculate a given n-jet rate we have considered all the graphs with n resolved gluons and any number of unresolvable ones and we expanded the Regge factors to order $\bar{\alpha}_S^3$. Doing so we found that the jet rates expressions calculated both in the multi-Regge (BFKL) approach and in the coherent (CCFM) approach are the same.

We have stressed the fact that in the calculation with coherence there exist stronger singularities ($\omega \to 0$) than occur in BFKL but these additional "coherence induced" logarithms cancel when we sum all the graphs contributing to the jet rates and the final results are identical to those obtained without coherence. We will show now how this cancellation persists for n-jet rates to all orders in $\bar{\alpha}_S$.

In Ref. [78] our results were extended to all orders, for any number of resolved gluons. The BFKL and CCFM formulations were shown to give the same jet rates in leading logarithmic approximation to order $\bar{\alpha}_s^n$ for any n. The factorization of collinear singularities was demonstrated, and a simple generating function for the jet multiplicity distribution was obtained. A summary of the whole approach can be found in [79].

Working within the multi-Regge (BFKL) approach, a simple expression for the n-jet rate was found

$$R_\omega^{(n\ \mathrm{jet})}(Q,\mu_R) = \frac{F_\omega^{(n\ \mathrm{jet})}(Q,\mu_R,\mu)}{F_\omega(Q,\mu)} = \frac{1}{n!}\,\frac{\partial^n}{\partial u^n} R_\omega(u,T)\bigg|_{u=0}, \tag{3.72}$$

where the jet-rate generating function R_ω is given by

$$R_\omega(u,T) = \exp\left(-\frac{2\bar{\alpha}_s}{\omega}T\right)\left[1+(1-u)\frac{2\bar{\alpha}_s}{\omega}T\right]^{\frac{u}{1-u}}. \tag{3.73}$$

The same jet-rate generating function is obtained taking account of coherence from the CCFM formulation of small-x dynamics. After convolution with the measured gluon structure function, it gives the predicted jet rates in the leading logarithmic region $\ln(1/x) \gg T = \ln(Q/\mu_R) \gg 1$, to all orders in α_s, proving that the CCFM results for the multijet contributions are equal to the BFKL predictions, thus completing the all-orders extension of our results. As an example if we apply Eq. 3.72 to calculate the 1-jet rate to order $\bar{\alpha}_s^4$ it gives the same results as ours to order $\bar{\alpha}_s^3$, i.e.

$$\begin{aligned} \text{“}1-\text{jet”} \;=\;& \frac{(2\bar{\alpha}_S)}{\omega}T + \frac{(2\bar{\alpha}_S)^2}{\omega^2}\left[TS - \frac{1}{2}T^2\right] + \frac{(2\bar{\alpha}_S)^3}{\omega^3}\left[\frac{1}{3}T^3 - \frac{1}{2}T^2S + \frac{1}{2}TS^2\right] \\ & + \frac{(2\bar{\alpha}_S)^4}{\omega^4}\left[\frac{1}{6}TS^3 - \frac{1}{4}T^2S^2 + \frac{1}{3}T^3S - \frac{1}{4}T^4\right] + \cdots \end{aligned} \tag{3.74}$$

It is important to note that the jet rate to all orders is collinear safe because all the collinear-divergent parts (carried in the S dependence) factored out in $F_\omega^{(n \text{ jet})}$ and disappeared when dividing by $F_\omega(Q,\mu)$. This gives a cut-off independent function as should be for an observable.

From this generating function it is possible to obtain interesting quantities to all orders, for example the mean number of jets and the mean square fluctuation in this number,

$$\langle n \rangle = \frac{\partial}{\partial u} R_\omega(u,T)\bigg|_{u=1} = \frac{2\bar{\alpha}_s}{\omega} T + \frac{1}{2}\left(\frac{2\bar{\alpha}_s}{\omega} T\right)^2 , \tag{3.75}$$

$$\langle n^2 \rangle - \langle n \rangle^2 = \frac{2\bar{\alpha}_s}{\omega} T + \frac{3}{2}\left(\frac{2\bar{\alpha}_s}{\omega} T\right)^2 + \frac{2}{3}\left(\frac{2\bar{\alpha}_s}{\omega} T\right)^3 . \tag{3.76}$$

In general, the pth central moment of the jet multiplicity distribution is a polynomial in $\bar{\alpha}_s T/\omega$ of degree $2p-1$, indicating that the distribution becomes relatively narrow in the limit of very small x and large Q/μ_R [78].

In Ref. [55, 56] the subject is developed even further and all subleading logarithms of Q^2/μ_R^2 were included. There the formalism was also applied to calculate the jet multiplicity at low values of the Bjorken variable x in processes like Higgs production at the future Large Hadron Collider (LHC). In Ref. [55] they extended the results from a $[\bar{\alpha}_s \ln(1/x)\ln(Q^2/\mu_R^2)]^n$ resummation to a $[\bar{\alpha}_s \ln(1/x)]^n[\ln(Q^2/\mu_R^2)]^m$ one with $0 < m \leq n$. It was shown that the simple quadratic and cubic forms of the mean and the variance found previously remain valid to the new logarithmic accuracy. Then the mean and variance of the jet multiplicity in Higgs boson production at LHC as a function of the Higgs mass was obtained.

The CCFM equation is the proper one to describe exclusive observables because it gives the correct leading logarithms at small x. But it has a practical disadvantage compared to the BFKL equation because it is much more difficult to solve, both numerically and analytically. All the work referred to in this section has been possible due to the equivalence of the BFKL and CCFM prescriptions at leading order. The calculations in the BFKL formalism turn out to be technically much simpler.

Recently, it has been now shown that for any sufficiently inclusive observables the CCFM formalism leads to the same results as the BFKL equation [80]. The key idea to understand this result comes if we try to obtain the results of Ref. [22] from those in the previous section in the limit $\mu_R \to 0$. To get the right solution we should consider subleading terms $\bar{\alpha}_s \ln^2 Q/\mu_R$ which must be resummed when taking the limit $\mu_R \to 0$ to obtain a continuous transition from the case where BFKL and CCFM results are equivalent, to that of them being different. If we also consider the effects of introducing the $z \to 1$ divergent part of the splitting function in the CCFM approach we will see that this leads to all BFKL and CCFM final-state properties being identical in the $[\bar{\alpha}_s \ln(1/x) \ln(Q^2/\mu_R^2)]^n$ approximation [80].

We should emphasise that these results have been obtained at leading order. If we go beyond this approximation differences in the BFKL and CCFM predictions arise making the latter mandatory for the description of final states. There have been some attempts to implement CCFM into an event generator, e.g. SMALLX [81, 82], LDCMC [83] and CASCADE [84]. There is a large debate about their validity because their predictions depend strongly on the treatment of the so-called *consistency constraint* $k_i^2 > z_i q_i^2$ in Eq. 3.25 and the inclusion of non-singular terms in the gluon splitting functions. More theoretical and phenomenological work is needed to understand how to treat non-leading effects which are important in the description of the data [85, 86, 87, 88, 89, 90].

Chapter 4

The BFKL equation at next-to-leading order

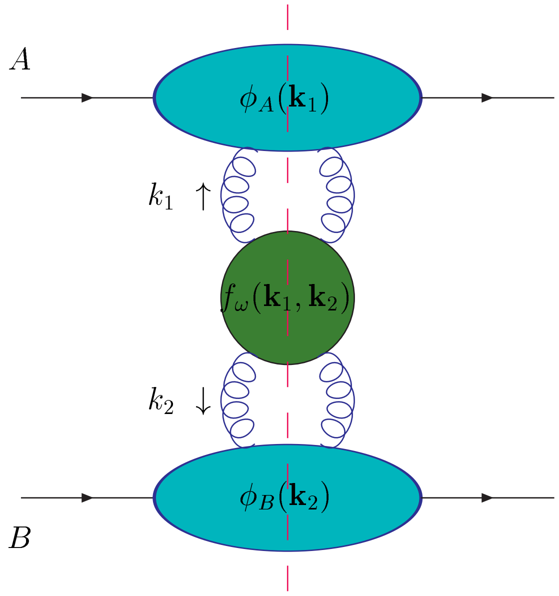

Figure 4.1: Elements for high energy factorization

4.1 Introduction

In this chapter we will introduce all the elements needed to obtain the next-to-leading expansion in $\ln(1/x)$. We will indicate how to resum the $\alpha_S(\alpha_S \ln(1/x))^n$ terms.

We would like to generalise the high energy $\mathbf{k}$-dependent leading-order factorization to the new accuracy. This factorization is based on the separation of the cross section into process dependent impact factors and a kernel which is supposed to be independent of the external probes. To proceed it is assumed that the factorization formula

$$\frac{d\sigma_{AB}(s)}{d\mathbf{k}_1 d\mathbf{k}_2} = \int \frac{d\omega}{2\pi i} \left(\frac{s}{s_0(\mathbf{k}_1, \mathbf{k}_2)} \right)^{\omega} \phi_A(\mathbf{k}_1) f_\omega(\mathbf{k}_1, \mathbf{k}_2) \phi_B(\mathbf{k}_2) \tag{4.1}$$

holds at NLO. The elements of this expression are indicated in Fig. 4.1.

The factorization scheme turns out not to be unique because some NLO terms can be included arbitrarily in the Green's function or in the impact factors. For consistency of the whole procedure, the factorization assumption in Eq. 4.1 must be proved at the end of the calculation. This means to check that the two key properties of factorization at LO, i.e., the dominance of the exchange of gluons in the t-channel and the reggeization of the gluon propagator still hold at NLO. It is important to note that the factorization formula 4.1 has been checked at one-loop [91] and two-loop [92] order but it has not been justified to all orders in the perturbative expansion so far.

4.2 The impact factors

An important issue in determining the impact factors is how to choose the scale s_0 in the $\left(\frac{s}{s_0}\right)^\omega$ term of the cross section. We have seen that the LO results did not depend upon this choice, at NLO the situation is different. If we assume that at NLO the kernel can be written as

$$f_\omega = (\omega - \mathcal{K})^{-1}, \tag{4.2}$$

and we expand the impact factors and the kernel in powers of $\bar{\alpha}_S$ we obtain the following expansion for the differential cross section

$$\frac{d\sigma_{AB}(s)}{d\mathbf{k}_1 d\mathbf{k}_2} = \int \frac{d\omega}{2\pi i} \frac{\left(\phi_A^{(0)}(\mathbf{k}_1) + \bar{\alpha}_S \phi_A^{(1)}(\mathbf{k}_1)\right) e^{\omega \ln \frac{s}{\eta s_0}} \left(\phi_B^{(0)}(\mathbf{k}_2) + \bar{\alpha}_S \phi_B^{(1)}(\mathbf{k}_2)\right)}{\omega - \bar{\alpha}_S \mathcal{K}^{(0)}(\mathbf{k}_1, \mathbf{k}_2) - \bar{\alpha}_S^2 \mathcal{K}^{(1)}(\mathbf{k}_1, \mathbf{k}_2)}, \tag{4.3}$$

where we have introduced the η term representing the freedom in the choice of the energy factor scaling s.

Now we can see how a change in s_0 introduces a shift in the definition of the impact factors corrections, after integrating in ω we find that

$$\begin{aligned} \frac{d\sigma_{AB}(s)}{d\mathbf{k}_1 d\mathbf{k}_2} &= \phi_A^{(0)}(\mathbf{k}_1)\phi_B^{(0)}(\mathbf{k}_2) + \bar{\alpha}_s \Big[\phi_A^{(0)}(\mathbf{k}_1)\mathcal{K}^{(0)}(\mathbf{k}_1, \mathbf{k}_2)\phi_B^{(0)}(\mathbf{k}_2) \ln \frac{s}{s_0} + \\ & \phi_A^{(1)}(\mathbf{k}_1)\phi_B^{(0)}(\mathbf{k}_2) + \phi_A^{(0)}(\mathbf{k}_1)\phi_B^{(1)}(\mathbf{k}_2) + \phi_A^{(0)}(\mathbf{k}_1)\mathcal{K}^{(0)}(\mathbf{k}_1, \mathbf{k}_2)\phi_B^{(0)}(\mathbf{k}_2) \ln \frac{1}{\eta}\Big]. \end{aligned} \tag{4.4}$$

The leading logarithmic term remains the same but the part proportional to $\ln \eta$ can be embedded in the definition of the impact factors at NLO. The fact that these probe-independent NLO terms can belong to either the impact factors or to the Green's function forces us to choose a scheme to fix the scale. We will follow reference [93] and choose as LO terms those consistent with the infrared and collinear features of

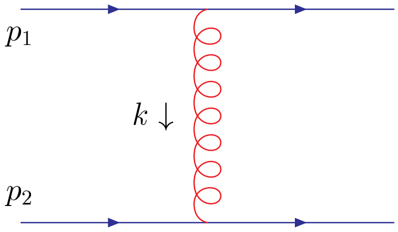

Figure 4.2: Born level amplitude in high energy scattering

the process under consideration. Any finite constants will be included in the NLO corrections.

We will give a hint to the derivation of the impact factors as calculated in Ref. [93]. We will obtain the expressions for the quark and gluon impact factors to LO and NLO accuracy. This will enable us to obtain a definite expression for the BFKL kernel, first at LO to illustrate the procedure and then at NLO which is the case of interest in this section.

In high energy parton-parton scattering it is hoped that we can define a process with two hard scales by fixing the transverse momenta $\mathbf{k}_1, \mathbf{k}_2$ of the fragmentation jets. The fragmentation region of the particle A is the region of phase space which corresponds to the outgoing particles being emitted almost collinear to A.

4.3 Leading order case

We want to study the high energy scattering of two partons which can be either quarks or gluons at LO. Our aim is to factorize it in terms of impact factors and gluon Green's function. Dimensional regularization in the $\overline{\mathrm{MS}}$ scheme in $4 + 2\epsilon$ dimensions is used to renormalize the coupling constant and to remove the infrared divergences found in the intermediate steps.

We first calculate the Born level amplitude of Fig. 4.2. As we are interested in

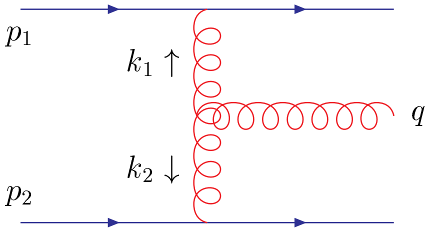

Figure 4.3: Amplitude for real gluon emission in the central region

the differential cross section, we use the transverse space measure

$$d[\mathbf{k}] = \frac{d^{2+2\epsilon}\mathbf{k}}{\pi^{1+\epsilon}}, \tag{4.5}$$

to obtain

$$\frac{d\sigma_{AB}^{\mathrm{Born}}}{d[\mathbf{k}]} = \phi_A^{(0)}(\mathbf{k})\phi_B^{(0)}(\mathbf{k}). \tag{4.6}$$

The Born impact factors are

$$\phi_i^{(0)}(\mathbf{k}) = \sqrt{\frac{\pi}{N_c^2-1}}\frac{2C_i\alpha_s(4\pi)^{\epsilon/2}}{\mathbf{k}^2\mu^{2\epsilon}\Gamma(1-\epsilon)} \tag{4.7}$$

with μ being the renormalization scale,

$$\alpha_s = \frac{g_s^2\Gamma(1-\epsilon)\mu^{2\epsilon}}{(4\pi)^{1+\epsilon}} \tag{4.8}$$

the dimensionless coupling constant, and the factor C_i different for quarks and gluons, i.e.

$$C_{\mathrm{quark}} = C_F = \frac{N_c^2-1}{2N_c}, \tag{4.9}$$

$$C_{\mathrm{gluon}} = C_A = N_c. \tag{4.10}$$

To get the one-loop kernel we add real and virtual contributions to the Born cross section. The LO kinematics favours the emission of a gluon of momentum q in the central region. We need to use the amplitude for the graph in Fig. 4.3 and after polarisation and colour averaging, and including the virtual one-loop corrections which reggeize the exchanged gluon propagators, the total leading contribution, up to one-loop order, is

$$\frac{d\sigma_{AB}^{LO}}{d[\mathbf{k}_1]d[\mathbf{k}_2]} = \phi_A^{(0)}(\mathbf{k}_1)\phi_B^{(0)}(\mathbf{k}_2)\left[\delta[\mathbf{q}] + \bar{\alpha}_s\mathcal{K}_0(\mathbf{k}_1,\mathbf{k}_2)\ln\frac{s}{s_0}\right], \tag{4.11}$$

where

$$\begin{aligned} \bar{\alpha}_s \mathcal{K}_0(\mathbf{k}_1, \mathbf{k}_2) &= \frac{\bar{\alpha}_s}{\mathbf{q}^2 \Gamma(1-\epsilon)\mu^{2\epsilon}} + 2\omega^{(1)}(\mathbf{k}_1^2)\delta[\mathbf{q}], && (4.12) \\ \delta[\mathbf{q}] &= \pi^{1+\epsilon}\delta^{2+2\epsilon}(\mathbf{q}), && (4.13) \\ \omega^{(1)}(\mathbf{k}^2) &= -\frac{g_s^2 C_A}{(4\pi)^{2+\epsilon}}\mathbf{k}^2 \int \frac{d[\mathbf{p}]}{\mathbf{p}^2(\mathbf{k}-\mathbf{p})^2} \\ &= -\frac{\bar{\alpha}_s}{2\epsilon}\frac{\Gamma^2(1+\epsilon)}{\Gamma(1+2\epsilon)}\left(\frac{\mathbf{k}^2}{\mu^2}\right)^{\epsilon}. && (4.14) \end{aligned}$$

The last term, $\omega^{(1)}(\mathbf{k}^2)$, is the $4+2\epsilon$ dimensional representation of the LO term in the reggeized gluon propagator, ie

$$\left(\frac{s}{\mathbf{k}^2}\right)^{\omega(\mathbf{k}^2)} = 1 + \omega^{(1)}(\mathbf{k}^2)\ln\frac{s}{\mathbf{k}^2} + \mathcal{O}(\bar{\alpha}_s^2). \tag{4.15}$$

The leading order gluon Green's function defined as

$$f_\omega^{LO} = \frac{1}{\omega - \bar{\alpha}_s \mathcal{K}_0} \tag{4.16}$$

satisfies the LO BFKL equation.

4.4 Next-to-leading order case

Quark impact factors at NLO

The calculation of the quark-parton scattering can be found in Ref. [91]. In that work arguments are given to favour the choice of

$$s_0(\mathbf{k}_1, \mathbf{k}_2) = \mathrm{Max}(\mathbf{q}, \mathbf{k}_1) \cdot \mathrm{Max}(\mathbf{q}, \mathbf{k}_2) \tag{4.17}$$

with $q^\mu = k_1^\mu + k_2^\mu$, as a convenient scale to calculate the impact factor with divergences consistent with the collinear singularities of the process. It was shown that the contribution to the NLO differential cross section for $qq \to qgq$ coming from real gluon emission has a dominant term in the region

$$|\mathbf{q}|(1-z_1) \gg |\mathbf{k}_1| z_1, \tag{4.18}$$

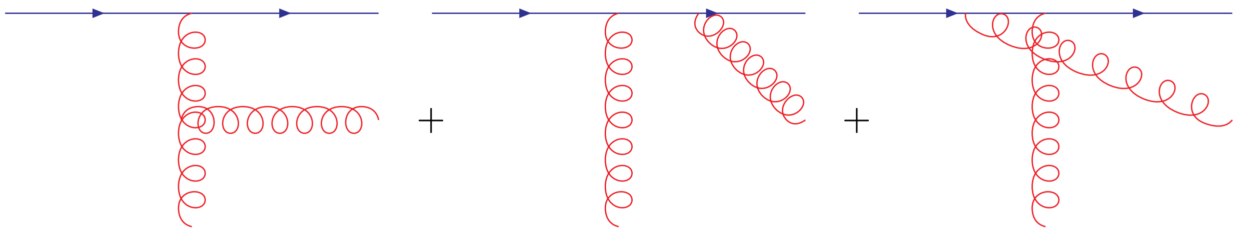

Figure 4.4: Graphs for real gluon emission in the fragmentation region

with

$$k_1^\mu \simeq z_1 p_1^\mu - \frac{\mathbf{k}_1^2}{(1-z_1)s} p_2^\mu + \mathbf{k}_1^\mu. \tag{4.19}$$

This is the *coherent* region where the gluon is emitted at angles larger than the $q_A q_{A'}$ scattering angle [73, 20]. After averaging in the azimuthal angle in $\mathbf{k}_1$ at fixed $|\mathbf{q}|$ we get (in the coherent region)

$$\frac{d\sigma^{NLO}}{d[\mathbf{k}_1]d[\mathbf{k}_2]} \sim \ln \frac{s}{\mathrm{Max}(\mathbf{q}, \mathbf{k}_1) \cdot \mathrm{Max}(\mathbf{q}, \mathbf{k}_2)}, \tag{4.20}$$

which suggests the natural choice of Eq. 4.17.

The relevant amplitudes to consider for quark impact factor at NLO are represented in Fig. 4.4. Notice that now the gluon does not need to be in the central region.

The result for the one-loop correction to the quark impact factor can be expressed in terms of the LO one as

$$\phi_q^{(1)}(\mathbf{k}) = \phi_q^{(0)}(\mathbf{k})\omega^{(1)}(\mathbf{k}^2)\left[\left(\frac{11}{6} - \frac{n_f}{3N_c}\right) + \left(\frac{3}{2} - \frac{\epsilon}{2}\right) - \frac{\mathcal{K}\epsilon}{N_c}\right], \tag{4.21}$$

with

$$\mathcal{K} = \left[N_c\left(\frac{67}{18} - \frac{\pi^2}{6}\right) - \frac{5n_f}{9}\right]. \tag{4.22}$$

The process dependent impact factors carry poles in $\frac{1}{\epsilon}$ corresponding to the collinear singularities at $\mathbf{k}^2 = 0$ of the $q \to g$ transition of the initial massless quark.

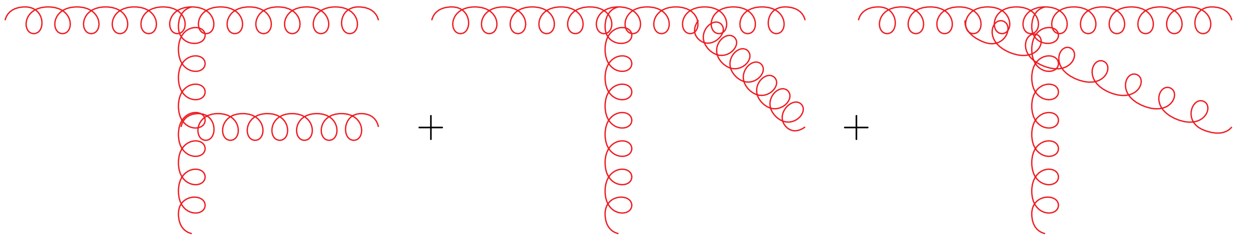

Figure 4.5: Graphs contributing to the $gB \to ggB$ amplitude

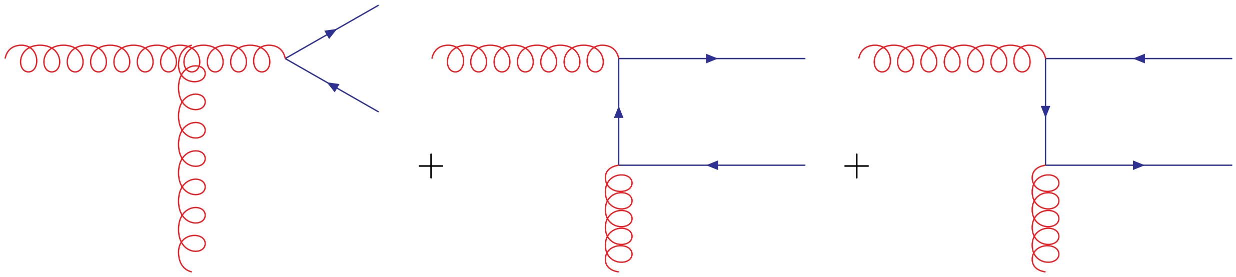

Figure 4.6: Graphs contributing to the $gB \to q\bar{q}B$ amplitude

Gluon impact factors at NLO

For the gluon-parton scattering there are two different final states for three-particle production. We can have the parton B and two gluons, as in Fig. 4.5, or the parton B and a quark-antiquark pair. In the last case the main contributions to the cross section come from the case when the q and the $\bar{q}$ are in the same fragmentation vertex, Fig. 4.6, because any other possibility implies a fermionic exchange which is suppressed by a factor $\frac{|t|}{s}$, see Fig. 4.7 for an example.

The final answer for the gluon impact factor turns out to be the expression

$$\phi_g^{(1)}(\mathbf{k}) = \phi_g^{(0)}(\mathbf{k})\omega^{(1)}(\mathbf{k}^2)\left[\left(\frac{11}{6} - \frac{n_f}{3N_c}\right) + \left(\frac{11}{6} + \frac{(2+\epsilon)n_f}{6N_c}\right)\right. \quad (4.23)$$

$$\left. - \frac{C_F n_f}{N_c^2}\left(\frac{2}{3} + \frac{\epsilon}{3}\right) - \frac{\mathcal{K}\epsilon}{N_c}\right], \quad (4.24)$$

with $\mathcal{K}$ as in Eq. 4.22.

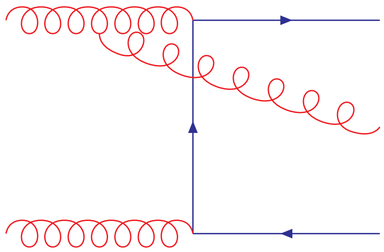

Figure 4.7: Non-contributing diagram at NLO for $gB \to q\bar{q}B$

Effect of the energy scale choice

For a proper study of the influence of a possible change in s_0 here we reproduce the analysis developed in Ref. [91]. The most general form for the Green's function in Eq. 4.1 at NLO can be written as

$$f_\omega = (1 + \bar{\alpha}_s H_{\text{left}})[\omega - \bar{\alpha}_s \mathcal{K}_0 - \bar{\alpha}_s^2 \mathcal{K}_{\text{NLO}}]^{-1}(1 + \bar{\alpha}_s H_{\text{right}}), \tag{4.25}$$

where the NLO kernel, which we will show explicitly in the next section, has the structure

$$\mathcal{K}_{\text{NLO}} = -b\mathcal{K}_0 \ln \frac{\mathbf{k}_1^2}{\mu^2} + \mathcal{K}_1, \tag{4.26}$$

with

$$b = \frac{11}{12} - \frac{n_f}{6N_c}. \tag{4.27}$$

Two new factors, $H_{\text{left}}(\mathbf{k}_1, \mathbf{k}_2)$, $H_{\text{right}}(\mathbf{k}_1, \mathbf{k}_2)$, have been introduced and the NLO kernel has a term with a β-function coefficient, coming from the running coupling contribution, and a renormalization scale independent term, $\mathcal{K}_1$.

The new factors are needed when we change to a different scale. If we choose a factorized scale $s_0 = \mathbf{k}_1\mathbf{k}_2$ then at one-loop accuracy the modification of the gluon Green's function is mandatory with

$$H_{\text{left}}(\mathbf{k}_1, \mathbf{k}_2) = H_{\text{right}}(\mathbf{k}_1, \mathbf{k}_2) = -\frac{\bar{\alpha}_s}{\pi^{1+\epsilon}\Gamma(1-\epsilon)\mu^{2\epsilon}} \theta(q - k_2) \ln \frac{q}{k_2}. \tag{4.28}$$

These new kernels carry double poles in ϵ and they must be included in f_ω if we want to have infrared finite impact factors with the new factorized energy scale. They are zero if we choose the scale as in previous sections.

The next-to-leading order BFKL kernel

We have already anticipated the general structure of the kernel at two loops accuracy, Eq. 4.26. To obtain the complete result the two loops differential cross section has to be calculated. Taking into account the expansion to order $\bar{\alpha}_s^2$ of all the factors present in the cross section and keeping only the logarithmic enhanced terms we obtain

$$\begin{aligned}\frac{d\sigma_{AB}(s)}{d\mathbf{k}_1 d\mathbf{k}_2} &= \phi_A^{(0)}(\mathbf{k}_1)\phi_B^{(0)}(\mathbf{k}_2) + \bar{\alpha}_s \left\{ \ln\frac{s}{s_0}\phi_A^{(0)}(\mathbf{k}_1)\mathcal{K}_0(\mathbf{k}_1,\mathbf{k}_2)\phi_B^{(0)}(\mathbf{k}_2)\right\} \\ &+ \bar{\alpha}_s^2 \left\{ \ln\frac{s}{s_0}\mathcal{K}_0(\mathbf{k}_1,\mathbf{k}_2)\left[\phi_A^{(0)}(\mathbf{k}_1)\phi_B^{(1)}(\mathbf{k}_2) + \phi_A^{(1)}(\mathbf{k}_1)\phi_B^{(0)}(\mathbf{k}_2)\right.\right. \\ &\qquad + \phi_A^{(0)}(\mathbf{k}_1)\left(H_{\rm left}(\mathbf{k}_1,\mathbf{k}_2) + H_{\rm right}(\mathbf{k}_1,\mathbf{k}_2)\right)\phi_B^{(0)}(\mathbf{k}_2) \\ &\qquad \left. + \left(\mathcal{K}_0(\mathbf{k}_1,\mathbf{k}_2)\right)^{-1}\phi_A^{(0)}(\mathbf{k}_1)\mathcal{K}_1(\mathbf{k}_1,\mathbf{k}_2)\phi_B^{(0)}(\mathbf{k}_2)\right] \\ &\left. + \frac{1}{2}\ln^2\frac{s}{s_0}\phi_A^{(0)}(\mathbf{k}_1)\mathcal{K}_0^2(\mathbf{k}_1,\mathbf{k}_2)\phi_B^{(0)}(\mathbf{k}_2)\right\} \qquad (4.29)\end{aligned}$$

If we are able to calculate this cross section and we know the impact factors at one loop and the functions $H_{\rm left}, H_{\rm right}$, for a given choice of the scale s_0, then we can obtain the NLO kernel $\mathcal{K}_1$ without any ambiguity.

To obtain this differential cross section at two loops in NLO is very complicated and only recently it has been completed. We refer the reader to the literature to find out about the details of the calculation [94, 92]. We will only indicate that to achieve the NLO accuracy it is necessary to relax the *multi-Regge kinematics* and take into account processes where an additional power of $\bar{\alpha}_s$ is not compensated by a $\ln s$, this approximation is known as *quasi-multi-Regge kinematics*. Relaxing the multi-Regge kinematics means that we should consider those amplitudes with emission of two gluons or a $q\bar{q}$ with similar rapidity. They can be emitted either in the forward-rapidity region as in Fig. 4.8 or in the central-rapidity region as in shown in Fig. 4.9.

For the sake of definiteness and with the intention of showing the result for the NLO kernel, we write the BFKL equation in $2+2\epsilon$ dimensions

$$\omega f_\omega(\mathbf{k}_1,\mathbf{k}_2) = \delta^{2+2\epsilon}(\mathbf{k}_1-\mathbf{k}_2) + \int d^{2+2\epsilon}\mathbf{k}\ \mathcal{K}(\mathbf{k}_1,\mathbf{k})f_\omega(\mathbf{k},\mathbf{k}_2). \qquad (4.30)$$

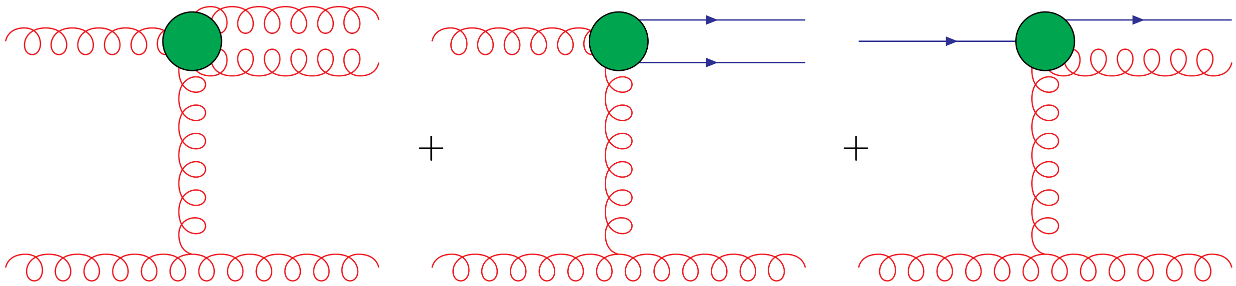

Figure 4.8: Amplitudes for three partons production with a pair produced in the forward-rapidity region

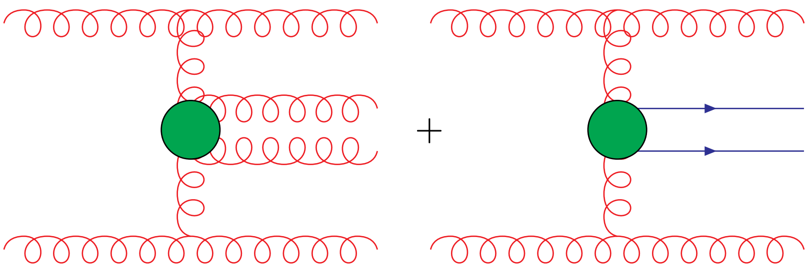

Figure 4.9: Amplitudes for four partons production with a pair produced in the central-rapidity region

The kernel can be written as an expansion over the QCD coupling constant as

$$\mathcal{K}(\mathbf{k}_1,\mathbf{k}_2) = 2\left(\omega^{(0)}(k_1)+\omega^{(2)}(k_1)+\cdots\right)\delta^{2+2\epsilon}(\mathbf{k}_1-\mathbf{k}_2)+\mathcal{K}_0(\mathbf{k}_1,\mathbf{k}_2)+\mathcal{K}_1(\mathbf{k}_1,\mathbf{k}_2)+\cdots. \tag{4.31}$$

The LO Born expressions are known

$$\omega^{(0)}(k) = -\frac{\alpha_s N_c}{4\pi\mu^{2\epsilon}}\left(\frac{2}{\epsilon}+2\ln\frac{k^2}{\mu^2}\right), \tag{4.32}$$

$$\mathcal{K}_0(\mathbf{k}_1,\mathbf{k}_2) = \frac{\alpha_s N_c}{\pi^{2+\epsilon}\Gamma(1-\epsilon)\mu^{4\epsilon}}\frac{1}{(\mathbf{k}_1-\mathbf{k}_2)^2}. \tag{4.33}$$

The two-loop correction to the gluon Regge trajectory for massless quarks was calculated in Ref. [95, 96] and reads

$$\begin{aligned}\omega^{(2)}(k) = & -\frac{\alpha_s^2 N_c^2}{(4\pi)^2\mu^{4\epsilon}}\left[\left(\frac{11}{3}-\frac{2}{3}\frac{n_f}{N_c}\right)\left(\frac{1}{\epsilon^2}-\ln^2\frac{k^2}{\mu^2}\right)\right. \\ & \left.+\left(\frac{67}{9}-\frac{\pi^2}{3}-\frac{10}{9}\frac{n_f}{N_c}\right)\left(\frac{1}{\epsilon}+2\ln\left(\frac{k^2}{\mu^2}\right)\right)-\frac{404}{27}+2\zeta(3)+\frac{56}{27}\frac{n_f}{N_c}\right].\end{aligned} \tag{4.34}$$

The poles correspond to infrared divergences and they will cancel out in the cross section.

The contributions to the NLO kernel have two origins, from the one-loop virtual correction to the one-gluon production cross section [97, 98, 99] and from the Born cross-sections for production of two gluons [100, 101] and $q\bar{q}$ pair [102, 103, 104, 105, 106]. Putting them together we obtain

$$\begin{aligned}
\mathcal{K}_1(\mathbf{k}_1,\mathbf{k}_2) &= \frac{\alpha_s N_c}{\pi^{2+\epsilon}\Gamma(1-\epsilon)\mu^{4\epsilon}} \\
&\times \left\{\frac{1}{(\mathbf{k}_1-\mathbf{k}_2)^2}\left[\left(\frac{11}{3}-\frac{2}{3}\frac{n_f}{N_c}\right)\frac{1}{\epsilon}\left(1-\left(\frac{(\mathbf{k}_1-\mathbf{k}_2)^2}{\mu^2}\right)^{\epsilon}\left(1-\epsilon^2\frac{\pi^2}{6}\right)\right)\right.\right. \\
&+ \left.\left(\frac{(\mathbf{k}_1-\mathbf{k}_2)^2}{\mu^2}\right)^{\epsilon}\left(\frac{67}{9}-\frac{\pi^2}{3}-\frac{10}{9}\frac{n_f}{N_c}+\epsilon\left(-\frac{404}{27}+14\zeta(3)+\frac{56}{27}\frac{n_f}{N_c}\right)\right)\right] \\
&-\left(1+\frac{n_f}{N_c^3}\right)\frac{2\mathbf{k}_1^2\mathbf{k}_2^2-3(\mathbf{k}_1\mathbf{k}_2)^2}{16\mathbf{k}_1^2\mathbf{k}_2^2}\left(\frac{2}{\mathbf{k}_1^2}+\frac{2}{\mathbf{k}_2^2}+(\frac{1}{\mathbf{k}_2^2}-\frac{1}{\mathbf{k}_1^2})\ln\frac{\mathbf{k}_1^2}{\mathbf{k}_2^2}\right)-\frac{1}{(\mathbf{k}_1-\mathbf{k}_2)^2}\left(\ln\frac{\mathbf{k}_1^2}{\mathbf{k}_2^2}\right)^2 \\
&+\frac{2(\mathbf{k}_1^2-\mathbf{k}_2^2)}{(\mathbf{k}_1-\mathbf{k}_2)^2(\mathbf{k}_1+\mathbf{k}_2)^2}\left(\frac{1}{2}\ln\frac{\mathbf{k}_1^2}{\mathbf{k}_2^2}\ln\left(\frac{\mathbf{k}_1^2\mathbf{k}_2^2(\mathbf{k}_1-\mathbf{k}_2)^4}{(\mathbf{k}_1^2+\mathbf{k}_2^2)^4}\right)+L\left(-\frac{\mathbf{k}_1^2}{\mathbf{k}_2^2}\right)+L\left(-\frac{\mathbf{k}_2^2}{\mathbf{k}_1^2}\right)\right) \\
&-\left(3+(1+\frac{n_f}{N_c^3})\left(1-\frac{(\mathbf{k}_1^2+\mathbf{k}_2^2)^2}{8\mathbf{k}_1^2\mathbf{k}_2^2}-\frac{2\mathbf{k}_1^2\mathbf{k}_2^2-3\mathbf{k}_1^4-3\mathbf{k}_2^4}{16\mathbf{k}_1^2\mathbf{k}_2^2}\right)\right)\int_0^\infty dx\frac{\ln\left|\frac{1+x}{1-x}\right|}{\mathbf{k}_1^2+x^2\mathbf{k}_2^2} \\
&- \left.\left(1-\frac{(\mathbf{k}_1^2-\mathbf{k}_2^2)^2}{(\mathbf{k}_1-\mathbf{k}_2)^2(\mathbf{k}_1+\mathbf{k}_2)^2}\right)\left(\int_0^1-\int_1^\infty\right)dz\frac{\ln\frac{(z\mathbf{k}_1)^2}{\mathbf{k}_2^2}}{(\mathbf{k}_2-z\mathbf{k}_1)^2}\right\}, \qquad (4.35)
\end{aligned}$$

with

$$L(z) = \int_0^z \frac{dt}{t}\ln(1-t), \qquad (4.36)$$

$$\zeta(n) = \sum_{k=1}^{\infty} k^{-n}. \qquad (4.37)$$

To analyse the physical implications of this kernel it is more convenient to apply it to the spherically symmetric eigenfunctions of the leading order kernel, $\mathbf{k}^{2(\gamma-1)}$,

$$\int d^{2+2\epsilon}\mathbf{k}_2\mathcal{K}(\mathbf{k}_1,\mathbf{k}_2)\mathbf{k}_2^{2(\gamma-1)} = \bar{\alpha}_s(\mathbf{k}_1^2)\left(\chi_0(\gamma)+\bar{\alpha}_s(\mathbf{k}_1^2)\chi_1(\gamma)\right)\mathbf{k}_1^{2(\gamma-1)}. \qquad (4.38)$$

The leading order kernel is given by

$$\chi_0(\gamma) = 2\psi(1)-\psi(\gamma)-\psi(1-\gamma) \qquad (4.39)$$

and χ_1 has recently become available [94, 92]:

$$
\begin{aligned}
\chi_1(\gamma) &= -\frac{1}{8}\left(\frac{11}{3}-\frac{2n_f}{3N_c}\right)\chi_0(\gamma)^2+\left(\frac{67}{36}-\frac{\pi^2}{12}-\frac{5n_f}{18N_c}\right)\chi_0(\gamma)+\frac{3}{2}\zeta(3)\\
&- \frac{\pi^2\cos\pi\gamma}{4(1-2\gamma)\sin^2\pi\gamma}\left(3+\left(1+\frac{n_f}{N_c^3}\right)\frac{2+3\gamma(1-\gamma)}{(3-2\gamma)(1+2\gamma)}\right)\\
&+ \frac{\psi''(\gamma)+\psi''(1-\gamma)}{4}+\frac{\pi^3}{4\sin\pi\gamma}-\phi(\gamma)
\end{aligned}
\tag{4.40}
$$

where

$$
\phi(\gamma)=\sum_{n=0}^{\infty}(-1)^n\left[\frac{\psi(n+1+\gamma)-\psi(1)}{(n+\gamma)^2}+\frac{\psi(n+2-\gamma)-\psi(1)}{(n+1-\gamma)^2}\right]. \tag{4.41}
$$

In the next chapter we will analyse the physical implications of these results. We will see how the NLO corrections to the BFKL kernel turn out to be huge and negative compared to the LO one and we will explain the methods developed in recent years to understand such a behaviour of the perturbative expansion.

Chapter 5

Improving the BFKL expansion

As we have seen, the original result at leading order obtained by Lipatov et al. more than twenty years ago predicted that the cross section for the scattering of hadronic objects in the high energy limit should grow as a power of s. This power turned out to be of the order of 0.5 for α_s with a typical value of 0.2. There has been a large experimental activity to check if this prediction is correct but it turned out that the cross sections rise with a power much smaller that 0.5.

The hope for the theorists was that the resummation of the terms $\alpha_s(\alpha_s \ln s)^n$ was going to give new light into the problem. The calculation of the next-to-leading order terms in the BFKL formalism and the fact that they turned out to be very large opened a debate about the validity of the whole approach. In this chapter we will show the techniques which have been proposed in order to cure the problem.

5.1 Structure of the next-to-leading order corrections

In chapter 2 we have sketched the derivation of the NLO terms in the BFKL approach. Immediately after they appeared these corrections were found to have quite a pathological behaviour. The problems come from two sides, one related to the running coupling term of the kernel, which we will discuss only at the end of this thesis, and other associated with the scale-invariant term, which will be studied throughly in the following.

We recall that the action of the next-to-leading BFKL kernel on the LO eigenfunction can be written as

$$\bar{\alpha}_s(\mathbf{k}^2)\left(\chi_0(\gamma)+\bar{\alpha}_s(\mathbf{k}^2)\chi_1(\gamma)\right), \tag{5.1}$$

and the QCD coupling, $\bar{\alpha}_s = \alpha_s N_c/\pi$, can be expressed as

$$\bar{\alpha}_s(\mathbf{k}^2) = \frac{\bar{\alpha}_s(\mu^2)}{1+\bar{\alpha}_s(\mu^2) b \ln\frac{\mathbf{k}^2}{\mu^2}} \simeq \bar{\alpha}_s(\mu^2)\left(1-\bar{\alpha}_s(\mu^2) b \ln\frac{\mathbf{k}^2}{\mu^2}\right), \tag{5.2}$$

with

$$b = \frac{11}{12} - \frac{n_f}{6N_c}. \tag{5.3}$$

This is a correct approximation within the accuracy of the calculation and gives us the freedom to write the NLO eigenvalue (5.1) as

$$\left[\bar{\alpha}_s(\mu^2)\chi_0(\gamma) + \bar{\alpha}_s^2(\mu^2)\chi_1(\gamma)\right]_{\text{scale invariant}} + \left[-\bar{\alpha}_s^2(\mu^2) b \ln\frac{\mathbf{k}^2}{\mu^2}\chi_0(\gamma)\right]_{\text{running coupling}}. \tag{5.4}$$

The first indication of the problem with the scale-invariant term was already noticed in the original work by Fadin and Lipatov in Ref. [94]. They pointed out that the corrections to the leading eigenvalue are large and negative. This is clear if we look at the scale invariant terms. The leading eigenvalue of the LO BFKL kernel is

$$\omega_0 = \bar{\alpha}_s\chi_0(\frac{1}{2}) = 2.77\bar{\alpha}_s, \tag{5.5}$$

but the NLO one calculated at $\gamma = 1/2$ gives

$$\bar{\alpha}_s\chi(\gamma)|_{\gamma=\frac{1}{2}} = \bar{\alpha}_s\chi_0(\gamma) + \bar{\alpha}_s^2\chi_1(\gamma)|_{\gamma=\frac{1}{2}} = \omega_0(1 - 6.61\bar{\alpha}_s) = 2.77\bar{\alpha}_s - 18.34\bar{\alpha}_s^2. \tag{5.6}$$

At a value of $\bar{\alpha}_s = 0.15$ the NLO corrections cancel the LO term and for larger values the eigenvalue becomes negative. To illustrate this comment it is convenient to look at Fig. 5.1 where the Pomeron intercept is shown as a function of ν for $\gamma = 1/2 + i\nu$, more plots will be shown in the next chapter together with a deeper interpretation of their meaning.

This analysis is based on the assumption that the structure of the saddle point at NLO is the same as at LO, i.e. focusing in on $\gamma = 1/2$. In Ref. [107] Ross showed that the NLO eigenvalue function has no longer a maximum at $\gamma = 1/2$ but two symmetric maxima at both sides of it. The steep change of $\chi_1(\nu)$ near $\nu = 0$ made it necessary to expand the kernel up to fourth order in ν to get a reliable saddle point approximation, it was found that the power behaviour of s had an exponent of 0.12 for $\bar{\alpha}_s = 0.15$ instead of 0.02 obtained from a naive analysis. But it turned out that the obtained cross sections were not even positive definite [107, 108]. To confirm these problems negative cross sections were also found when the resummed anomalous dimensions at small x using NLO BFKL were calculated to study DIS at small x [109, 110].

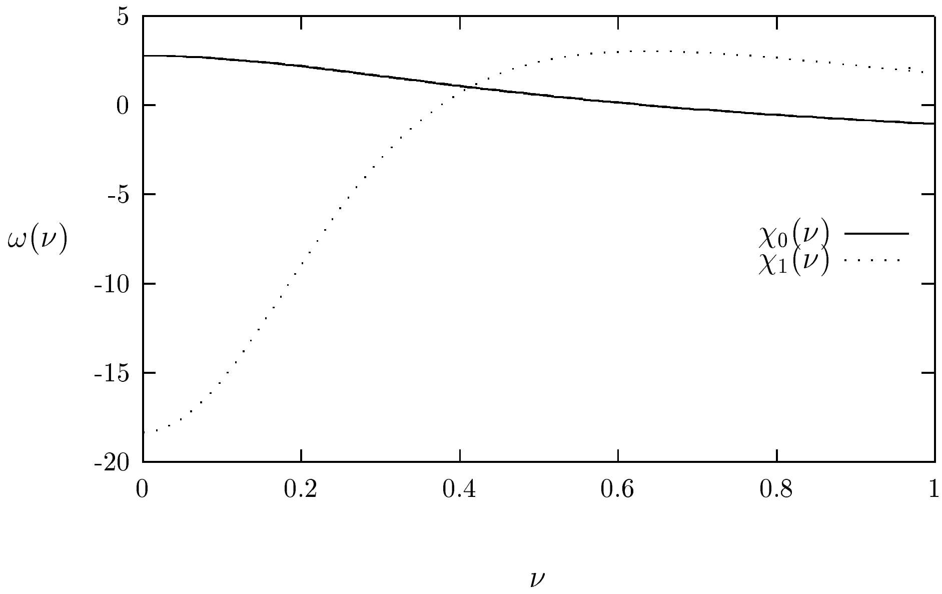

Figure 5.1: Comparison between LO and NLO kernels at $\gamma = \frac{1}{2} + i\nu$

A possible way out of this situation would be to study the NNLO terms but this 3-loops calculation is unfeasibly complicated due to the large number of graphs to be evaluated and their mixing with unitarity effects *, so it is very probable that those terms will never be available. In any case it is perfectly possible that the whole perturbative expansion has problems of convergence and those terms will not give too much light into the physical picture of the problem.

In the next section we take a different approach and following the formulae of Ref. [111] we will show that although the full NLO kernel has many contributions, its behaviour can be reproduced by just taking into account three collinear corrections which can be found when determining the divergences of the kernel around $\gamma = 0$ and $\gamma = 1$. These are coming from the running coupling effects, the non singular part of the splitting functions and the choice of the energy scale (s_0 in our derivation of the

*The violation of unitarity is closely related to the sub-leading logarithm contributions [112]. At LO in the amplitude we consider cut ladders with only gluons in the intermediate states which are emitted from a single reggeized gluon. Unitarity corrections are expected to explain saturation and require to consider the sum over all possible intermediate states, not only those due to colour octet state. It means going from a single ladder approach (t-channel iteration) to more than one ladders (s-channel iteration).

LO terms). We will see that the crisis at NLO is fundamentally related to the choice of scales.

5.2 Collinear limit of the BFKL kernel

Running coupling effects

When investigating the LO BFKL equation we kept the coupling α_s fixed as an external parameter. We have seen that in the derivation of the NLO kernel there exist graphs which contribute to the running of the coupling. For the time being let us analyse their effects in a very 'naive' way, we will give an explanation of how to properly treat running coupling effects at the end of this thesis.

We can write the BFKL equation as [111]

$$f(x,k^2) \quad = \quad f^{(0)}(x,k^2) + \int \frac{dz}{z} \int dk'^2 \mathcal{K}(k^2,k'^2) f(\frac{x}{z},k'^2), \tag{5.7}$$

with

$$f(x,k^2) = x\frac{\partial g(x,k^2)}{\partial k^2} \tag{5.8}$$

being the unintegrated gluon distribution.

A very simple way of making the QCD coupling run in the equation is to introduce the kernel

$$\mathcal{K}^{\mathrm{RC}}(k^2,k'^2) = \bar{\alpha}_s(k^2)\frac{\theta(k^2-k'^2)}{k^2} + \bar{\alpha}_s(k'^2)\frac{\theta(k'^2-k^2)}{k'^2}, \tag{5.9}$$

with the coupling running as in Eq. 5.2. The Mellin transform of this kernel is

$$\frac{\bar{\alpha}_s(k^2)}{\gamma} + \frac{\bar{\alpha}_s(k^2)}{1-\gamma} - \frac{b\bar{\alpha}_s^2(k^2)}{(1-\gamma)^2}. \tag{5.10}$$

The first two contributions belong to the LO approximation but we have an extra piece proportional to b corresponding to NLO accuracy which we will define as

$$\chi_1^{RC}(\gamma) = -\frac{b}{(1-\gamma)^2}. \tag{5.11}$$

The introduction of the running coupling has immediately broken the conformal $\gamma \leftrightarrow 1-\gamma$ symmetry of the kernel.

Splitting function effects

At leading order only the singular part of the splitting function

$$P_{gg}(z) = 6\left[\frac{z}{(1-z)_+} + \frac{1-z}{z} + z(1-z) + \left(\frac{11}{12} - \frac{n_f}{18}\right)\delta(1-z)\right] \tag{5.12}$$

is taken into account but at NLO it is fundamental to include the finite components as well. After a Mellin transform with respect to x and for $n_f = 0$ the contribution to the NLO kernel coming from this inclusion of finite extra terms can be proved to be [111]

$$\chi_1^{SF}(\gamma) = -\frac{11}{12}\left(\frac{1}{\gamma^2} + \frac{1}{(1-\gamma)^2}\right). \tag{5.13}$$

There are other terms coming from a non-zero number of flavours and from graphs involving the convolution of the gluon-quark and quark-gluon splitting functions.

Energy scale effects

When we calculated the LO BFKL equation we left a free parameter in our derivation, it is the factor s_0 which scales the centre-of-mass energy in the terms

$$(\bar{\alpha}_s \ln \frac{s}{s_0})^n. \tag{5.14}$$

Different choices for s_0 only affect the derivation beyond the LO approximation. For a process where the partonic evolution takes place between two objects with similar transverse size, $k_1^2 \sim k_2^2$, the natural choice for the scale is the most symmetric one, i.e. $s_0 = k_1 k_2$. For this choice the LO BFKL approximation resums the terms

$$\left(\bar{\alpha}_s \ln \frac{s}{k_1 k_2} \ln \frac{k_1^2}{k_2^2}\right)^n. \tag{5.15}$$

It is perfectly possible to choose a different scale, for example, in DIS where one of the transverse momenta is hard and the other is at the non-perturbative threshold, i.e. $k_1^2 = Q^2 \gg k_2^2 = Q_0^2$, we could express the same terms as (here we consider only $n = 2$)

$$\left(\bar{\alpha}_s \ln \frac{s}{k_1 k_2} \ln \frac{k_1^2}{k_2^2}\right)^2 = \left(\bar{\alpha}_s \ln \frac{s}{Q^2} \ln \frac{Q^2}{Q_0^2}\right)^2 + \frac{1}{4}\bar{\alpha}_s^2 \ln^4 \frac{Q^2}{Q_0^2} + \bar{\alpha}_s^2 \ln \frac{s}{Q^2} \ln^3 \frac{Q^2}{Q_0^2}. \tag{5.16}$$

This result is not consistent with the renormalization group analysis for DIS where the cross section written in terms of Q^2/s and Q^2/Q_0^2 only has as many collinear logarithms as powers of $\bar{\alpha}_s$. The last two terms of Eq. 5.16 do not fulfill this condition. If we want to be consistent with RG results the NLO corrections should cancel these terms arising from a different scale scheme at LO. As we are trying to build up the NLO kernel from simple collinear arguments naively we could think to eliminate these terms just by introducing at NLO the same second term in Eq. 5.16 but with a negative sign. In the Mellin transform space this corresponds to having $1/\gamma^3$ poles at NLO. Let see how to get rid of these terms in the Mellin-transform space. The cross section is proportional to

$$\sim \int d\omega \int d\gamma \left(\frac{s}{QQ_0}\right)^{\omega} \left(\frac{Q^2}{Q_0^2}\right)^{\gamma} \frac{1}{\omega - \bar{\alpha}_s \chi(\gamma)}. \tag{5.17}$$

To implement the new energy scale $s_0 = Q^2$ is equivalent to the change $\gamma \to \gamma - \frac{\omega}{2}$ in $\chi(\gamma)$ because

$$\left(\frac{s}{QQ_0}\right)^{\omega} \left(\frac{Q^2}{Q_0^2}\right)^{\gamma} = \left(\frac{s}{Q^2}\right)^{\omega} \left(\frac{Q^2}{Q_0^2}\right)^{\gamma+\frac{\omega}{2}}. \tag{5.18}$$

Therefore we can write the expression 5.17 as

$$\sim \int d\omega \int d\gamma \left(\frac{s}{Q^2}\right)^{\omega} \left(\frac{Q^2}{Q_0^2}\right)^{\gamma} \frac{1}{\omega - \bar{\alpha}_s \chi(\gamma - \frac{\omega}{2})}. \tag{5.19}$$

The pole in the ω-space can be estimated by an expansion of the kernel at $\bar{\alpha}_s \sim 0$, i.e.

$$\begin{aligned} \chi(\gamma - \frac{\omega}{2}) &= \chi(\gamma - \frac{\bar{\alpha}_s \chi}{2}) \qquad (5.20)\\ &= \chi\left(\gamma - \frac{\bar{\alpha}_s \chi}{2}\right)\Bigg|_{\bar{\alpha}_s=0} + \frac{\partial}{\partial \bar{\alpha}_s} \chi\left(\gamma - \frac{\bar{\alpha}_s \chi}{2}\right)\Bigg|_{\bar{\alpha}_s=0} \bar{\alpha}_s + \cdots = \chi(\gamma) - \frac{\bar{\alpha}_s \chi \chi'}{2} + \cdots \\ &\to \chi(\gamma) + \frac{\bar{\alpha}_s}{2\gamma^3} \text{ when } \gamma \to 0, \\ &\to \chi(\gamma) + \frac{\bar{\alpha}_s}{2(1-\gamma)^3} \text{ when } \gamma \to 1. \end{aligned}$$

So we have identified the unwanted cubic poles and we can now define the NLO contribution coming from the energy scale such that it annihilates them

$$\chi_1^{ES} = -\frac{1}{2\gamma^3} - \frac{1}{2(1-\gamma)^3}. \tag{5.21}$$

This completes the naive NLO analysis, the final kernel is

$$\begin{aligned}\chi_1^{\text{collinear}} &= \chi_1^{RC}(\gamma)+\chi_1^{SF}(\gamma)+\chi_1^{ES}(\gamma) \\ &= \left[-\frac{b}{(1-\gamma)^2}\right]+\left[-\frac{11}{12}\left(\frac{1}{\gamma^2}+\frac{1}{(1-\gamma)^2}\right)\right]+\left[-\frac{1}{2\gamma^3}-\frac{1}{2(1-\gamma)^3}\right].\end{aligned} \tag{5.22}$$

It is very remarkable that this simple approximation reproduces the true NLO kernel by more than a 93% in the range $0<\gamma<1$ [111] and gives the correct cubic and quadratic divergences at $\gamma=0$ and $\gamma=1$.

5.3 Estimating the higher order corrections

Now that we have been able to reproduce most of the NLO kernel just by studying its collinear contributions we face the issue of improving the convergence of the real expression. The pathological behaviour will be cured by including those higher order terms which remove the sub-leading double transverse logarithms which we know must absent in the DGLAP limits (with scale choices k_1^2 or k_2^2).

In the DGLAP limit where one of the scales is much larger than the other ($k_1^2 \gg k_2^2$ or $k_2^2 \gg k_1^2$) the cross section has terms of the form

$$\left(\bar{\alpha}_s \ln\frac{s}{k_1^2}\ln\frac{k_1^2}{k_2^2}\right)^n. \tag{5.23}$$

If we write them in terms of $s_0 = k_1 k_2$ we get double transverse logarithms

$$\left(\bar{\alpha}_s \ln^2\frac{k_1^2}{k_2^2}\right)^{n-m}\left(\bar{\alpha}_s \ln\frac{s}{k_1 k_2}\ln\frac{k_1^2}{k_2^2}\right)^m \tag{5.24}$$

These terms are formally subleading but form an important part of the NLO corrections. The DGLAP limit $\gamma\to 0$ must be free of these double logarithms. In Ref. [113] a method is shown which for a general kernel given at fixed order up to $\bar{\alpha}_s^N$ can resum those terms of the form

$$\frac{\bar{\alpha}_s^n}{\gamma^k}, \frac{\bar{\alpha}_s^n}{(1-\gamma)^k}, \text{ with } 2n+1-N \le k \le 2n+1, \tag{5.25}$$

i.e. the terms in (5.24) expressed in the Mellin space. The strategy to construct a kernel with the correct set of double logarithms is to substitute the previous divergences in 5.25 with terms

$$\frac{\bar{\alpha}_s^n}{(\gamma+\frac{\omega}{2})^k}, \frac{\bar{\alpha}_s^n}{(1-\gamma+\frac{\omega}{2})^k} \tag{5.26}$$

but maintaining the correct expansion to order $\bar{\alpha}_s^n$.

This technique was applied in Ref. [113] to the NLO BFKL kernel and new kernels were constructed where the most divergent double logarithms were eliminated. The procedure is not unique because it introduces uncontrollable sub-sub-leading double logarithms. The treatment of these terms gives rise to different resummation schemes. An extensive analysis of these schemes is given in chapter 6.

Chapter 6

Rapidity veto effects

The central idea of this thesis is based on the assumption that some small x processes are governed by partonic cascades where each parton emission is far away in rapidity from the previous one. This is the so called *multi-Regge* kinematics and sets the basis to construct the leading order terms in the perturbative expansion. A crucial test for the validity of this expansion is to check if when taking into account higher order corrections, i.e. allowing for emissions close by in rapidity (*quasi-multi-Regge* kinematics), these are small relative to the leading order ones. In chapter 4 we have seen that this is the case if we account not only for the next-to-leading order terms but also for higher order corrections estimated from the collinear limit of the kernel.

In this section we want to test this result by artificially suppressing the emission of gluons which are close by in rapidity in the BFKL framework [114]. We will show that, after removing the unphysical collinear logarithms which typically arise in formally higher orders of the perturbative expansion, the effect of the rapidity veto is greatly reduced. This is an important result, since it supports the use of multi-Regge and quasi-multi-Regge kinematics which are implemented in the leading and next-to-leading order BFKL perturbative expansion.

6.1 Eliminating unphysical logarithms

As we have already shown, in the case of fixed coupling the leading eigenvalue of the BFKL kernel, to next-to-leading logarithmic accuracy, is determined by solving the equation

$$\omega = \chi(\gamma, \bar{\alpha}_s) = \bar{\alpha}_s \chi_0(\gamma) + \bar{\alpha}_s^2 \chi_1(\gamma) \tag{6.1}$$

where $\bar{\alpha}_s = N_c \alpha_s / \pi$. We also know that the leading order kernel is given by

$$\chi_0(\gamma) = 2\psi(1) - \psi(\gamma) - \psi(1-\gamma) \tag{6.2}$$

and χ_1 has recently become available [94, 92] (see Eq. 4.40).

In this section we take $n_f = 3$ although our results depend only very weakly upon

n_f. For our purposes, it is sufficient to consider the gluon Green's function:

$$f(s,k_1,k_2) = \int \frac{d\omega}{2\pi i}\frac{d\gamma}{2\pi i} \left(\frac{s}{s_0}\right)^{\omega} \left(\frac{k_1^2}{k_2^2}\right)^{\gamma} \frac{1}{\omega - \chi(\gamma,\bar{\alpha}_s)}. \tag{6.3}$$

With $s_0 = k_1 k_2$ the kernel is as given explicitly above.

Let us now recall some of the results we have proved so far in this thesis. It has been pointed out that the NLO kernel induces unphysical logarithms in the ratio k_1/k_2 at NNLO and beyond [92, 113]. If $k_1 \gg k_2$ then the unphysical logs are induced by the singular behaviour of the kernel at $\gamma = 0$, i.e. $\chi_0 \approx 1/\gamma$ and $\chi_1 \approx -1/(2\gamma^3)$ (the symmetry under interchange of k_1 and k_2 is reflected in the fact that the kernel is even about $\gamma = 1/2$). Although these logarithms lie formally beyond the boundary of the NLO approach, they can induce spurious large effects, especially if the external momenta are strongly ordered ($k_1 \gg k_2$ or $k_1 \ll k_2$). For consistency with the DGLAP approach we know that they must really be absent. At NLO all spurious logs are indeed cancelled. Salam demonstrated how to extend the NLO kernel so as to guarantee the cancellation of unphysical logs to all orders. The prescription for modifying the kernel is not unique and Salam investigated a variety of different schemes. Let us summarise the four schemes he used in [113].

For the scale choice $s_0 = k_1 k_2$ the resummed kernels will have the general structure

$$\begin{aligned}\bar{\chi}(\gamma,\omega,\bar{\alpha}_s) &= \bar{\alpha}_s \chi^{(1)}(\gamma) = \\ &\bar{\alpha}_s\chi_0(\gamma) + \bar{\alpha}_s^2\chi_1(\gamma) + \sum_{n=2}^{\infty} \bar{\alpha}_s^{n+1}\chi_n^{(1)}(\gamma),\end{aligned} \tag{6.4}$$

where $\chi_n^{(1)}$ has γ^{-k} and $(1-\gamma)^{-k}$ divergences with coefficients $d_{nk}^{(1)}$*.

Each scheme is characterized by a set of functions $\mathcal{D}_k(\gamma)$ with the properties of being regular when $\gamma > \frac{1}{2}$ and only γ^{-k} divergent at $\gamma = 0$. To obtain $\bar{\chi}(\gamma,\omega,\bar{\alpha}_s)$ we first need a correct kernel at leading order and free of unphysical logarithms, i.e.

$$\begin{aligned}\chi^{(0)}(\gamma) &= \chi^{(0)}(\gamma,\omega=\bar{\alpha}_s\chi^{(0)}) = \\ &\chi_0(\gamma) + d_{01}\left[\mathcal{D}_1(\gamma+\frac{\omega}{2}) - \mathcal{D}_1(\gamma) + \mathcal{D}_1(1-\gamma+\frac{\omega}{2}) - \mathcal{D}_1(1-\gamma)\right],\end{aligned} \tag{6.5}$$

*In general the coefficients for the divergencies at $\gamma \sim 0$ and at $\gamma \sim 1$ can be different but for the kernels studied here this is not the case.

where $d_{01} = 1$ is the coefficient of the γ^{-1} and $(1-\gamma)^{-1}$ divergences of the exact kernel $\chi_0(\gamma)$. The general expression for the kernel $\chi^{(1)}(\gamma)$ of Eq. 6.4 derived in Ref. [113] is

$$\begin{aligned}
\chi^{(1)}(\gamma) &= \chi^{(1)}(\gamma, \omega = \bar{\alpha}_s \chi^{(1)}) = \\
& \chi^{(0)}(\gamma,\omega) + \bar{\alpha}_s \Big\{ \chi_1(\gamma) - \chi_1^{(0)}(\gamma) + \qquad (6.6)\\
& \Big[\left(d_{11} - d_{11}^{(0)}\right) \Big(\mathcal{D}_1(\gamma + \frac{\omega}{2}) - \mathcal{D}_1(\gamma) + \mathcal{D}_1(1-\gamma+\frac{\omega}{2}) - \mathcal{D}_1(1-\gamma) \Big) \Big] + \\
& \Big[\left(d_{12} - d_{12}^{(0)}\right) \Big(\mathcal{D}_2(\gamma + \frac{\omega}{2}) - \mathcal{D}_2(\gamma) + \mathcal{D}_2(1-\gamma+\frac{\omega}{2}) - \mathcal{D}_2(1-\gamma) \Big) \Big] \Big\},
\end{aligned}$$

where d_{11} and d_{12} are the coefficients of the divergences of the exact kernel $\chi_1(\gamma)$ given in Eq. 6.19 ($d_{11} = \delta_1$, $d_{12} = \delta_2$). $\chi^{(0)}$ generates some NLO terms ($\chi^{(0)} = \chi_0 + \bar{\alpha}_s \chi_1^{(0)} + \ldots$) which might produce a double counting when the genuine NLO kernel, χ_1, is introduced. The last term in the second line of Eq. 6.6 cures this problem. The coefficients corresponding to the divergences of $\chi_1^{(0)}$ at $\gamma^{-1,\,-2}$ and $(1-\gamma)^{-1,\,-2}$ are $d_{11}^{(0)}$ and $d_{12}^{(0)}$.

This new kernel is correct to NLO order because the whole $\mathcal{O}(\bar{\alpha}_s)$ contribution comes from $\chi_1(\gamma)$, the other parts in the equation do not contain terms at this order. To show that this function is free of unphysical logarithms when it is expressed in the scale $s_0 = k_1^2$ it is convenient to make the transformation

$$\begin{aligned}
\chi^{(1)}(\gamma) &= \mathcal{R}_0(\gamma) + d_{01}\Big(\mathcal{D}_1(\gamma+\frac{\omega}{2}) + \mathcal{D}_1(1-\gamma+\frac{\omega}{2}) \Big) + \\
& \bar{\alpha}_s \Big\{ \mathcal{R}_1(\gamma) + \left(d_{11} - d_{11}^{(0)}\right) \Big(\mathcal{D}_1(\gamma+\frac{\omega}{2}) + \mathcal{D}_1(1-\gamma+\frac{\omega}{2}) \Big) + \\
& \left(d_{12} - d_{12}^{(0)}\right) \Big(\mathcal{D}_2(\gamma+\frac{\omega}{2}) + \mathcal{D}_2(1-\gamma+\frac{\omega}{2}) \Big) \Big\}, \qquad (6.7)
\end{aligned}$$

with

$$\begin{aligned}
\mathcal{R}_0(\gamma) &= \chi_0(\gamma) - d_{01}\left(\mathcal{D}_1(\gamma) + \mathcal{D}_1(1-\gamma)\right), \qquad (6.8)\\
\mathcal{R}_1(\gamma) &= \chi_1(\gamma) - \chi_1^{(0)} - (d_{11} - d_{11}^{(0)})\left(\mathcal{D}_1(\gamma) + \mathcal{D}_1(1-\gamma)\right) \\
& -(d_{12} - d_{12}^{(0)})\left(\mathcal{D}_2(\gamma) + \mathcal{D}_2(1-\gamma)\right). \qquad (6.9)
\end{aligned}$$

Now, taking into account that when $\gamma \sim 0$ then

$$\chi_0(\gamma) \sim \frac{d_{01}}{\gamma}, \qquad (6.10)$$

$$\chi_1(\gamma) \sim \frac{d_{11}}{\gamma} + \frac{d_{12}}{\gamma^2} + \frac{d_{13}}{\gamma^3}, \tag{6.11}$$

$$\chi_1^{(0)}(\gamma) \sim \frac{d_{11}^{(0)}}{\gamma} + \frac{d_{12}^{(0)}}{\gamma^2} + \frac{d_{13}^{(0)}}{\gamma^3}, \tag{6.12}$$

we can see that for the functions $\mathcal{R}_0$ and $\mathcal{R}_1$ to be regular at $\gamma = 0$ we need the extra condition

$$d_{13} = d_{13}^{(0)}. \tag{6.13}$$

The same considerations apply for the $\gamma = 1$ case. To analyse the rest of the kernel we transform it to the scale $s_0 = k_1^2$ applying $\gamma \to \gamma - \frac{\omega}{2}$. The result is the kernel η:

$$\begin{aligned}\eta^{(1)}(\gamma) &= \eta^{(1)}(\gamma, \omega = \bar{\alpha}_s \eta^{(1)}) = \mathcal{R}_0(\gamma - \frac{\omega}{2}) + d_{01}\left(\mathcal{D}_1(\gamma) + \mathcal{D}_1(1-\gamma+\omega)\right) + \\ & \bar{\alpha}_s \Big\{ \mathcal{R}_1(\gamma - \frac{\omega}{2}) + \left(d_{11} - d_{11}^{(0)}\right)\left(\mathcal{D}_1(\gamma) + \mathcal{D}_1(1-\gamma+\omega)\right) + \\ & \left(d_{12} - d_{12}^{(0)}\right)\left(\mathcal{D}_2(\gamma) + \mathcal{D}_2(1-\gamma+\omega)\right)\Big\}. \end{aligned} \tag{6.14}$$

The only divergences produced by the terms in (γ) are of the form $\frac{1}{\gamma}$, $\frac{\bar{\alpha}_s}{\gamma}$ and $\frac{\bar{\alpha}_s}{\gamma^2}$. These are allowed by DGLAP and when introduced in the terms in $(1 - \gamma + \omega)$ generate at most divergences of the type $\frac{\bar{\alpha}_s}{\gamma}$ and $\frac{\bar{\alpha}_s^2}{\gamma^2}$ which are also consistent with the renormalization group appoach. The same arguments apply for the scale $s_0 = k_2^2$. In [113] it was shown that the kernels constructed with this method have $\bar{\alpha}_s^n \gamma^{-n-1}$ as the most divergent terms for $s_0 = k_1^2$ and $\bar{\alpha}_s^n (1-\gamma)^{-n-1}$ as the most divergent ones for $s_0 = k_2^2$. It turns out that any modification of the most divergent unknown term, $\bar{\alpha}_s^2 \gamma^{-3}$, can only change at most the sub-sub-leading double logarithms $\bar{\alpha}_s^n \gamma^{-2n+1}$ with $n \geq 2$, i.e. we have a method to correctly eliminate the worst unphysical divergences at all orders. In the following we will study the different schemes proposed in Ref.[113].

In the so called scheme 1 the choice for the $\mathcal{D}_k$ functions is

$$\begin{aligned}\mathcal{D}_1(\gamma) &= \psi(1) - \psi(\gamma) \\ \mathcal{D}_2(\gamma) &= \psi'(\gamma).\end{aligned} \tag{6.15}$$

The expression for $\chi^{(0)}$ is

$$\chi^{(0)}(\gamma) = 2\psi(1) - \psi(\gamma + \frac{\omega}{2}) - \psi(1 - \gamma + \frac{\omega}{2}), \tag{6.16}$$

and its NLO terms are

$$\chi_1^{(0)}(\gamma) = -\frac{1}{2}\chi_0(\gamma)\left(\psi'(\gamma)+\psi'(1-\gamma)\right), \tag{6.17}$$

and now it is easy to obtain the coefficients of its divergences

$$\begin{aligned} d_{11}^{(0)} &= -\frac{\pi^2}{6} \\ d_{12}^{(0)} &= 0 \\ d_{13}^{(0)} &= -\frac{1}{2} \quad (= d_{13}). \end{aligned}$$

Therefore, in scheme 1, using Eqs. 6.4, 6.5 and 6.6 one replaces $\chi(\gamma,\bar{\alpha}_s)$ of 6.1, 6.3 with

$$\begin{aligned} \bar{\chi}(\gamma,\omega,\bar{\alpha}_s) &= \bar{\alpha}_s[\, 2\psi(1)-\psi(\gamma+\omega/2)-\psi(1-\gamma+\omega/2)\,] \\ &+ \bar{\alpha}_s^2\Big[\chi_1(\gamma)+\frac{1}{2}\chi_0(\gamma)(\psi'(\gamma)+\psi'(1-\gamma)) \\ &+ \left(\delta_1+\frac{\pi^2}{6}\right)[\psi(\gamma)+\psi(1-\gamma)-\psi(\gamma+\omega/2)-\psi(1-\gamma+\omega/2)] \\ &- \delta_2[\psi'(\gamma)+\psi'(1-\gamma)-\psi'(\gamma+\omega/2)-\psi'(1-\gamma+\omega/2)]\Big] \end{aligned} \tag{6.18}$$

where

$$\begin{aligned} \delta_1 &= -\frac{5n_f}{18N_c}-\frac{13n_f}{36N_c^3} \\ \delta_2 &= -\frac{11}{8}+\frac{n_f}{12N_c}-\frac{n_f}{6N_c^3} \end{aligned} \tag{6.19}$$

are the coefficients of the singular parts of the NLO kernel, i.e.

$$\mathrm{Lim}_{\ \gamma\to 0}\ \chi_1(\gamma) = -\frac{1}{2\gamma^3}+\frac{\delta_2}{\gamma^2}+\frac{\delta_1}{\gamma}. \tag{6.20}$$

This new kernel is identical to the NLO kernel to order $\bar{\alpha}_s^2$ but is completely free from any singularities as $\gamma\to 0,1$.

The leading ω-plane singularity is found by solving

$$\omega = \bar{\chi}(\gamma,\omega,\bar{\alpha}_s). \tag{6.21}$$

In scheme 2, the $\mathcal{D}_k$ functions are

$$\begin{aligned} \mathcal{D}_1 &= \frac{1}{\gamma} \\ \mathcal{D}_2 &= \frac{1}{\gamma^2}, \end{aligned}$$

and $\chi^{(0)}$ is

$$\chi^{(0)} = \chi_0(\gamma) - \frac{\chi_0(\gamma)}{2}\left(\frac{1}{\gamma^2} + \frac{1}{(1-\gamma)^2}\right)\bar{\alpha}_s + \cdots \tag{6.22}$$

with coefficients

$$\begin{aligned} d_{11}^{(0)} &= -\frac{1}{2} \\ d_{12}^{(0)} &= 0 \\ d_{13}^{(0)} &= -\frac{1}{2} \quad (= d_{13}). \end{aligned}$$

Therefore the new kernel in scheme 2 is

$$\begin{aligned} \bar{\chi}(\gamma,\omega,\bar{\alpha}_s) &= \bar{\alpha}_s\left[\chi_0(\gamma) - \frac{1}{\gamma} - \frac{1}{1-\gamma} + \frac{1}{\gamma+\omega/2} + \frac{1}{1-\gamma+\omega/2}\right] \\ &+ \bar{\alpha}_s^2\left[\chi_1(\gamma) + \frac{1}{2}\chi_0(\gamma)\left(\frac{1}{\gamma^2} + \frac{1}{(1-\gamma)^2}\right)\right. \\ &- \left(\delta_1 + \frac{1}{2}\right)\left(\frac{1}{\gamma} + \frac{1}{1-\gamma} - \frac{1}{\gamma+\omega/2} - \frac{1}{1-\gamma+\omega/2}\right) \\ &- \left.\delta_2\left(\frac{1}{\gamma^2} + \frac{1}{(1-\gamma)^2} - \frac{1}{(\gamma+\omega/2)^2} - \frac{1}{(1-\gamma+\omega/2)^2}\right)\right]. \end{aligned} \tag{6.23}$$

In scheme 3 the role of the $\mathcal{D}_k$ functions is now played by two constants A and B chosen such that $d_{11}^{(0)} = \delta_1$ and $d_{12}^{(0)} = \delta_2$. The $\chi^{(0)}$ part of the kernel is

$$\begin{aligned} \chi^{(0)}(\gamma) &= \chi^{(0)}(\gamma, \omega = \bar{\alpha}_s\chi^{(0)}) = \\ &= (1-\bar{\alpha}_s A)\left[2\psi(1) - \psi(\gamma + \frac{\omega}{2} + \bar{\alpha}_s B) - \psi(1-\gamma+\frac{\omega}{2} + \bar{\alpha}_s B)\right] \\ &= \chi_0(\gamma) - \bar{\alpha}_s\left[A\chi_0(\gamma) + \left(B + \frac{\chi_0(\gamma)}{2}\right)(\psi'(\gamma) + \psi'(1-\gamma))\right] + \cdots \end{aligned} \tag{6.24}$$

and the coefficients of the divergences are

$$\begin{aligned} d_{11}^{(0)} &= -A - \frac{\pi^2}{6} \quad (= d_{11}) \\ d_{12}^{(0)} &= -B \quad (= d_{12}) \\ d_{13}^{(0)} &= -\frac{1}{2} \quad (= d_{13}). \end{aligned}$$

The final form of the scheme 3 is

$$\begin{aligned} \bar{\chi}(\gamma,\omega,\bar{\alpha}_s) &= \bar{\alpha}_s(1-\bar{\alpha}_s A)[2\psi(1) - \psi(\gamma+\omega/2+\bar{\alpha}_s B) - \psi(1-\gamma+\omega/2+\bar{\alpha}_s B)] \\ &+ \bar{\alpha}_s^2\left[\chi_1(\gamma) + \left(\frac{1}{2}\chi_0(\gamma) + B\right)(\psi'(\gamma) + \psi'(1-\gamma)) + A\chi_0(\gamma)\right] \end{aligned} \tag{6.25}$$

where

$$\begin{aligned} A &= -\delta_1 - \frac{\pi^2}{6}, \\ B &= -\delta_2. \end{aligned} \tag{6.26}$$

Finally, in scheme 4, the same idea is applied with the initial kernel being

$$\begin{aligned} \chi^{(0)}(\gamma) &= \chi^{(0)}(\gamma, \omega = \bar{\alpha}_s \chi^{(0)}) = \qquad (6.27) \\ &= \chi_0(\gamma) - \frac{1}{\gamma} - \frac{1}{1-\gamma} + (1 - \bar{\alpha}_s A') \left[\frac{1}{\gamma + \frac{w}{2} + \bar{\alpha}_s B} + \frac{1}{1 - \gamma + \frac{w}{2} + \bar{\alpha}_s B} \right] \\ &= \chi_0(\gamma) - \bar{\alpha}_s \left[A' \left(\frac{1}{\gamma} + \frac{1}{1-\gamma} \right) + \left(B + \frac{\chi_0(\gamma)}{2} \right) \left(\frac{1}{\gamma^2} + \frac{1}{(1-\gamma)^2} \right) \right] + \cdots \end{aligned}$$

and the coefficients of the divergences are

$$\begin{aligned} d_{11}^{(0)} &= -A' - \frac{1}{2} \quad (= d_{11}) \\ d_{12}^{(0)} &= -B \quad (= d_{12}) \\ d_{13}^{(0)} &= -\frac{1}{2} \quad (= d_{13}). \end{aligned}$$

Hence, the kernel is

$$\begin{aligned} \bar{\chi}(\gamma, \omega, \bar{\alpha}_s) &= \bar{\alpha}_s \left[\chi_0(\gamma) - \frac{1}{\gamma} - \frac{1}{1-\gamma} \right. \\ &+ \left. (1 - \bar{\alpha}_s A') \left(\frac{1}{\gamma + \omega/2 + \bar{\alpha}_s B} + \frac{1}{1 - \gamma + \omega/2 + \bar{\alpha}_s B} \right) \right] \\ &+ \bar{\alpha}_s^2 \left[\chi_1(\gamma) + \left(B + \frac{1}{2} \chi_0(\gamma) \right) \left(\frac{1}{\gamma^2} + \frac{1}{(1-\gamma)^2} \right) + A' \left(\frac{1}{\gamma} + \frac{1}{1-\gamma} \right) \right] \end{aligned} \tag{6.28}$$

where B is as above and

$$A' = -\delta_1 - \frac{1}{2}. \tag{6.29}$$

There are other schemes in the literature [116] but in this work we will be only interested in the analysis of those previously shown. It was demonstrated in [113] that the all orders kernel is much better behaved than the NLO kernel. In particular, in schemes 3 and 4 it was shown that the subsequent integral over γ in Eq. 6.3 is again dominated by the saddle point at $\gamma = 1/2$ and that the leading eigenvalue of the kernel does not pick up huge higher order corrections (although they do still lead to a

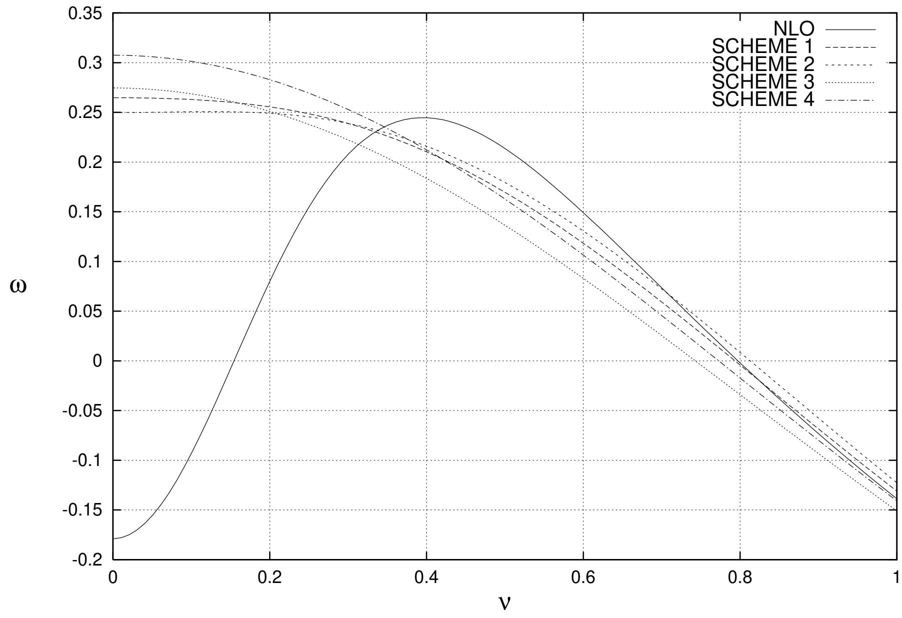

Figure 6.1: Behaviour of the next-to-leading order kernel compared to the collinear improved ones

significant reduction in its value). To illustrate these points, in Fig. 6.1 we show the behaviour of the all order kernels as a function of ν where $\gamma = 1/2 + i\nu$, with $\bar{\alpha}_s = 0.2$, and compare with the behaviour of the NLO kernel (which no longer has the saddle point at $\gamma = 1/2$ [107]). It can be seen that for these modest values of $\bar{\alpha}_s$ the result is not very sensitive to the scheme used. In this chapter we follow Salam in maintaining that schemes 3 and 4 are the most realistic schemes and focus upon them.

6.2 Limiting the gluon emission.

Now we are going to impose the constraint that subsequent gluon emissions must be separated by some minimum interval in rapidity, b, which we will call the *rapidity veto* [114]. We are interested in studying the stability of the previous kernels under changes in the value of b. This is readily accomplished if we write the BFKL equation as an integral equation in rapidity

$$\tilde{f}_\nu(y) = \int dy' \; \theta(y - y' - b) \; \bar{\alpha}_s \chi_0(\gamma) \; \tilde{f}_\nu(y'), \tag{6.30}$$

with the Heaviside function implementing the rapidity veto condition

$$y_{i+1} - y_i > b \tag{6.31}$$

for each gluon emission i in the BFKL ladder and $K_0(\nu)$ being the Mellin transform of the kernel.

As we want to express this condition in the ω plane we use the transformation

$$f_\nu(\omega) = \int dy\ e^{-\omega y}\ \tilde{f}_\nu(y), \tag{6.32}$$

and we introduce it in the original equation:

$$\begin{aligned} f_\nu(\omega) &= \int dy\ e^{-\omega y} \int dy'\ \theta(y - y' - b)\ \bar{\alpha}_s \chi_0(\gamma)\ \tilde{f}_\nu(y') \\ &= \bar{\alpha}_s \chi_0(\gamma) \int dy'\ \tilde{f}_\nu(y') \int_{y'+b} dy\ e^{-\omega y} \\ &= \frac{e^{-\omega b}}{\omega} \bar{\alpha}_s \chi_0(\gamma)\ f_\nu(\omega). \end{aligned} \tag{6.33}$$

Therefore, the effect of imposing the veto on the LO BFKL equation leads to a leading eigenvalue which is determined by the solution to

$$\omega = \bar{\alpha}_s e^{-b\omega} \chi_0(\gamma), \tag{6.34}$$

with

$$\chi_{\text{veto}}^{\text{LO}}(\gamma, \omega, \bar{\alpha}_s) = \bar{\alpha}_s e^{-b\omega} \chi_0(\gamma) \tag{6.35}$$

being the new LO kernel and encoding the rapidity veto to all orders in $\bar{\alpha}_s$.

It has been suggested that a veto of $b \sim 1$ may well be a good approximation to real physics and as such may account for a large part of the NLO corrections to the leading eigenvalue of the kernel [90, 115, 117]. Our intention in this work is not to further investigate this point but to prove that the collinear resummation of the kernel really has the effect of reducing the effect of emissions very close in rapidity.

Expanding the condition (6.34) in powers of $\bar{\alpha}_s$ gives

$$\begin{aligned} \omega &\approx (1 - b\ \omega)\ \omega_0 \\ \omega &\approx \frac{\omega_0}{1 + b\ \omega_0} \\ &\approx \omega_0 (1 - b\ \omega_0) \end{aligned} \tag{6.36}$$

and $\omega_0 = \bar{\alpha}_s \chi_0(1/2)$, which is relevant if we assume that the saddle point at $\gamma = 1/2$ is reliable. This is to be compared with the NLO kernel, which gives

$$\omega = \omega_0(1 - 2.4\ \omega_0). \tag{6.37}$$

If a veto of 2 units were physics then we see that it saturates most of the NLO correction, leaving behind a genuinely small correction. The study of a rapidity veto has also been pursued in [118].

In order to impose a veto at NLO we add a term $\Delta(\gamma)$ which allows us to match the NLO kernel to order $\bar{\alpha}_s^2$, i.e.

$$\begin{aligned} \omega &= \bar{\alpha}_s e^{-b\omega} \left[\chi_0(\gamma) + \bar{\alpha}_s \Delta(\gamma)\right] \\ &\simeq \bar{\alpha}_s \left[\chi_0(\gamma) + \bar{\alpha}_s \Delta(\gamma) - \bar{\alpha}_s b\ \chi_0^2(\gamma)\right]. \end{aligned} \tag{6.38}$$

Hence, to match the NLO kernel we need

$$\Delta(\gamma) = \chi_1(\gamma) + b\ \chi_0^2(\gamma). \tag{6.39}$$

And, finally, we get

$$\chi_{\mathrm{veto}}^{\mathrm{NLO}}(\gamma, \omega, \bar{\alpha}_s) = \bar{\alpha}_s e^{-b\omega}[\chi_0(\gamma) + \bar{\alpha}_s \chi_1(\gamma) + \bar{\alpha}_s b \chi_0^2(\gamma)]. \tag{6.40}$$

The next step is to solve the transcendental equations just obtained and study the dependence of ω upon $\gamma = 1/2 + i\nu$ and $\bar{\alpha}_s$. In Figs. 6.2–6.5 we show the effect of imposing the veto on the LO and NLO BFKL equations. We show separately the dependence of the kernels upon ν and the variation of the kernels evaluated at $\nu = 0$ with $\bar{\alpha}_s$. In each case we show results for three different values of b, $b = 0$ (no veto), $b = 1$ and $b = 2$. As a cross check for our calculations we note that the LO and NLO original results are recovered in the $b = 0$ case. Clearly the imposition of the veto has a dramatic effect upon the behaviour of the kernel.

In the next section, we wish to investigate the effect of imposing a rapidity veto in conjunction with the removal of the unphysical logarithms. Our philosophy is as follows. If, after removing the unphysical logarithms, the imposition of a rapidity veto

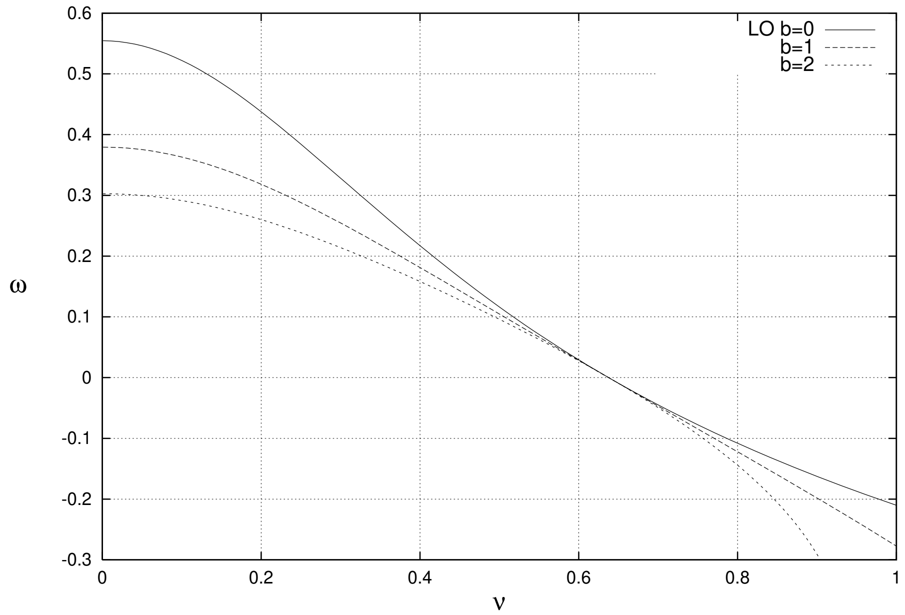

Figure 6.2: Dependence of the LO kernel plus veto upon ν for $\bar{\alpha}_s = 0.2$

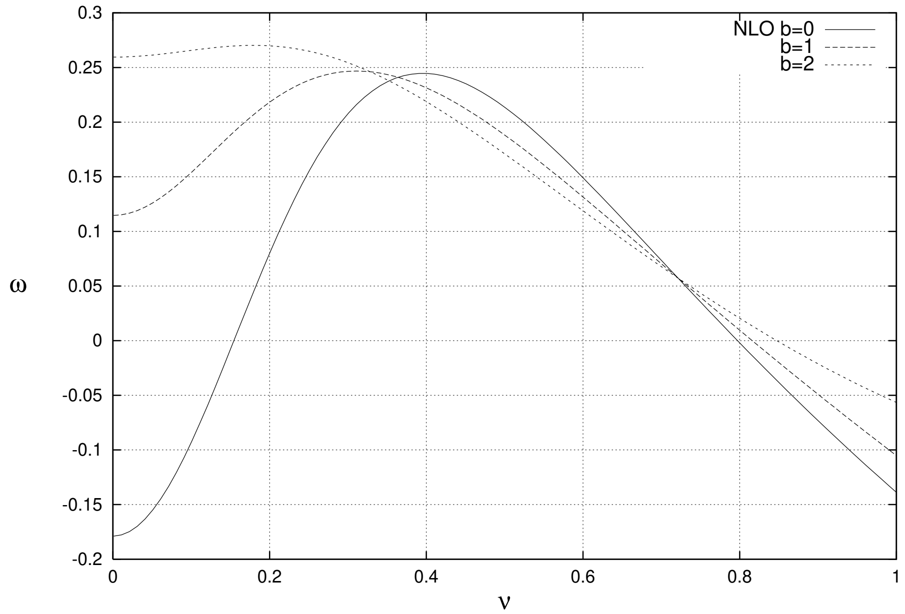

Figure 6.3: Dependence of the NLO kernel plus veto upon ν for $\bar{\alpha}_s = 0.2$

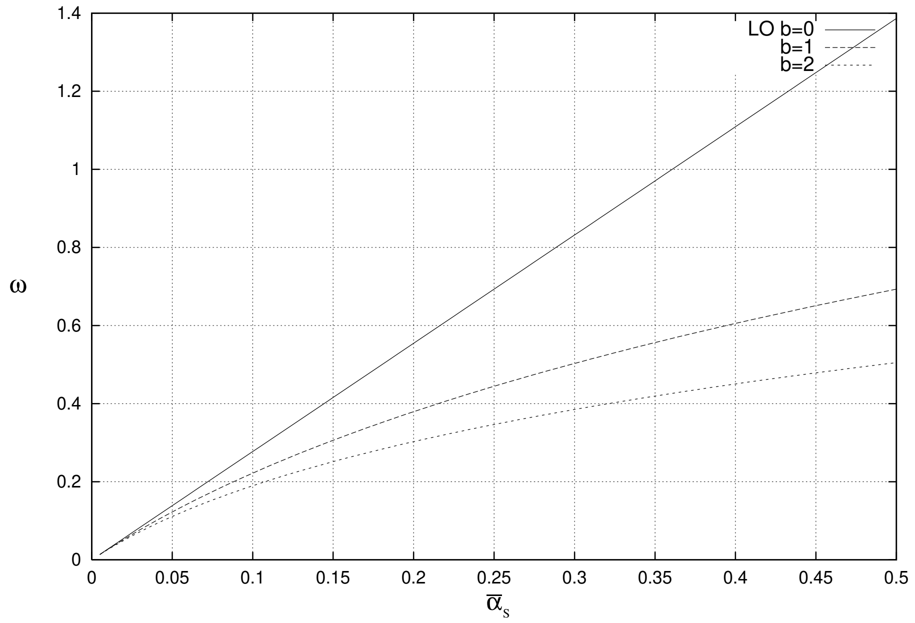

Figure 6.4: Dependence of the LO kernel plus veto upon $\bar{\alpha}_s$ for $\nu = 0$

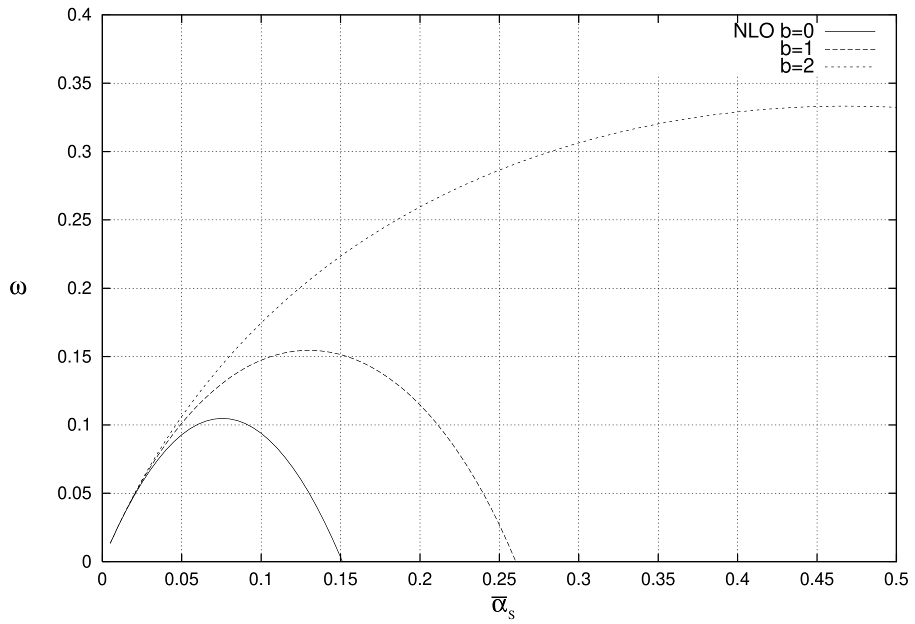

Figure 6.5: Dependence of the NLO kernel plus veto upon $\bar{\alpha}_s$ for $\nu = 0$

has little effect then we have internal consistency. This is because the BFKL approach relies on the assumption of multi-Regge kinematics, i.e. that successive emissions are infinitely far apart in rapidity, at LO and it assumes that subsequent corrections should be small. It follows that cutting out emissions which are nearby in rapidity should have a relatively small effect. We will show that this is indeed the case.

6.3 The Rapidity Veto to all orders.

The rapidity veto can be implemented in a way which ensures that the cancellation of the unphysical logarithms is not disturbed. The procedure is scheme dependent, just as in the case without any veto. We need to introduce the term $b\chi_0^2$ from Eq. 6.39 to match the genuine NLO kernel. This generates extra divergences at NLO which we choose to eliminate modifying the constant B. This constant will have the same factor $-\delta_2$ as before in order to ensure the correct treatment of the unphysical logarithms but it will also have a factor $-b$ to cancel the extra $b\frac{\bar{\alpha}_s^2}{\gamma^2}$ divergences.

Consequently, for scheme 3 we write

$$\begin{aligned}\chi_{\text{veto}}(\gamma,\omega,\bar{\alpha}_s) &= \bar{\alpha}_s e^{-b\omega}\{(1-\bar{\alpha}_s A)[2\psi(1) \\ &- \psi(\gamma+\omega/2+\bar{\alpha}_s B') - \psi(1-\gamma+\omega/2+\bar{\alpha}_s B')] \\ +\bar{\alpha}_s &\left[\chi_1(\gamma)+b\chi_0(\gamma)^2+\left(\frac{1}{2}\chi_0(\gamma)+B'\right)(\psi'(\gamma)+\psi'(1-\gamma))+A\chi_0(\gamma)\right]\}\end{aligned} \tag{6.41}$$

where A is as before but B' is now

$$B' = -\delta_2 - b, \tag{6.42}$$

which is required to ensure that the introduction of the rapidity gap does not destroy the elimination of the unphysical logarithms.

For scheme 4 the procedure is the same and we obtain

$$\begin{aligned}\chi_{\text{veto}}(\gamma,\omega,\bar{\alpha}_s) &= \bar{\alpha}_s e^{-b\omega}\left\{\left[\chi_0(\gamma)-\frac{1}{\gamma}-\frac{1}{1-\gamma}\right.\right. \\ &+ \left.(1-\bar{\alpha}_s A')\left(\frac{1}{\gamma+\omega/2+\bar{\alpha}_s B'}+\frac{1}{1-\gamma+\omega/2+\bar{\alpha}_s B'}\right)\right]\end{aligned} \tag{6.43}$$

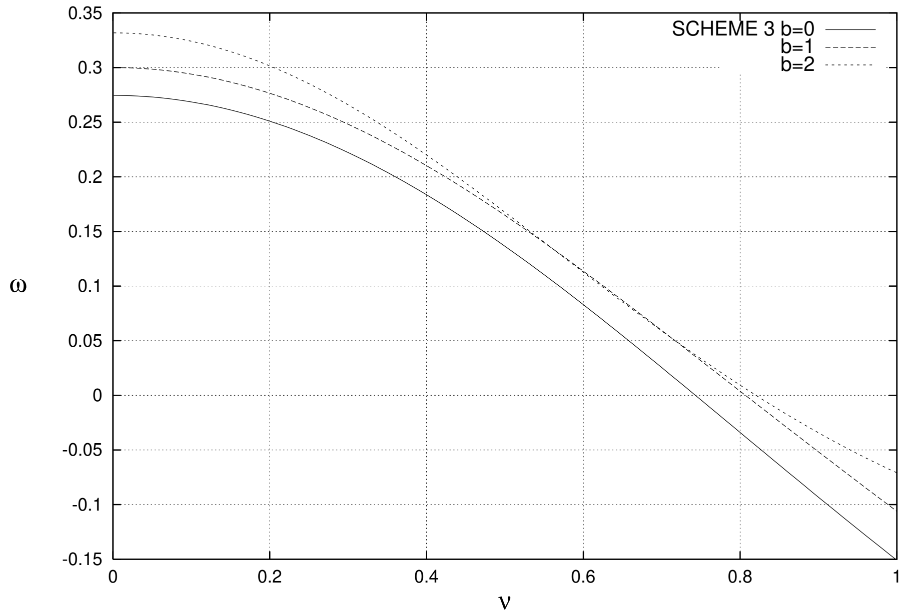

Figure 6.6: Dependence of the 'Scheme 3 plus veto' NLO kernel upon ν for $\bar{\alpha}_s = 0.2$

$$+ \bar{\alpha}_s \left[\chi_1(\gamma) + b\chi_0(\gamma)^2 + \left(B' + \frac{1}{2}\chi_0(\gamma) \right) \left(\frac{1}{\gamma^2} + \frac{1}{(1-\gamma)^2} \right) + A' \left(\frac{1}{\gamma} + \frac{1}{1-\gamma} \right) \right] \Bigg\} .$$

These new kernels implement the veto, are matched to NLO, and are free from any singularities as $\gamma \to 0, 1$.

In Figs. 6.6, 6.7, we do as in Figs. 6.2–6.5 but using the new Scheme 3 kernel and in Fig. 6.8, 6.9 we show the results for the Scheme 4 kernel. Having subtracted the unphysical logarithms we can see clearly that the dependence upon the rapidity veto is greatly diminished. We interpret this as supporting the use of (quasi-)multi-regge kinematics.

In the case of the pure LO and NLO kernels and their collinear corrected variants, the behaviour of the kernel near $\nu = 0$ (see Eq. 2.48) drives the asymptotic ($s/s_0 \to \infty$) behaviour of the Green function of (6.3). However, the situation is far from clear after implementing the veto.

For definiteness, let us take the kernel of (6.35). After imposing the veto the gluon Green's function can be obtained from the expression

$$f(s, k_1, k_2) = \int \frac{d\omega}{2\pi i} \frac{d\gamma}{2\pi i} \left(\frac{s}{s_0} \right)^{\omega} \left(\frac{k_1^2}{k_2^2} \right)^{\gamma} \frac{1}{\omega - \bar{\alpha}_s e^{-b\omega} \chi_0(\gamma)} . \tag{6.44}$$

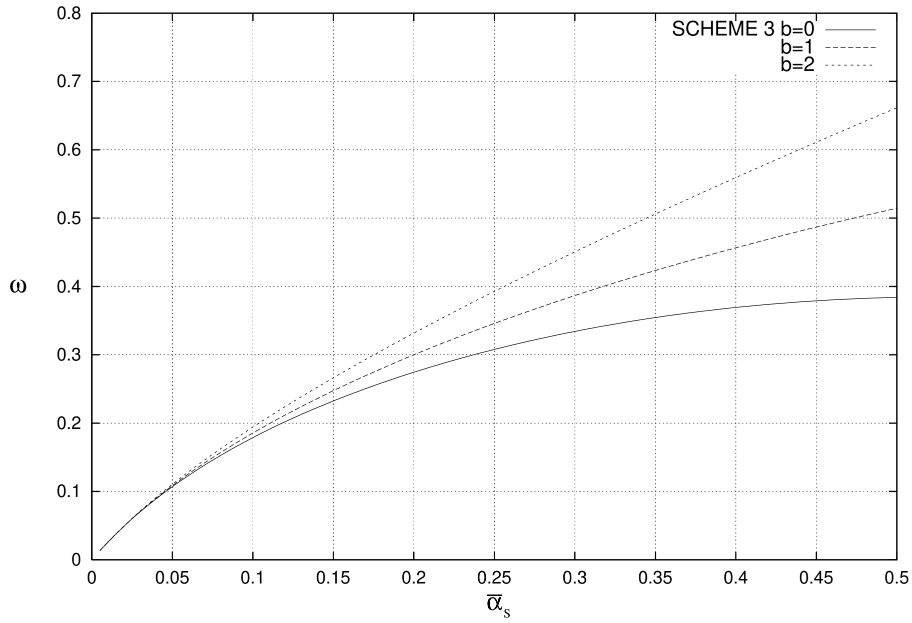

Figure 6.7: Dependence of the ‘Scheme 3 plus veto’ NLO kernel upon $\bar{\alpha}_s$ for $\nu = 0$

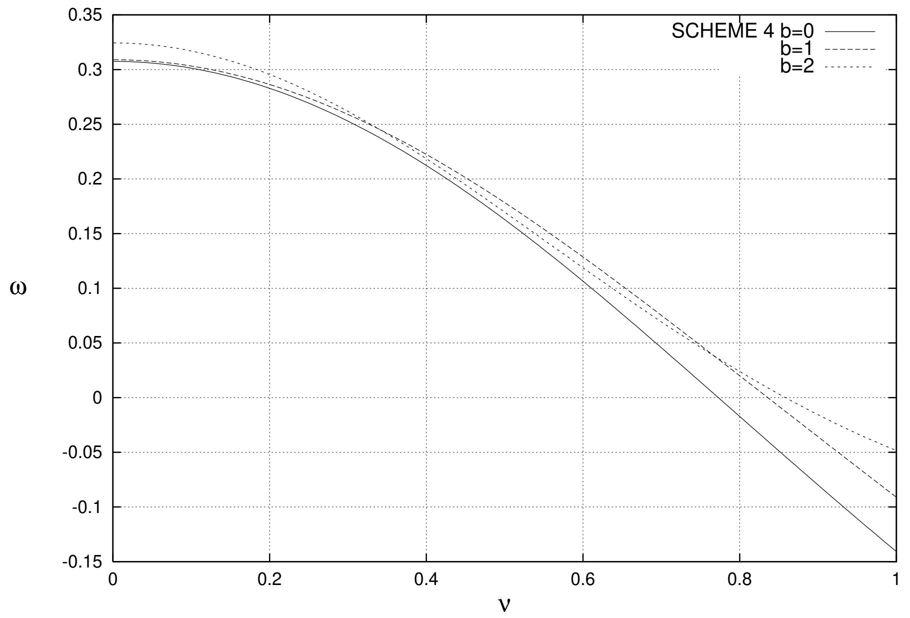

Figure 6.8: Dependence of the ‘Scheme 4 plus veto’ NLO kernel upon ν for $\bar{\alpha}_s = 0.2$

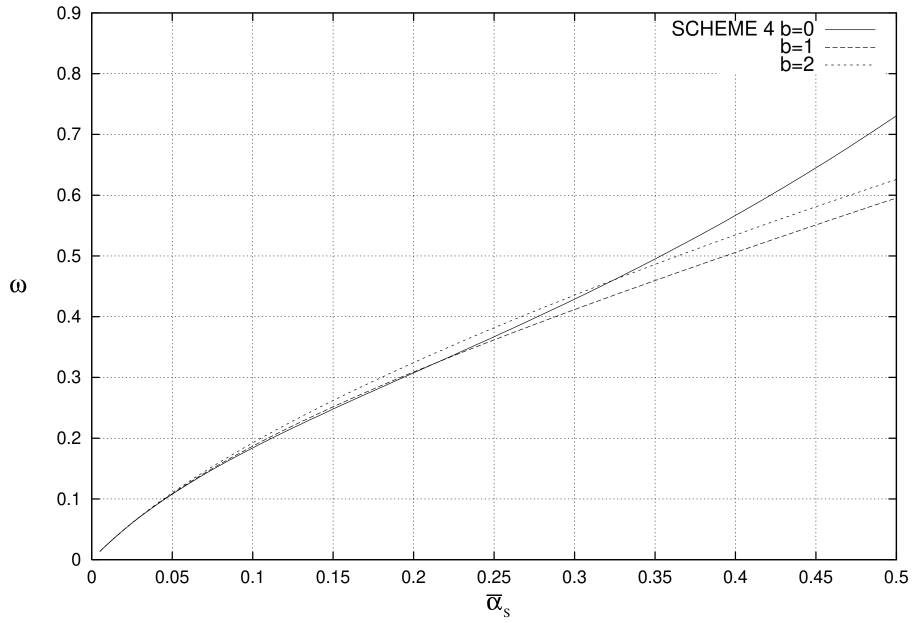

Figure 6.9: Dependence of the 'Scheme 4 plus veto' NLO kernel upon $\bar{\alpha}_s$ for $\nu = 0$

If we perform the integral over ω the Green's function of (6.3) becomes

$$f(s, k_1, k_2) = \int \frac{d\nu}{2\pi} \left(\frac{s}{s_0}\right)^{\omega_0(\nu)} \left(\frac{k_1^2}{k_2^2}\right)^{\frac{1}{2}+i\nu} \frac{1}{1 + b\omega_0(\nu)} \tag{6.45}$$

where $\omega_0(\gamma)$ is the solution to (6.34) and we have set $\gamma = \frac{1}{2} + i\nu$. We note that the solution to (6.34) develops cuts along the line $\gamma = 1/2$ with branch points at $\pm\nu_0$:

$$\chi_0\left(\frac{1}{2} + i\nu_0\right) = -\frac{e^{-1}}{\bar{\alpha}_s b}. \tag{6.46}$$

However, these cuts have no physical origin. They arise because we summed over arbitrarily large numbers of gluon emissions with each emission some minimum distance in rapidity from its neighbours. For any finite energy this is not possible. The result of truncating the number of emissions is to remove the cuts. To see this we can expand the RHS of Eq. 6.45 as a power series in $\bar{\alpha}_s$ [118]:

$$\frac{e^{\omega_0(\gamma)y}}{1 + b\ \omega_0(\gamma)} = \sum_{n=0}^{\infty} \frac{[\bar{\alpha}_s \chi_0(\gamma)\ (y - nb)]^n}{n!} \tag{6.47}$$

where $y \equiv \ln(s/s_0)$. Limiting the number of emitted gluons forces us to truncate the summation of the RHS of (6.47) and since the only singularities of $\chi_0(\gamma)$ are poles at $\gamma = 0, -1, -2, ...$ it follows that the cuts are absent.

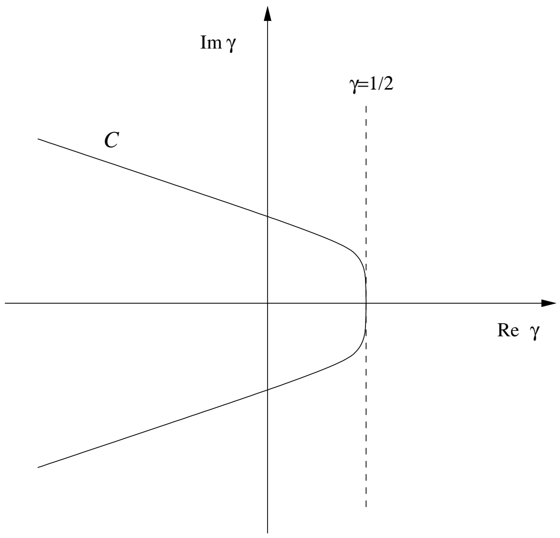

Figure 6.10: A suitable contour of integration for $k_1 > k_2$

Our claim that imposing the veto has a small effect is still not complete. We must also show that the asymptotic behaviour is driven by the behaviour of the kernel near $\nu = 0$. This is not as obvious as in the cases without a veto since the solution to (6.34), $\omega_0(\gamma)$, does not fall monotonically as $\gamma \to \infty$. In fact it grows slowly as

$$\omega_0(\gamma) \sim \ln[\ln \gamma(1-\gamma)].$$

However, the presence of the $(k_1^2/k_2^2)^\gamma$ term in the integral ensures that the integrand falls monotonically from its maximum in the vicinity of $\nu = 0$. For example, for $k_1 > k_2$ any γ-plane contour which heads to Re $\gamma \to -\infty$, e.g. the contour C shown in Fig. 6.10, is suitable. For large enough y we can therefore approximate (6.45) by

$$f(s, k_1, k_2) \approx \frac{e^{\tilde{\omega}_0 y}}{1 + b\,\tilde{\omega}_0} \int_{-\infty}^{\infty} \frac{d\nu}{2\pi} \left(\frac{k_1^2}{k_2^2}\right)^{1/2+i\nu} e^{-Ay\nu^2} \tag{6.48}$$

where $\omega_0(\gamma) \approx \tilde{\omega}_0 - A\nu^2$ in the vicinity of $\nu = 0$. The argument runs through in precisely the same fashion for the other kernels which include a veto. In Figs. 6.11 and 6.12 we show how the infinite sum is a good approximation down to low values of y for $\bar{\alpha}_s = 0.2$. In these plots we compare the LHS and RHS of Eq. 6.47 for y=4 and y=10 taking a typical value of $b = 1$ and notice how the approximation is accurate (for the truncated sum we took $N = 5, 8$ and 11). Therefore, for large enough s/s_0, the truncated sum can be approximated by the infinite sum and the integral over γ

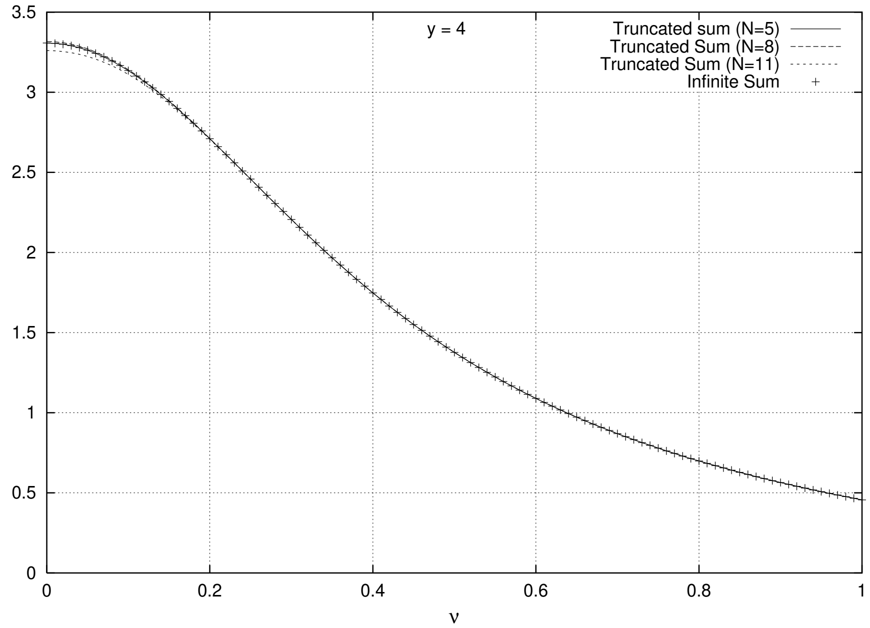

Figure 6.11: Value of the infinite sum and the truncated sum for $N = 5, 8, 11$ of Eq. 6.47 for y =4

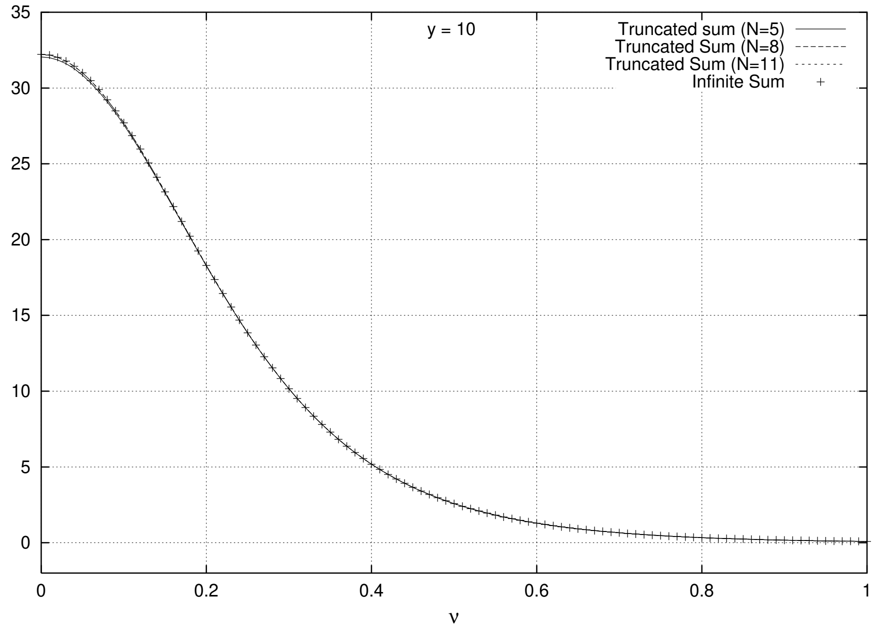

Figure 6.12: Value of the infinite sum and the truncated sum for $N = 5, 8, 11$ of Eq. 6.47 for y =10

can be approximated using the saddle point method, i.e. the asymptotic behaviour is driven by the value of the kernel at $\nu = 0$ (i.e. $\gamma = 1/2$). It is precisely this region of the kernel the one we have shown to be unaffected by the imposition of the veto.

Chapter 7

Solving the BFKL equation with running coupling

So far we have understood and solved the problems arising from the scale invariant terms of the BFKL kernel. The remaining question is how to treat the running coupling effects, i.e. those arising from the last term of Eq. 5.4.

In this chapter we will describe a formalism [119] for solving the BFKL equation with a coupling that runs for momenta above a certain infrared cutoff. By suitably choosing matching conditions proper account will be taken of the fact that the BFKL diffusion implies that the solution in the infrared (fixed coupling) regime depends upon the solution in the ultraviolet (running coupling) regime and vice versa. Expanding the BFKL kernel to a given order in the ratio of the transverse momenta will allow arbitrary accuracy to be achieved.

There has been a continuous effort in the literature to understand how to run the coupling in the BFKL equation. As we have seen in the case of fixed coupling, the energy dependence of diffractive processes is determined by the emergence of a branch cut in the Mellin transform plane ($\omega-$plane), with a branch point at $\omega > 0$. Lipatov [120] has demonstrated that accounting for the running of the strong coupling together with some (non-perturbative) information about the infrared behaviour of QCD leads to a separation of the $\omega-$plane singularity structure into a series of isolated poles. More recently, Thorne [121, 122] has shown that if one uses the solution to the BFKL equation with running coupling, the factor in the amplitude which is totally calculable in perturbative QCD has an essential singularity at $\omega = 0$, such that there is no power-like energy dependence. This is in accord with the recent work of Ciafaloni, Colferai and Salam, who have shown that the leading ω-plane singularity is of non-perturbative origin [127, 128].

We will treat the infrared region assuming that the strong coupling ceases to run below a certain scale. In this case, we expect that for sufficiently low values of the transverse momenta of the exchanged gluons, the $s-$behaviour will be dominated by the fixed coupling solution, whereas for large enough transverse momenta the solution of [121, 122] will dominate. In this chapter we want to understand the smooth extrapolation between these two extremes. We describe a formalism for solving the BFKL equation with strong coupling running above some infrared scale, in which we can see how the transition from the fixed coupling to the running coupling solution arises.

7.1 Formalism to solve the equation at leading order

To begin with we consider only the leading order BFKL kernel and describe later how the formalism may be extended in order to include the substantial part of the higher order corrections.

Since the BFKL equation is a diffusion equation there is always diffusion into the infrared regime, where renormalization group improved perturbation theory breaks down and one needs supplementary information about the behaviour of QCD beyond perturbation theory. For our purposes we simulate this infrared behaviour by assuming that the coupling freezes below a critical value of $t \equiv \ln(k^2/\Lambda^2_{QCD})$, $t = t_0$. We also make the assumption that $\alpha_s(t_0)$ is sufficiently small that perturbative results in the infrared regime maintain some level of credibility.

The full BFKL equation is solved in terms of a complete set of eigenfunctions $f_\omega(t)$ of the kernel with eigenvalue ω. For any ω there will be some diffusion into the infrared regime. We therefore write $f_\omega(t)$ as

$$f_\omega(t) \;=\; f^<_\omega(t)\,\theta(t_0-t) + f^>_\omega(t)\,\theta(t-t_0) \tag{7.1}$$

and the kernel as

$$\begin{aligned} K(t,t') \;=\; & \left[\frac{1}{b\,t_0}\mathcal{K}^<(t,t')\,\theta(t_0-t') + \frac{1}{b\,t}\mathcal{K}^<(t,t')\,\theta(t'-t_0)\right]\,\theta(t-t') \;+ \\ & \left[\frac{1}{b\,t_0}\mathcal{K}^>(t,t')\,\theta(t_0-t') + \frac{1}{b\,t'}\mathcal{K}^>(t,t')\,\theta(t'-t_0)\right]\,\theta(t'-t) \end{aligned} \tag{7.2}$$

where $b = \beta_0/12$, $\beta_0 = 11 - 2n_f/3$, being the first coefficient of the $\beta-$function for the running of the QCD coupling. We define $\mathcal{K}^<(t,t')$ and $\mathcal{K}^>(t,t')$ as the limits of sums, i.e.

$$\mathcal{K}^<(t,t') \;=\; \lim_{N\to\infty} \mathcal{K}^<_N(t,t')$$

$$\mathcal{K}^{>}(t,t') \;=\; \lim_{N\to\infty} \mathcal{K}^{>}_{N}(t,t')$$

where

$$\mathcal{K}^{<}_{N}(t,t') \;=\; \sum_{r=0}^{N} \left\{ e^{(r+1/2)(t'-t)} - \frac{1}{r+1}\delta(t-t') \right\} \tag{7.3}$$

$$\mathcal{K}^{>}_{N}(t,t') \;=\; \sum_{r=0}^{N} \left\{ e^{(r+1/2)(t-t')} - \frac{1}{r+1}\delta(t-t') \right\}. \tag{7.4}$$

The functions $e^{\gamma t}$ are eigenfunctions of these kernels with eigenvalues $\chi^{<}_{N}(\gamma)$ and $\chi^{>}_{N}(\gamma)$ respectively, i.e.

$$\begin{aligned}\int_{-\infty}^{t} \mathcal{K}^{<}_{N}(t,t')e^{\gamma t'}dt' &= \chi^{<}_{N}(\gamma)e^{\gamma t}\\ \int_{t}^{\infty} \mathcal{K}^{>}_{N}(t,t')e^{\gamma t'}dt' &= \chi^{>}_{N}(\gamma)e^{\gamma t}\end{aligned} \tag{7.5}$$

where

$$\chi^{<}_{N}(\gamma) \;=\; \sum_{r=0}^{N} \left\{ \frac{1}{r+1/2+\gamma} - \frac{1}{r+1} \right\} \tag{7.6}$$

$$\chi^{>}_{N}(\gamma) \;=\; \sum_{r=0}^{N} \left\{ \frac{1}{r+1/2-\gamma} - \frac{1}{r+1} \right\}. \tag{7.7}$$

Note that $\chi^{<}_{\infty}(\gamma) = \gamma_E - \psi(1/2+\gamma)$ and $\chi^{>}_{\infty}(\gamma) = \gamma_E - \psi(1/2-\gamma)$, and we have the leading order BFKL kernel.

In this paper we truncate the kernel after N terms. Note that the case $N=0$ reduces to the collinear model of [127, 128]. For this truncated kernel the spectrum of eigenvalues is

$$-\sum_{r=0}^{N} \frac{2}{r+1} \;\le b\,t_0\,\omega\; \le \sum_{r=0}^{N} \frac{2}{(2r+1)(r+1)}. \tag{7.8}$$

The infrared part of the eigenfunction $f^{<}_{\omega}(t)$ obeys the integral equation

$$\begin{aligned}b\,t_0\,\omega\, f^{<}_{\omega}(t) \;&=\; \int_{-\infty}^{t} \mathcal{K}^{<}_{N}(t,t') f^{<}_{\omega}(t')\,dt' \;+\; \int_{t}^{t_0} \mathcal{K}^{>}_{N}(t,t') f^{<}_{\omega}(t')\,dt'\\ &\quad+\; \int_{t_0}^{\infty} \mathcal{K}^{>}_{N}(t,t')\frac{t_0}{t'} f^{>}_{\omega}(t')dt'\end{aligned} \tag{7.9}$$

whereas the ultraviolet part of the solution $f^{>}_{\omega}(t)$, obeys the integral equation

$$\begin{aligned}b\,t\omega\, f^{>}_{\omega}(t) \;&=\; \int_{t_0}^{t} \mathcal{K}^{<}_{N}(t,t') f^{>}_{\omega}(t')\,dt' \;+\; \int_{t}^{\infty} \mathcal{K}^{>}_{N}(t,t')\frac{t}{t'} f^{>}_{\omega}(t')\,dt'\\ &\quad+\; \int_{-\infty}^{t_0} \mathcal{K}^{<}_{N}(t,t') f^{<}_{\omega}(t')\,dt'.\end{aligned} \tag{7.10}$$

We note that these equations are both inhomogeneous, reflecting the fact that even for $t < t_0$, where the coupling is fixed, the BFKL equation involves diffusion into the running coupling regime and vice versa.

We can convert these two equations into homogeneous integro-differential equations by operating on both sides of Eq.7.9 with the operator

$$\mathcal{O}^N_<(t) \;=\; \frac{d}{dt}\left(\frac{d}{dt}-1\right)\cdots\left(\frac{d}{dt}-N\right)e^{-t/2}$$

and operating on both sides of Eq.7.10 with the operator

$$\mathcal{O}^N_>(t) \;=\; \frac{d}{dt}\left(\frac{d}{dt}+1\right)\cdots\left(\frac{d}{dt}+N\right)e^{t/2}.$$

These equations are $(N+1)^{th}$ order in derivatives and so each one of these has solutions which contain $N+1$ arbitrary constants of integration. However, these constants are fixed by the requirement that the original integral equations, 7.9 and refbfkl¿, must be obeyed, together with the requirements the eigenfunctions should be normalizable, which means that $f^<_\omega(t)$ must be square integrable as $t \to -\infty$ and $f^>_\omega(t)$ must be square integrable as $t \to \infty$.

The general solution to the integro-differential equation for $f^<_\omega(t)$ is

$$f^<_\omega(t) \;=\; \sum_{j=1}^{N+2} a_j e^{\gamma^0_j t}, \tag{7.11}$$

where γ^0_j are the solutions to

$$b\,\omega\,t_0 \;=\; \chi^<_N(\gamma)+\chi^>_N(\gamma) \;\equiv\; \chi_N(\gamma) \tag{7.12}$$

with $\Re e(\gamma) \geq 0$ to ensure square integrability as $t \to -\infty$. In the allowed range of eigenvalues, Eq. 7.8, there will be $N+2$ such solutions. For example, in the case $N=0$ the solutions are

$$\gamma^0_j \;=\; \pm\, i\sqrt{\left(\lambda_0-\frac{1}{4}\right)} \tag{7.13}$$

where

$$\lambda_0 = \frac{1}{b\,\omega\,t_0+2}.$$

For the allowed range, $\lambda_0 > 1/4$, and so these values are purely imaginary. In the case $N = 1$ we have

$$\gamma_j^0 = \pm\sqrt{\left(\frac{10}{8} - 2\lambda_1 \pm \sqrt{1 - 2\lambda_1 + 4\lambda_1^2}\right)} \tag{7.14}$$

where

$$\lambda_1 = \frac{1}{b\,\omega\,t_0 + 3}.$$

For the allowed range, $\lambda_1 > 3/16$ and we see that two of the solutions are purely imaginary, $\pm i\nu_1$, and two purely real $\pm\beta_1$. Thus the general solution is

$$f_\omega^<(t) = a_1 e^{i\nu_1 t} + a_2 e^{-i\nu_1 t} + a_3 e^{\beta_1 t}. \tag{7.15}$$

For the integro-differential equation for $f_\omega^>(t)$, it is convenient to work in terms of the Laplace transform $\tilde{f}_\omega(\gamma)$ defined by

$$\frac{f_\omega^>(t)}{t} = \frac{1}{2\pi i}\int d\gamma\, \tilde{f}_\omega(\gamma) e^{\gamma t}, \tag{7.16}$$

in which the integral over γ is performed over some suitable contour, described below. The function $\tilde{f}_\omega(\gamma)$ obeys the differential equation

$$\omega\, b\, \tilde{f}_\omega''(\gamma) + \chi_N(\gamma)\tilde{f}_\omega'(\gamma) + \chi_N^>{}'\tilde{f}_\omega(\gamma) = 0, \tag{7.17}$$

where the prime indicates differentiation with respect to γ. This equation can be solved in WKB approximation yielding the result

$$\tilde{f}_\omega(\gamma) = \frac{1}{\left(V(\gamma,\omega)\right)^{1/4}} \exp\left\{-\frac{1}{2\omega b}\int^\gamma \left(\chi_N(\gamma') + \sqrt{V(\gamma',\omega)}\right) d\gamma'\right\}, \tag{7.18}$$

where

$$V(\gamma,\omega) = \chi_N^2(\gamma) - 4\,\omega\, b\, \chi_N^>{}'(\gamma).$$

Note that if we set the term $\chi_N^>{}'(\gamma)$ to zero we recover the expression obtained in [121, 122] for the case of deep-inelastic scattering in which the transverse momenta are ordered and the coupling is chosen to run always with t.

The solution 7.18 is a valid approximation except near the points where $V(\gamma)$ vanishes. We could improve the solution by expanding $V(\gamma)$ to linear order around the zeroes and matching the solutions either side to an Airy function. However, the singularities in $\tilde{f}_\omega$ at these zeroes are integrable so that such an improvement would have negligible effect on the inverse Laplace transform.

For $t < t_c$ the solution is oscillatory. The value of this critical value t_c can be estimated by approximating the integral of Eq. 7.16 by the saddle point at

$$2\,\omega\,b\,t \;=\; \chi_N(\gamma) + \sqrt{V(\gamma,\omega)}.$$

t_c is the minimum value of t for which this has a solution for purely real γ. Again, if we were to neglect $\chi_N^{>\prime}(\gamma)$, this would occur at $\gamma = 0$ and we have approximately

$$t_c \;=\; \frac{1}{b\,\omega}\chi_N(0).$$

This oscillatory part is "matched" to the fixed-coupling solution by requiring consistency with the original integral equations 7.9 and 7.10. To see how this is possible, we need to examine in more detail the possible contours of integration for Eq. 7.16.

7.1.1 The γ-contours

From the positions of the simple poles in $\chi_N^<(\gamma)$ and $\chi_N^>(\gamma)$, we note that $\tilde{f}_\omega(\gamma)$ has branch points on the real axis at $\gamma = r + 1/2$ and $\gamma = -1/2 - r$ for $r = 0, \cdots N$. The branch cuts can be "combed" in the direction of the positive or negative real axis in such a way as to leave a portion of the real axis between $n - 1/2$ and $n + 1/2$ for which $\tilde{f}_\omega(\gamma)$ is analytic. n runs from $-N$ to N.

For each such "combing" a contour, $\mathcal{C}_n$ can be chosen that crosses the real axis between $n - 1/2$ and $n + 1/2$. Since $t > 0$ we require that the ends of the contour turn over so that at the ends of the contour $\Re e\,\gamma \to -\infty$, thus ensuring that the inverse Laplace transform integral exists. The integral over each such contour is a valid solution to the integro-differential equation for $f_\omega^>(t)$ and since this equation is linear, the most general solution which is square integrable as $t \to \infty$ is the sum of the integrals over these contours with $-N \le n \le 0$, with arbitrary coefficients b_n, i.e.

$$\sum_{n=-N}^{0} b_n \int_{\mathcal{C}_n} d\gamma \tilde{f}_\omega(\gamma) e^{\gamma t}, \tag{7.19}$$

with $\tilde{f}_\omega(\gamma)$ given by Eq. 7.18.* As an example we consider the $N = 1$ case. The four "combings" are shown in Fig. 7.1 together with the four contours, $\mathcal{C}_n$. Only $\mathcal{C}_{-1}$ and $\mathcal{C}_0$ give a square integrable solution, so the general solution is

$$f_\omega^>(t) \;= t\left\{ \; b_{-1} \int_{-\infty}^{\infty} d\nu \, e^{-t} \, \tilde{f}_\omega(i\nu - 1) e^{i\nu t} \; + \; b_0 \int_{-\infty}^{\infty} d\nu \tilde{f}_\omega(i\nu) e^{i\nu t} \right\}. \tag{7.20}$$

Returning now to the original equations 7.9 and 7.10, we see that these are obeyed by the solutions 7.19 and 7.11 provided

$$\sum_{j=1}^{N+2} a_j \frac{e^{\gamma_j^0 t_0}}{(\gamma_j^0 - r - 1/2)} - t_0 \sum_{n=-N}^{0} b_n \int_{\mathcal{C}_n} d\gamma \frac{\tilde{f}_\omega(\gamma)\, e^{\gamma t_0}}{(\gamma - r - 1/2)} \;=\; 0 \quad (r = 0 \cdots N), \tag{7.21}$$

$$\sum_{j=1}^{N+2} a_j \frac{e^{\gamma_j^0 t_0}}{(\gamma_j^0 + r + 1/2)} + \sum_{n=-N}^{0} b_n \int_{\mathcal{C}_n} d\gamma \frac{\tilde{f}'_\omega(\gamma)\, e^{\gamma t_0}}{(\gamma + r + 1/2)} \;=\; 0 \quad (r = 0 \cdots N). \tag{7.22}$$

Thus we obtain $2N + 2$ relations between the $N + 2$ coefficients a_j and the $N + 1$ coefficients b_k (the overall normalization of these coefficients is determined by the normalization condition of the eigenfunctions). This then determines uniquely the required eigenfunctions.

Equations 7.9 and 7.10 guarantee the continuity of the eigenfunctions at $t = t_0$, i.e. $f_\omega^<(t_0) = f_\omega^>(t_0)$, but the derivative is not continuous. This results from the fact that we have taken an expression for the coupling as a function of t, whose derivative is not continuous at $t = t_0$.

7.1.2 Qualitative analysis of the solution for N=0

We can now see how the inverse Mellin transform, $f(s,t)$ of the solution $f_\omega(t)$ extrapolates smoothly between the power-like behaviour for $t \sim t_0$ and the softer behaviour (with at most logarithmic dependence on s) for $t \gg t_0$.

*We have absorbed the factor of $2\pi i$ in the denominator in eq.(7.16) into the definition of the coefficients b_n.

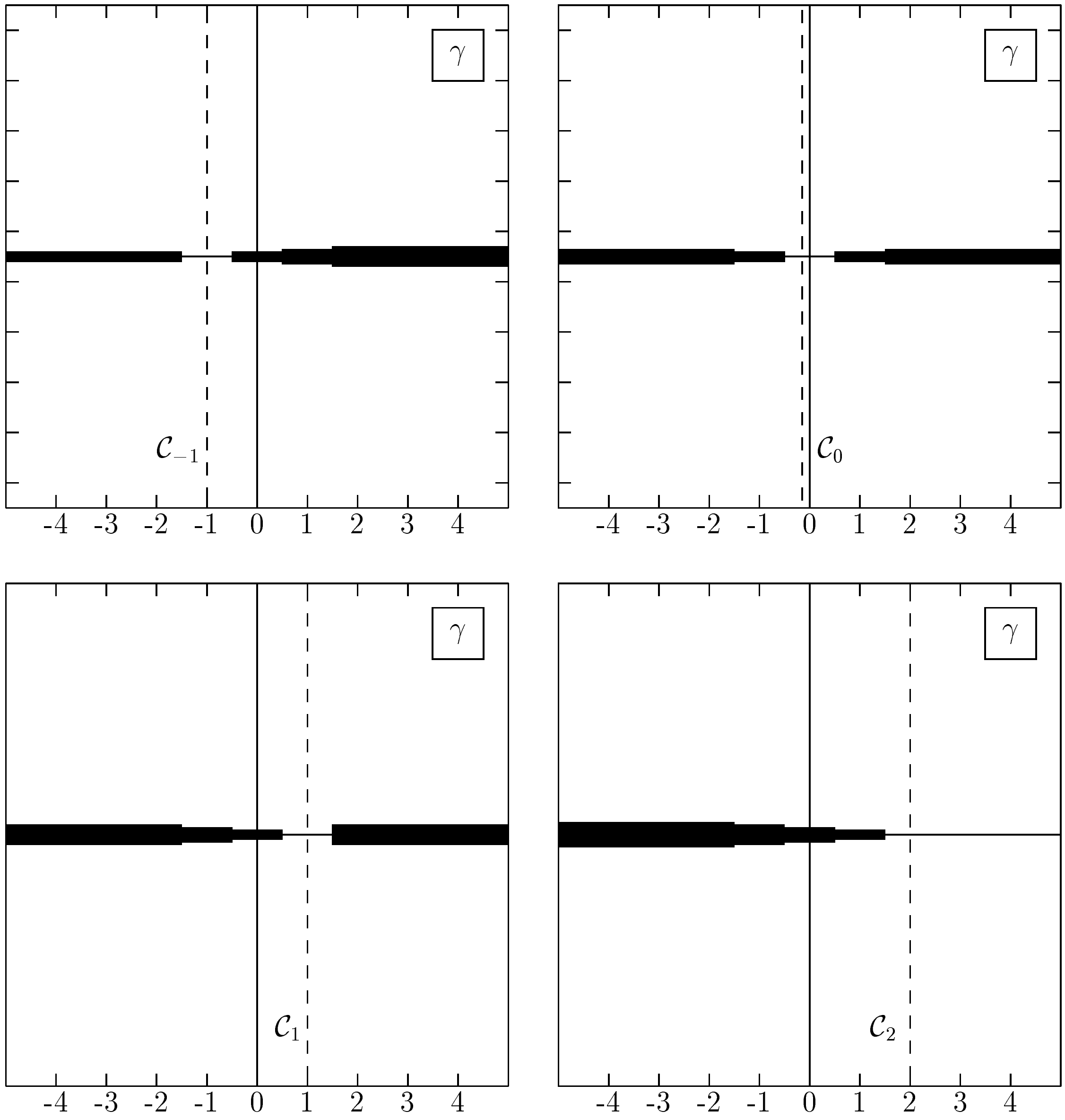

Figure 7.1: The four contours for the case $N = 1$ corresponding to the four different ways of "combing" the branch cuts.

Examining the $\gamma-$ integral for one particular contour, $\mathcal{C}_n$, and for $t > t_0$, we see that this will be dominated by a saddle point $\gamma_s(\omega, t)$, which is the solution to

$$2b\,\omega\,t \;=\; \chi_N(\gamma) + \sqrt{V(\gamma,\omega)}. \tag{7.23}$$

This is multi-valued and the dominant saddle point will be the one closest to the integration contour. We call this saddle point $\gamma_s^n(\omega, t)$. In other words, $f_\omega^>(t)$ of Eq. 7.16 from the contour $\mathcal{C}_n$ will contain an $\omega-$dependent prefactor, which may be written (after a suitable integration by parts)

$$\exp\left\{\int^t \gamma_s^n(\omega, t')dt'\right\}.$$

The essential singularity at $\omega = 0$ is now encoded in $\gamma_s^n(\omega, t)$ which acquires a singularity as $\omega \to 0$, i.e. the R.H.S. of 7.23 can only tend to zero as $|\gamma| \to \infty$.

Now examining Eqs. 7.21 and 7.22, we see that the contour integrals multiplying the coefficients b_n are also dominated by a similar saddle point but with t set to t_0. Thus these coefficients appear in Eqs. 7.21 and 7.22 with a prefactor

$$\exp\left\{\int^{t_0} \gamma_s^n(\omega, t')dt'\right\}.$$

Therefore these coefficients also possess an essential singularity at $\omega = 0$. Furthermore b_n will contain factors of the form $\exp(\gamma_0^j(\omega)t_0)$ from the L.H.S. of 7.21 and 7.22.

For t close to t_0 each term in the sum of Eq. 7.19 , i.e. the product of b_n and the contribution to $f_\omega^>(t)$ from the integral over the contour $\mathcal{C}_n$ will have a dominant $\omega-$dependence of the form

$$\exp\left\{\gamma_s^n(\omega, t_0)(t - t_0) + \gamma_0^j(\omega)t_0\right\}. \tag{7.24}$$

Note that due to the partial cancellation, the coefficient of the term that gives rise to the essential singularity vanishes as $t \to t_0$.

For sufficiently large s, the inverse Mellin transform probes small ω, where the term in the exponent proportional to $\gamma_s^n(\omega, t_0)$ will dominate even if $(t - t_0)$ is small and the s-behaviour is dominated by the essential singularity in the Laplace transform,

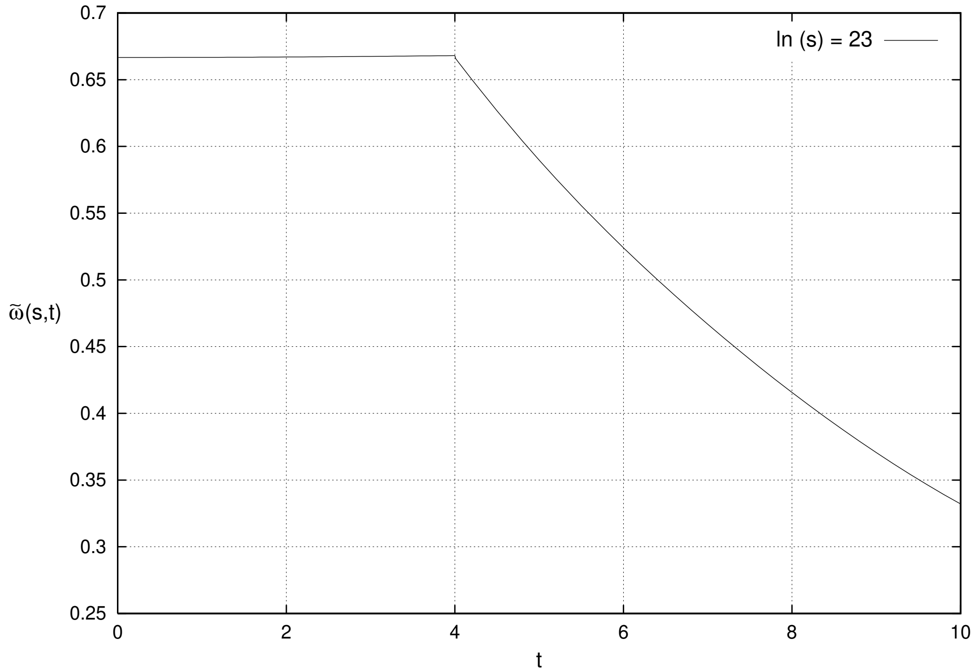

Figure 7.2: $\tilde{\omega}(s,t)$ against t for $\ln s = 23$

$\tilde{f}_\omega(\gamma)$. However, for more moderate values of s we can neglect this term when t is sufficiently close to t_0 and the $s-$dependence will be dominated by the fixed coupling power-like behaviour. As t is increased away from t_0, the boundary in s where the soft behaviour takes over from the power-like behaviour decreases and we see that as $t \to \infty$ we recover the solution of [121, 122].

This formalism is considerably simplified if we assume that t_0 is sufficiently large that $\exp(-t_0) \ll 1$. In this case we only need consider the right-most contour consistent with square-integrability as $t \to \infty$. This is the contour $\mathcal{C}_0$. In this case, within the approximation of performing the $\gamma-$contour integral and the inverse Mellin transform by the saddle-point method, the $s-$dependence may be written as $s^{\tilde{\omega}(s,t)}$, where $\tilde{\omega}(s,t)$ is the solution to

$$\ln(s) \;=\; -\frac{d}{d\omega}\left\{\theta(t-t_0)\int_{t_0}^{t}\gamma_s^0(\omega,t')dt' + \gamma_0^m(\omega)\mathrm{Min}(t,t_0)\right\}, \qquad (7.25)$$

and $\gamma_0^m(\omega)$ is the solution to Eq. 7.12 with the largest real part. In Fig. 7.2 we plot $\tilde{\omega}(s,t)$ against t for a large value of s ($\ln s = 23$). For simplicity we have taken the $N = 0$ case, although we expect the result to be qualitatively the same for higher values of N, and we take $t_0 = 4$. We see that it is almost constant for $t < t_0$ and

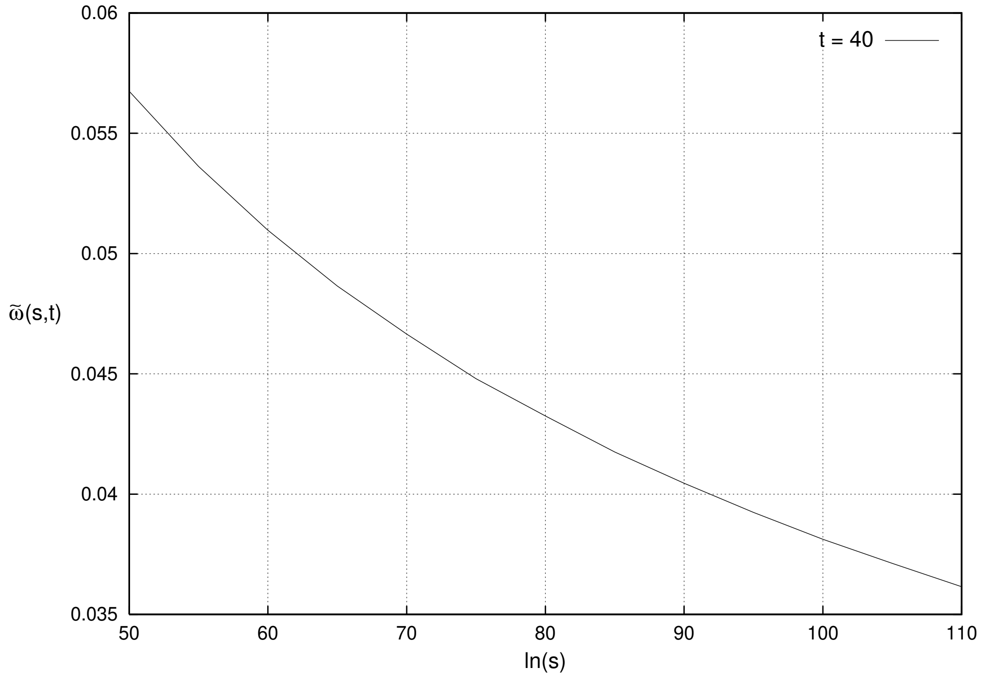

Figure 7.3: $\tilde{\omega}(s,t)$ against $\ln s$ for $t = 40$

diminishes as one increases t from t_0, indicating the smooth transition from hard to soft $s-$dependence as t is increased. The discontinuity of the slope at $t = t_0$ is a reflection of the fact that we have taken a sharp discontinuity in the slope of the running coupling at t_0 and would be smoothed out if a smoother transition were taken.

The asymptotic behaviour is only obtained for much larger values of t and in Fig. 7.3 we show the s dependence of $\tilde{\omega}(s,t)$ for $t = 40$ and notice that it is much closer to zero than the case where $t \sim t_0$ and decreases as $\ln s$ increases, resulting in an $s-$dependence for the amplitude that has no fixed power of s.

7.2 Accounting for Higher Order Corrections

The higher order BFKL kernel does not lend itself readily to an expansion in powers of $e^{t-t'}$. Furthermore, it is known that these corrections are large.

However, as we have seen in previous chapter we know that a substantial part of the higher order corrections consist of "collinear corrections" which are required to ensure correct behaviour when the formalism is applied to deep inelastic scattering. We have shown that once these corrections are accounted for, the remaining higher order corrections are modest. The simplest way of encoding these collinear corrections and summing them is to replace γ by $(\gamma - \omega/2)$ in $\chi_N^<(\gamma)$ and by $(\gamma + \omega/2)$ in $\chi_N^>(\gamma)$ [90, 113].

This formalism is readily adapted to the procedure described here. In the expression 7.11 for $f_\omega^<(t)$ the quantities $\gamma_j^0(\omega)$ are taken to be the solutions to the implicit equation

$$\chi_N^<(\gamma - \omega/2) + \chi_N^>(\gamma + \omega/2) \;=\; \omega b t_0, \tag{7.26}$$

and the expression for the Laplace transform of $f_\omega^>(t)$ becomes

$$\begin{aligned}\tilde{f}_\omega(\gamma) \;=\; & \frac{1}{(V(\gamma,\omega))^{1/4}} \\ & \exp\left\{-\frac{1}{2\omega b}\int^{\gamma}\left(\chi_N^<(\gamma' - \omega/2) + \chi_N^>(\gamma' + \omega/2) + \sqrt{V(\gamma',\omega)}\right)d\gamma'\right\},\end{aligned} \tag{7.27}$$

where

$$V(\gamma,\omega) \;=\; \left(\chi_N^<(\gamma - \omega/2) + \chi_N^>(\gamma + \omega/2)\right)^2 - 4\omega b\, \chi_N^{>\prime}(\gamma + \omega/2). \tag{7.28}$$

Provided that we restrict our analysis to the case $|\omega| < 1$, the singularity structure and consequently the analysis of the contours of integration remains unchanged from the leading order case, although the exact positions of the branch points will have moved.

This approach is very promising because it provides a general method to study running coupling effects for the whole BFKL kernel, including the higher order corrections. Work is in progress [129] to fully solve the problem beyond the saddle point approximation for $N > 0$ and including the collinear improved corrections.

Chapter 8

Conclusions and future work

In this thesis we have reviewed the BFKL resummation program at leading and next-to-leading order. For high energy processes where the centre-of-mass energy is much larger that the momentum transfer the scattering is dominated by gluon exchange in the t channel. The BFKL equation is derived in the multi-regge kinematics and resums terms of the form $(\alpha_s \ln s/s_0)^n$ assuming that the produced gluons are strongly ordered in rapidity and have similar transverse momenta. The precise definition of the scale s_0 does not modify the LO predictions and it is only constrained by the fact that the logarithms $\ln s/s_0$ must be large, i.e. $s \gg s_0$. The asymptotic energy behaviour of the cross section is given by the LO eigenvalue, i.e.

$$\left(\frac{s}{s_0}\right)^{4\ln 2\bar{\alpha}_s}. \tag{8.1}$$

The experimental situation reveals that, so far, there is no definite need of BFKL to explain the data. There seem not to be deviations from the NLO DGLAP conventional approach in the scaling violations to the evolution of the F_2 structure function in DIS. For other processes like forward jet production in DIS, dijet production at large rapidity intervals or high energy $\gamma^*\gamma^*$ scattering, more work to reduce the theoretical uncertainties and more data are needed.

Introducing the concept of QCD coherence and soft emissions in the BFKL ladder is believed to be the correct way to describe more exclusive observables like multi-jet rates. This can be achieved using the CCFM equation. Although, as we originally pointed out in this work [75, 79], the BFKL and CCFM predictions for final states coincide at LO, to achieve a correct phenomenology we should go to higher orders where the predictions from both approaches are different. At this accuracy Monte Carlo event generators are mandatory due to the difficulty of solving the CCFM equation. Work is in progress in this direction but still there is a lack of complete understanding of the CCFM equation.

The solution of the BFKL equation at LO is scale invariant because the strong coupling α_s has been considered as constant. If we relax the multi- regge kinematics allowing emissions to be close by in rapidity we obtain the next-to-leading order terms $\alpha_s(\alpha_s \ln s/s_0)^n$. If the BFKL resummation is based on a correct expansion these emissions should have little effect, at most they would reduce the value of the power of the energy growth in the cross sections 8.1. The NLO expansion contains the one-loop running of the coupling (Eq. 1.26) and it can be expressed in terms of the effect of the NLO kernel on the LO eigenfunctions as

$$\begin{aligned}
\omega(\gamma) &= \bar{\alpha}_s(Q^2)\chi_0(\gamma) + \bar{\alpha}_s(Q^2)^2\chi_1(\gamma) \\
&= \bar{\alpha}_s(\mu^2)\chi_0(\gamma) + \bar{\alpha}_s(\mu^2)^2\chi_1(\gamma) \\
&\quad -b\ln\frac{Q^2}{\mu^2}\bar{\alpha}_s(\mu^2)^2\chi_0(\gamma), \qquad (8.2)
\end{aligned}$$

where μ is the $\overline{\rm MS}$ renormalization scale. The kernels $\chi_0(\gamma)$ and $\chi_1(\gamma)$ are those in expressions 6.2 and 4.40 respectively. At NLO the scale invariance is explicitly broken by the last term of Eq. 8.2.

The NLO corrections in the scale invariant terms turned out to be large and negative compared to the LO ones. This is a feature of the BFKL expansion which has its origin in spurious double transverse logarithms. These logs appear in the expansion because of the freedom in the choice of the scale s_0 at LO. When we go to NLO the value of s_0 is relevant and can introduce NNLO and beyond terms which, although formally higher orders, can affect the properties of the Green's function. The problem can be cured by considering higher order contributions which cancel those logarithms not allowed when considering the DGLAP limit of the expansion. By introducing a veto on gluons emitted nearby in rapidity we have shown in this thesis that, after removing the unphysical logarithms, the contribution from nearby emissions is genuinely a higher order effect [114]. This supports the use of the multi-regge kinematics which is fundamental to the BFKL program.

Recently there have been remarkable results leading to a better understanding of the BFKL formalism in DIS. As we have seen the cross sections can be factorized into a non-perturbative and a perturbative part, with the evolution of the latter being calculable within DGLAP. It has been suggested that this factorization breaks down at very small x [124] and based on this result it has been argued that the splitting functions at small x can only be fitted because they are not calculable [125, 126]. This is in contrast with the results of a collinear model in ref. [127] which is like the BFKL case in that the emissions are not ordered in transverse scale. It also has the correct collinear limit. In this model factorization was found to be valid for all values of x. Also of note is the solution, in this model, for the gluon Green's function: [127]:

$$\mathcal{G}(s;k) \simeq \underbrace{\frac{1}{\sqrt{2\pi\chi_m''\bar{\alpha}_s \ln\frac{s}{s_0}}}\left(\frac{s}{s_0}\right)^{\omega_s(k)} \cdot [1+\mathcal{O}(\alpha_s^5 \ln^3\frac{s}{s_0})]}_{\text{Hard}} + \underbrace{\left(\frac{s}{s_0}\right)^{\omega_{\mathcal{P}}} R_{\mathcal{P}}\left(\frac{\Lambda^2}{k^2}\right)^{1+\omega_{\mathcal{P}}}}_{\text{Soft}}, \tag{8.3}$$

where the exponent $\omega_s(k)$ is observable at intermediate values of s with corrections of the order $\sim \alpha_s^5 \ln^3 \frac{s}{s_0}$. The non-perturbative Pomeron $\omega_{\mathcal{P}}$ dominates for larger energies but is higher-twist. These results need to be confirmed and we have provided an alternative general solution to the problem which will allow us to solve the full BFKL kernel introducing the running of the coupling in a consistent way [119]. Work is in progress to generate the whole solution to the BFKL equation with running coupling and to understand the transition from the fixed coupling regime to the running one [129].

Finally, to obtain a BFKL phenomenology with a firm theoretical basis we need not only the Green's function at NLO but also the process dependent NLO impact factors which, convoluted with the former, will give the physical cross sections. Some of them have already been derived [91, 93, 130] or have started to be calculated [131, 132].

Appendix A

Example of integration in two-dimensional gluon phase space

We want to calculate the following integral

$$\begin{aligned}
&\int_{\mu^2}^{Q^2} \frac{d^2 q_1}{\pi q_1^2} \int_{\mu^2}^{Q^2} \frac{d^2 q_2}{\pi q_2^2} \ln \frac{(\mathbf{q_1}+\mathbf{q_2})^2}{\mu^2} \\
&= \int_{\mu^2}^{Q^2} \frac{dq_1^2}{q_1^2} \int_{\mu^2}^{Q^2} \frac{dq_2^2}{2\pi q_2^2} \int_0^{2\pi} d\theta \ln \left(\frac{q_1^2}{\mu^2} + \frac{q_2^2}{\mu^2} + 2\frac{q_1 q_2}{\mu^2}\cos\theta \right).
\end{aligned} \tag{A.1}$$

We are now going to analyse the angular integral with the help of Ref. [123]. Using the notation

$$A \equiv \frac{q_1^2}{\mu^2} + \frac{q_2^2}{\mu^2} \text{ and } B \equiv 2\frac{q_1 q_2}{\mu^2}, \tag{A.2}$$

we can write

$$\begin{aligned}
&\int_0^{2\pi} d\theta \ln \left(\frac{q_1^2}{\mu^2} + \frac{q_2^2}{\mu^2} + 2\frac{q_1 q_2}{\mu^2}\cos\theta \right) \\
&= \frac{d}{d\lambda} \int_0^{2\pi} d\theta (A + B\cos\theta)^\lambda \bigg|_{\lambda=0} \\
&= 2\pi \frac{d}{d\lambda} \left[A^\lambda {}_2F_1\left(\frac{1-\lambda}{2}, -\frac{\lambda}{2}; 1; \frac{B^2}{A^2} \right) \right]_{\lambda=0}.
\end{aligned} \tag{A.3}$$

${}_2F_1(a,b;c;z)$ is the hypergeometric function which in our case where $c=1$ and $2(a-b)=1$ has the nice property [123] of having the quadratic transformation

$${}_2F_1(a, a+\frac{1}{2}; c; z) = (1+\sqrt{z})^{-2a} {}_2F_1(2a, c-\frac{1}{2}; 2c-1; \frac{2\sqrt{z}}{1+\sqrt{z}}). \tag{A.4}$$

This property is very convenient because applying the symmetry condition

$$
\begin{aligned}
& {}_2F_1\left(\frac{1-\lambda}{2}, -\frac{\lambda}{2}; 1; \frac{B^2}{A^2}\right) \\
= & {}_2F_1\left(-\frac{\lambda}{2}, \frac{1-\lambda}{2}; 1; \frac{B^2}{A^2}\right) = \left(1+\frac{B}{A}\right)^{\lambda} {}_2F_1\left(-\lambda, \frac{1}{2}; 1; \frac{2B}{A+B}\right)
\end{aligned}
\tag{A.5}
$$

we can express our integral as

$$
\begin{aligned}
& 2\pi \frac{d}{d\lambda}\left[A^{\lambda} {}_2F_1\left(\frac{1-\lambda}{2}, -\frac{\lambda}{2}; 1; \frac{B^2}{A^2}\right)\right]_{\lambda=0} \\
= \; & 2\pi \frac{d}{d\lambda}\left[(A+B)^{\lambda} {}_2F_1\left(-\lambda, \frac{1}{2}; 1; \frac{2B}{A+B}\right)\right]_{\lambda=0} \\
= \; & 2\pi \frac{d}{d\lambda}\left[\left(\frac{q_1}{\mu}+\frac{q_2}{\mu}\right)^{2\lambda} {}_2F_1\left(-\lambda, \frac{1}{2}; 1; \frac{4q_1q_2}{(q_1+q_2)^2}\right)\right]_{\lambda=0} \\
= \; & 2\pi \left\{\ln\left(\frac{q_1}{\mu}+\frac{q_2}{\mu}\right)^2 {}_2F_1\left(0, \frac{1}{2}; 1; \frac{4q_1q_2}{(q_1+q_2)^2}\right)\right. \\
& \left. + \sum_{k=0}^{\infty}\left[\frac{d}{d\lambda}(-\lambda)_k|_{\lambda=0}\right] \frac{(\frac{1}{2})_k}{(1)_k k!}\left[\frac{4q_1q_2}{(q_1+q_2)^2}\right]^k\right\},
\end{aligned}
\tag{A.6}
$$

where $(m)_k$ is the Pochhammer's symbol

$$
(m)_k = \frac{\Gamma(m+k)}{\Gamma(m)}. \tag{A.7}
$$

Using now the relations

$$
{}_2F_1(0, b; c; z) = 1, \quad \frac{d}{d\lambda}(-\lambda)_k\bigg|_{\lambda=0} = -\Gamma(k) = -(k-1)!, \text{ and } (1)_k = k!, \tag{A.8}
$$

we get for our angular integral the expression

$$
2\pi \left\{\ln\left(\frac{q_1}{\mu}+\frac{q_2}{\mu}\right)^2 - \sum_{k=1}^{\infty}\frac{1}{k!\;k}\left(\frac{1}{2}\right)_k\left[\frac{4q_1q_2}{(q_1+q_2)^2}\right]^k\right\}. \tag{A.9}
$$

For a general function F of the form

$$
F(z) = \sum_{k=1}^{\infty}\frac{1}{k!\;k}\left(\frac{1}{2}\right)_k z^k, \tag{A.10}
$$

we can find a logarithmic expression by derivating it

$$
F'(z) = \frac{1}{z}\sum_{k=1}^{\infty}\frac{z^k}{k!}\left(\frac{1}{2}\right)_k = \frac{1}{z}\left(\frac{1}{\sqrt{1-z}}-1\right), \tag{A.11}
$$

and integrating back

$$F(z) = -\ln\left(z\frac{1+\sqrt{1-z}}{1-\sqrt{1-z}}\right) + \ln 4, \tag{A.12}$$

where we have used the fact that $F(0) = 0$.

With this information we can now write A.9 as

$$2\pi\left\{\ln\left(\frac{q_1}{\mu}+\frac{q_2}{\mu}\right)^2 + \ln\left(\frac{(|q_1+q_2|+|q_1-q_2|)}{(|q_1+q_2|-|q_1-q_2|)}\frac{4q_1q_2}{|q_1+q_2|^2}\right) - \ln 4\right\}$$

$$= 2\pi\ln\left(\frac{(|q_1+q_2|+|q_1-q_2|)}{(|q_1+q_2|-|q_1-q_2|)}\frac{q_1q_2}{\mu^2}\right)$$

$$= 2\pi\left\{\Theta(q_1-q_2)\ln\frac{q_1^2}{\mu^2} + \Theta(q_2-q_1)\ln\frac{q_2^2}{\mu^2}\right\}. \tag{A.13}$$

Finally, implementing this in our original equation A.1 we obtain

$$\begin{aligned}
&\int_{\mu^2}^{Q^2}\frac{d^2q_1}{\pi q_1^2}\int_{\mu^2}^{Q^2}\frac{d^2q_2}{\pi q_2^2}\ln\frac{(\mathbf{q_1}+\mathbf{q_2})^2}{\mu^2} \\
&= \int_{\mu^2}^{Q^2}\frac{dq_2^2}{q_2^2}\int_{q_2^2}^{Q^2}\frac{dq_1^2}{q_1^2}\ln\frac{q_1^2}{\mu^2} + \int_{\mu^2}^{Q^2}\frac{dq_1^2}{q_1^2}\int_{q_1^2}^{Q^2}\frac{dq_2^2}{q_2^2}\ln\frac{q_2^2}{\mu^2} \\
&= 2\int_{\mu^2}^{Q^2}\frac{dk^2}{k^2}\int_{k^2}^{Q^2}\frac{dq^2}{q^2}\ln\frac{q^2}{\mu^2} \\
&= \frac{\mathbf{16}}{\mathbf{3}}\mathbf{T^3},
\end{aligned} \tag{A.14}$$

with $T = \ln\frac{Q}{\mu}$ in the notation of the text.

References

[1] M. E. Peskin and D. V. Schroeder, *Reading, USA: Addison-Wesley (1995) 842 p.*

[2] D. E. Groom *et al.*, Eur. Phys. J. **C15** (2000) 1.

[3] S. Bethke, J. Phys. G **G26** (2000) R27 [hep-ex/0004021].

[4] J. C. Collins, D. E. Soper and G. Sterman, Nucl. Phys. **B261**, 104 (1985).

[5] M. L. Mangano, *1998 European School of High-Energy Physics, St. Andrews, Scotland, 23 Aug - 5 Sep 1998.*

[6] V. Barger and R. J. Phillips, "Collider Physics," *Redwood city, USA: Addison-Wesley (1987) 592 P. (Frontiers in physics, 71).*

[7] F. Bloch and A. Nordsieck, Phys. Rev. **52** (1937) 54.

[8] T. Kinoshita, J. Math. Phys. **3** (1962) 650.

[9] T. D. Lee and M. Nauenberg, Phys. Rev. **133** (1964) B1549.

[10] V. N. Gribov and L. N. Lipatov, Yad. Fiz. **15**, 781 (1972).

[11] L. N. Lipatov, Sov. J. Nucl. Phys. **20**, 94 (1975).

[12] G. Altarelli and G. Parisi, Nucl. Phys. **B126**, 298 (1977).

[13] Y. L. Dokshitzer, Sov. Phys. JETP **46** (1977) 641.

[14] R. K. Ellis, W. J. Stirling and B. R. Webber, "QCD and collider physics," *Cambridge, UK: Univ. Pr. (1996) 435 p. (Cambridge monographs on particle physics, nuclear physics and cosmology: 8).*

[15] A. D. Martin, R. G. Roberts, W. J. Stirling and R. S. Thorne, Eur. Phys. J. **C4** (1998) 463 [hep-ph/9803445].

[16] A. De Rujula, S. L. Glashow, H. D. Politzer, S. B. Treiman, F. Wilczek and A. Zee, Phys. Rev. **D10** (1974) 1649.

[17] L. N. Lipatov, Sov. J. Nucl. Phys. **23** (1976) 338.

[18] E. A. Kuraev, L. N. Lipatov and V. S. Fadin, Sov. Phys. JETP **45** (1977) 199.

[19] I. I. Balitsky and L. N. Lipatov, Sov. J. Nucl. Phys. **28**, 822 (1978).

[20] S. Catani, F. Fiorani and G. Marchesini, Nucl. Phys. **B336**, 18 (1990).

[21] S. Catani, F. Fiorani and G. Marchesini, Phys. Lett. **B234**, 339 (1990).

[22] G. Marchesini, Nucl. Phys. **B445**, 49 (1995) [hep-ph/9412327].

[23] S. Catani, hep-ph/9406325.

[24] L. V. Gribov, E. M. Levin and M. G. Ryskin, Phys. Rept. **100** (1983) 1.

[25] M. Kuhlen, hep-ph/9712505.

[26] I. Abt *et al.* [H1 Collaboration], Nucl. Phys. **B407**, 515 (1993).

[27] M. Derrick *et al.* [ZEUS Collaboration], Phys. Lett. **B316**, 412 (1993).

[28] J. Breitweg *et al.* [ZEUS Collaboration], Phys. Lett. **B407**, 432 (1997) [hep-ex/9707025].

[29] S. Aid *et al.* [H1 Collaboration], Nucl. Phys. **B470** (1996) 3 [hep-ex/9603004].

[30] P. D. Collins, "An Introduction To Regge Theory And High-Energy Physics," *Cambridge 1977, 445p.*

[31] J. J. Sakurai, Annals Phys. **11**, 1 (1960).

[32] M. Froissart, Phys. Rev. **123** (1961) 1053.

[33] H. Abramowicz and A. Caldwell, Rev. Mod. Phys. **71** (1999) 1275 [hep-ex/9903037].

[34] A. V. Barnes *et al.*, Phys. Rev. Lett. **37** (1976) 76.

[35] J. R. Forshaw and D. A. Ross, "Quantum chromodynamics and the pomeron," *Cambridge, UK: Univ. Pr. (1997) 248 p. (Cambridge lecture notes in physics. 9).*

[36] A. Donnachie and P. V. Landshoff, Nucl. Phys. **B231** (1984) 189.

[37] A. Donnachie and P. V. Landshoff, Phys. Lett. **B191** (1987) 309.

[38] A. Donnachie and P. V. Landshoff, Phys. Lett. **B296** (1992) 227 [hep-ph/9209205].

[39] I.Ya. Pomeranchuk, Sov. Phys. JEPT **7** (1958) 499.

[40] M. Derrick *et al.* [ZEUS Collaboration], Phys. Lett. **B315**, 481 (1993).

[41] T. Ahmed *et al.* [H1 Collaboration], Nucl. Phys. **B429**, 477 (1994).

[42] Y. I. Azimov, Y. L. Dokshitzer, V. A. Khoze and S. I. Troian, Z. Phys. **C27** (1985) 65.

[43] A. H. Mueller, J. Phys. G **G17** (1991) 1443.

[44] W. Tang, Phys. Lett. **B278** (1992) 363.

[45] J. Bartels, A. de Roeck and M. Loewe, Z. Phys. **C54** (1992) 635.

[46] B. Foster, hep-ex/0008069.

[47] C. Adloff *et al.* [H1 Collaboration], Phys. Lett. **B462** (1999) 440 [hep-ex/9907030].

[48] J. R. Forshaw and M. G. Ryskin, Z. Phys. **C68** (1995) 137 [hep-ph/9501376].

[49] A. H. Mueller and W. K. Tang, Phys. Lett. **B284** (1992) 123.

[50] V. Del Duca and W. Tang, hep-ph/9308207.

[51] B. Abbott *et al.* [D0 Collaboration], Phys. Rev. Lett. **84** (2000) 5722 [hep-ex/9912032].

[52] B. Cox, J. Forshaw and L. Lonnblad, JHEP **9910** (1999) 023 [hep-ph/9908464].

[53] B. E. Cox, J. R. Forshaw and L. Lonnblad, hep-ph/9912489.

[54] C. Ewerz, L. H. Orr, W. J. Stirling and B. R. Webber, J. Phys. G **G26** (2000) 696 [hep-ph/9912469].

[55] C. Ewerz and B. R. Webber, JHEP **9904** (1999) 022 [hep-ph/9904244].

[56] C. Ewerz and B. R. Webber, JHEP **9908** (1999) 019 [hep-ph/9907430].

[57] M. Acciarri *et al.* [L3 Collaboration], Phys. Lett. **B453** (1999) 333.

[58] P. Achard [L3 Collaboration], Nucl. Phys. Proc. Suppl. **82** (2000) 61 [hep-ex/9907016].

[59] M. Wadhwa, hep-ex/9909001.

[60] J. Kwiecinski, hep-ph/0009055.

[61] M. Gell-Mann and M. L. Goldberger, Phys. Rev. Lett. **9** (1962) 275.

[62] M. Gell-Mann, M. L. Goldberger, F. E. Low, E. Marx and F. Zachariasen, Phys. Rev. **133B** (1964) 145.

[63] M. Gell-Mann, M. L. Goldberger, F. E. Low, V. Singh and F. Zachariasen, Phys. Rev. **133B** (1964) 161.

[64] J. C. Polkinghorne, J. Math. Phys. **5** (1964) 1491.

[65] L. Tyburski, Phys. Rev. **D13** (1976) 1107.

[66] L. L. Frankfurt and V. E. Sherman, *Sov.J.Nucl.Phys.(English Transl.) 23 (1976) 581-587.Yadern.Fiz.23 (1976) 1099-1110 and Leningrad Inst Nucl Phys - 180 (75,REC.OCT) 31p.*

[67] C. Y. Lo and H. Cheng, Phys. Rev. **D13** (1976) 1131.

[68] A. L. Mason, Nucl. Phys. **B120** (1977) 275.

[69] H. Cheng and C. Y. Lo, Phys. Rev. **D15** (1977) 2959.

[70] E. A. Kuraev, L. N. Lipatov and V. S. Fadin, Sov. Phys. JETP **44** (1976) 443.

[71] V. Del Duca, hep-ph/9503226.

[72] P. Chiappetta, CPT-88-P-2178

[73] M. Ciafaloni, Nucl. Phys. **B296**, 49 (1988).

[74] S. Catani, F. Fiorani, G. Marchesini and G. Oriani, Nucl. Phys. **B361**, 645 (1991).

[75] J. R. Forshaw and A. Sabio Vera, Phys. Lett. **B440** (1998) 141 [hep-ph/9806394].

[76] J. Kwiecinski, C. A. Lewis and A. D. Martin, Phys. Rev. **D54**, 6664 (1996) [hep-ph/9606375].

[77] L. H. Orr and W. J. Stirling, hep-ph/9804431.

[78] B. R. Webber, Phys. Lett. **B444** (1998) 81 [hep-ph/9810286].

[79] J. R. Forshaw, A. Sabio Vera and B. R. Webber, J. Phys. G **G25** (1999) 1511 [hep-ph/9812318].

[80] G. P. Salam, JHEP **9903** (1999) 009 [hep-ph/9902324].

[81] G. Marchesini and B. R. Webber, Nucl. Phys. **B349** (1991) 617.

[82] G. Marchesini and B. R. Webber, Nucl. Phys. **B386** (1992) 215.

[83] H. Kharraziha and L. Lonnblad, JHEP **9803** (1998) 006 [hep-ph/9709424].

[84] H. Jung, hep-ph/9908497.

[85] M. A. Kimber, J. Kwiecinski, A. D. Martin and A. M. Stasto, hep-ph/0006184.

[86] L. Lonnblad and H. Jung, hep-ph/0006166.

[87] L. Goerlich and J. Turnau, *Prepared for Workshop on Monte Carlo Generators for HERA Physics (Plenary Starting Meeting), Hamburg, Germany, 27-30 Apr 1998*.

[88] H. Jung, Nucl. Phys. Proc. Suppl. **79** (1999) 429 [hep-ph/9905554].

[89] G. Bottazzi, G. Marchesini, G. P. Salam and M. Scorletti, JHEP **9812** (1998) 011 [hep-ph/9810546].

[90] B. Andersson, G. Gustafson and J. Samuelsson, Nucl. Phys. **B467** (1996) 443.

[91] M. Ciafaloni, Phys. Lett. **B429**, 363 (1998) [hep-ph/9801322].

[92] M. Ciafaloni and G. Camici, Phys. Lett. **B430**, 349 (1998) [hep-ph/9803389].

[93] M. Ciafaloni and D. Colferai, Nucl. Phys. **B538**, 187 (1999) [hep-ph/9806350].

[94] V. S. Fadin and L. N. Lipatov, Phys. Lett. **B429**, 127 (1998) [hep-ph/9802290].

[95] V. S. Fadin, M. I. Kotsky and R. Fiore, Phys. Lett. **B359** (1995) 181.

[96] V. S. Fadin, R. Fiore and M. I. Kotsky, Phys. Lett. **B387** (1996) 593 [hep-ph/9605357].

[97] V. S. Fadin and L. N. Lipatov, Nucl. Phys. **B406** (1993) 259.

[98] V. Fadin, R. Fiore and A. Quartarolo, Phys. Rev. **D50** (1994) 5893 [hep-th/9405127].

[99] V. S. Fadin, R. Fiore and M. I. Kotsky, Phys. Lett. **B389** (1996) 737 [hep-ph/9608229].

[100] V. S. Fadin and L. N. Lipatov, Nucl. Phys. **B477** (1996) 767 [hep-ph/9602287].

[101] V. S. Fadin, M. I. Kotsky and L. N. Lipatov, Phys. Lett. **B415** (1997) 97

[102] S. Catani, M. Ciafaloni and F. Hautmann, Phys. Lett. **B242**, 97 (1990).

[103] S. Catani, M. Ciafaloni and F. Hautmann, Nucl. Phys. **B366**, 135 (1991).

[104] G. Camici and M. Ciafaloni, Phys. Lett. **B386**, 341 (1996) [hep-ph/9606427].

[105] G. Camici and M. Ciafaloni, Nucl. Phys. **B496**, 305 (1997) [hep-ph/9701303].

[106] V. S. Fadin, R. Fiore, A. Flashi, M. I. Kotsky Phys. Lett. **B422** 287 (1998)

[107] D. A. Ross, Phys. Lett. **B431** (1998) 161 [hep-ph/9804332].

[108] E. Levin, hep-ph/9806228.

[109] R. D. Ball and S. Forte, hep-ph/9805315.

[110] J. Blumlein, V. Ravindran, W. L. van Neerven and A. Vogt, hep-ph/9806368.

[111] G. P. Salam, Acta Phys. Polon. **B30** (1999) 3679 [hep-ph/9910492].

[112] J. Bartels, Nucl. Phys. **B175** (1980) 365.

[113] G. P. Salam, JHEP **9807** (1998) 019 [hep-ph/9806482].

[114] J. R. Forshaw, D. A. Ross and A. Sabio Vera, Phys. Lett. **B455** (1999) 273 [hep-ph/9903390].

[115] L. N. Lipatov, talk presented at the 4th Workshop on Small-x and Diffractive Physics, FNAL, September 1998.

[116] M. Ciafaloni and D. Colferai, Phys. Lett. **B452**, 372 (1999) [hep-ph/9812366].

[117] B. Andersson, G. Gustafson, J. Hakkinen, M. Ringner and P. Sutton, JHEP **9809**, 014 (1998) [hep-ph/9807541].

[118] C. R. Schmidt, Phys. Rev. **D60**, 074003 (1999) [hep-ph/9901397].

[119] J. R. Forshaw, D. A. Ross and A. Sabio Vera, to be published in Phys. Lett. B. [hep-ph/0011047].

[120] L. N. Lipatov, Sov. Phys. JETP **63**, 904 (1986).

[121] R. S. Thorne, Phys. Rev. **D60**, 054031 (1999)

[122] R. S. Thorne, Phys. Lett. **B474**, 372 (2000)

[123] W. Magnus, F. Oberhettinger, R.P. Soni, "Formulas and theorems for the special functions of mathematical physics", Springer, 1966.

[124] A. H. Mueller, Phys. Lett. **B396** (1997) 251 [hep-ph/9612251].

[125] G. P. Salam, in *NONE*, hep-ph/0005304.

[126] G. Altarelli, R. D. Ball and S. Forte, Nucl. Phys. **B575** (2000) 313 [hep-ph/9911273].

[127] M. Ciafaloni, D. Colferai and G. P. Salam, JHEP **9910** (1999) 017

[128] M. Ciafaloni, D. Colferai and G. P. Salam, JHEP **0007** (2000) 054

[129] J. R. Forshaw, D. A. Ross and A. Sabio Vera, in preparation.

[130] V. Del Duca and C. R. Schmidt, Phys. Rev. **D57** (1998) 4069 [hep-ph/9711309].

[131] V. Fadin, D. Ivanov and M. Kotsky, in , hep-ph/0007119.

[132] J. Bartels, S. Gieseke and C. F. Qiao, hep-ph/0009102.